PRACA DOKTORSKA

ICHF
Instytut Chemii Fizycznej PAN

Warsaw-4-PhD
Warsaw Doctoral School
in Natural and BioMedical Sciences

Photochemistry and spectroscopy of small, cryogenically isolated organopnictogen molecules

Elavenil Ganesan

Ph.D. Thesis

prepared within the Warsaw Doctoral School in Natural and BioMedical Sciences
at the Institute of Physical Chemistry, Polish Academy of Sciences,
ul. Kasprzaka 44/52, 01-224, Warsaw, Poland
under the supervision of Professor Robert Kołos
and auxiliary supervision of Dr. ArunLibertsen Lawzer

Warsaw, February 2025

Acknowledgement

It gives me immense pleasure to write this acknowledgment section. This thesis would not have been possible without the patience, guidance, and countless efforts of my mentors: Prof. Robert Kołos, Dr. Arun-Libertsen Lawzer, and Dr. Thomas Custer. I extend my heartfelt gratitude to our collaborators—Prof. Jean-Claude Guillemin, for providing the necessary chemicals, and Prof. Claudine Crépin-Gilbert, for her invaluable support during my visit to ISMO, France. I am also deeply grateful to Dr. Marcin Gronowski for contributing some of the theoretical results used in this thesis.

After five years of struggle, marked by moments of stress and unfortunate circumstances, I have finally reached this milestone. My PhD journey has been a spectrum of fleeting joys, intense mental battles, and overwhelming care and love. This journey would not have been possible without the unwavering support and affection of those I am privileged to call friends.

To my undergraduate friends—Subramani, Karthi, Shankar, Nikki, Senthil, Kishore and Durgu—who have stood by me through every personal challenge: We started as friends, but over time, you became family. I deeply cherish the bond we share. Similarly, I am grateful to my postgraduate friends (too many to name here, but each of you holds a special place in my heart). Despite the physical distance, your support never wavered.

I must also thank my "Warsaw machans," who stood beside me through the struggles I faced. While some spend a lifetime searching for one true companion, I was fortunate to find an entire group of extraordinary individuals. Together, we explored countless places, creating memories I will always treasure. The kindness, care, and mutual respect within this group are beyond words. Our sleepless nights, deep conversations, and shared meals made connections on a profoundly personal level. A special mention goes to Sharat, Sangami, Sakthi, Karthika Ka, Moni Ma, Deb, Arun Anna, and the newest addition to our circle, Kaaviya. Their names bring a smile to my face and pride to my heart. I only wish I had built similar bonds with all the incredible people I met in Warsaw.

Life can often be overwhelming, and it is easy to become consumed by personal struggles. Yet, family always finds a way to ensure you are okay. I am blessed with a family—Amma, Appa, and Anna—whose love and support have carried me through every stage of life. My PhD is not just my achievement; it is the realization of a dream and the hard work of three generations.

During my time in Warsaw, one constant presence helped me navigate solitude and mental battles. This remarkable individual ensured my well-being, provided solace when I needed it most, and always seemed to understand my emotions without ever meeting me in person. His music became my refuge. This extraordinary figure is none other than the legendary Ilaiyaraaja. His compositions consoled me, inspired me, and remained my unwavering companion throughout this thesis journey.

To all the incredible people I have mentioned here—and to those I may have unintentionally left out—I am forever grateful. As a tribute to this thesis, I have written a poem in my mother tongue, Tamil.

தேடல் பட்டறை செய்த
உளி கண்ட சிற்பமிங்கே
கேள்விக் கடல் உலர்த்தி
தேடிப் பிடித்த பதில்களிங்கே
பரந்த அண்டத்தில் நீந்தி
சிறுதுளி அவிழ்த்த அழியா ஆற்றலிங்கே
உள்ளக் கனலில் கரைந்த
மேகம் பொழிந்த அருவியிங்கே
எண்ணச் சிறகுகள் விரித்து
அசைந்து இசைத்த பாடலிங்கே
பலயானை பலம் பொருந்தி
வேடம் பல உடுத்தி
காண்பதற்கரிய மாய உண்மையிங்கே
ஏன் என துவங்கி
ஏன் என முடியும்
முடியா விந்தையிங்கே

-Elavenil (இளவேனில்)

Dedicated to Tamil (என் தமிழுக்காக)

Funding

1. The Polish National Agency for Academic Exchange "STER" project No. BPI/STE/2021/1/00034/U/00001

2. PHC Polonium project No. BPN/BFR/2021/1/00028/U/00001

List of publications

1. **Ganesan, E**., Custer, T., Lawzer, A., Guillemin, J. and Kołos, R.; "Unusual Quartet-Doublet Phosphorescence from the Phosphaethynyl Radical CP"; *Angewandte Chemie Int. Ed*. (2022) e202210521 https://doi.org/10.1002/anie.202210521

2. Lawzer, A., **Ganesan, E**., Gronowski, M., Custer, T., Guillemin, J. and Kołos, R.; "Free ethynylarsinidene and ethynylstibinidene: Heavier analogues of nitrenes and phosphinidenes"; *Chemistry-A European Journal* (2023) **29**, e202300887 https://doi.org/10.1002/chem.202300887

3. Lawzer, A.-L., **Ganesan, E**., Custer, T., Guillemin, J.-C., & Kołos, R. "Isomerisation of phosphabutyne and a photochemical route to phosphabutadiyne (HC_3P), a phosphorus analogue of cyanoacetylene"; *Phys. Chem. Chem. Phys.* (2024) https://doi.org/10.1039/D4CP04182H

4. **Ganesan, E**., Lawzer, A., Custer, T., Guillemin, J. and Kołos, R., "Photochemical dehydrogenation of methylpnictines (CH_3PH_2, CH_3AsH_2, CH_3SbH_2) in solid argon"; *in preparation*

Scientific presentations

1. **“**Spectroscopy of Small Phosphorus-Containing Molecules of Astrophysical Interest” (poster), conference *Chemical processes in solar-type star-forming regions*, 2023, Toulouse, France.

2. “Laboratory astrochemistry” (oral presentation) and “Infrared and electronic spectroscopy of small organo-phosphorus molecules in rare gas matrices” (poster), summer school *Space missions: Ground-based observations and science communication*, 2023, Vilnius, Lithuania.

3. “Photochemistry of methylpnictines (CH_3XH_2; X= P, As, Sb) in cryogenic matrices” (poster & flash talk), *Nanospace Astrochemistry Training School*, 2024, Groningen, The Netherlands.

Acronyms and abbreviations

0-0 – vibrationless origin of an electron transition

CASSCF – complete active space self-consistent field

CCD – charge-coupled device

DBU - 1,8-diazabicyclo[5.4.0]undec-7-ene

DFT – density functional theory

FTIR - Fourier transform infrared

GASCI - generalized active space configuration interaction

HOMO – Highest occupied molecular orbital

IC – internal conversion

IPC PAS – Institute of Physical Chemistry, Polish Academy of Sciences

IR - infrared

ISC – intersystem crossing

LED – light emitting diode

LUMO – lowest unoccupied molecular orbital

MRCI – multi-reference configuration interaction

OPO – optical parametric oscillator

PEC – potential energy curve

PES – potential energy surface

PMT – photomultiplier Tube

SOMO – singly occupied molecular orbital

S/N – signal-to-noise ratio

TD-DFT - time-dependent density functional theory

TS – transition state

UV/Vis – ultraviolet and visible

UV - ultraviolet

VUV – vacuum Ultraviolet

VR – vibrational relaxation

Abstract

This dissertation deals with select simple, yet poorly known phosphorous-, arsenic-, and antimony-containing molecules. Their vacuum- and/or mid-ultraviolet photochemistry was investigated, starting with single-carbon species: phosphaethyne (HCP), methylphosphine (CH_3PH_2), methylarsine (CH_3AsH_2), and methylstibine (CH_3SbH_2). Next, two-carbon molecule, ethynylstibine ($HCCSbH_2$) was studied, and finally a three-carbon one: propadienylphosphine ($H_2C=C=CH-PH_2$). Except for HCP, all these compounds represented the family of pnictines ($R-XH_2$, where X = P, As, or Sb).

Highly reactive products generated during photolysis experiments were at the heart of this doctoral work. They were trapped within cryogenic rare-gas matrices and characterized with vibrational (Fourier-transform infrared) absorption spectroscopy and electronic spectroscopy (both absorption and luminescence). Photoinduced dehydrogenation and C-X bond cleavage emerged as the dominant reactions giving access to previously underexplored or unknown chemical compounds. The main achievements of this research include the following:

- Quartet-doublet luminescence emitted by the radical CP was discovered. This very rare type of phosphorescence was thoroughly analyzed and explained (Chapter 3).
- Differences in photochemical properties observed here for the methylpnictines, namely CH_3PH_2, CH_3AsH_2, and CH_3SbH_2, were rationalized. Spectroscopic characterization of their exotic photolysis products $CH_2=PH$, $CH_2=AsH$, $H-C\equiv As$, CH_3Sb, and CD_3Sb was provided (Chapter 4).
- Photodehydrogenation of ethynylstibine produced the previously unknown species $H-C\equiv C-Sb$ (ethynylstibinidene, the compound of monovalent antimony). Its spectroscopic properties were juxtaposed with those of HCCN, HCCP, and HCCAs. Luminescence emissions attributed to HCCAs and HCCSb were discovered (Chapter 5).
- Photodehydrogenation of propadienylphosphine turned out to be an efficient way leading to the astrochemically significant molecule $H-C\equiv C-C\equiv P$ (Chapter 6).

The prospects for future advancement of the research described in this dissertation are provided.

Streszczenie rozprawy doktorskiej

Rozprawa dotyczy wybranych prostych, lecz słabo dotychczas poznanych związków chemicznych zawierających fosfor, arsen i antymon. Zbadano ich fotochemię w zakresie próżniowego i/lub średniego nadfioletu, zaczynając od cząsteczek jednowęglowych: fosfaetynu (HCP), metylofosfiny (CH_3PH_2), metylarsyny (CH_3AsH_2) i metylostibiny (CH_3SbH_2). Kolejnymi obiektami badań były cząsteczki dwuwęglowe, tj. etynylostibina ($HCCSbH_2$) i etynyloarsyna ($HCCAsH_2$) oraz trójwęglowa propadienylofosfina ($H_2C=C=CH-PH_2$). Wspólny elementem strukturalnym tych związków (z wyjątkiem HCP) jest ugrupowanie $-XH_2$, gdzie X oznacza P, As lub Sb.

W centrum uwagi znalazły się wysoce reaktywne produkty reakcji fotochemicznych. Pułapkowanie w matrycy z zestalonego gazu szlachetnego zapewniało im trwałość pozwalającą na scharakteryzowanie za pomocą spektroskopii oscylacyjnej (absorpcyjnej w podczerwieni) oraz elektronowej (zarówno absorpcji, jak i luminescencji). Fotoindukowane odwodornienie oraz dysocjacja wiązania C-X były dominującymi procesami, dającymi dostęp do uprzednio nieznanych lub słabo scharakteryzowanych związków chemicznych. Do głównych osiągnięć doktoratu należą:

- odkrycie luminescencji kwartet-dublet emitowanej przez rodnik CP; ten bardzo rzadki rodzaj fosforescencji został dokładnie przeanalizowany i znalazł wyjaśnienie (Rozdział 3);
- opisanie i wytłumaczenie różnic we właściwościach fotochemicznych cząsteczek CH_3PH_2, CH_3AsH_2 i CH_3SbH_2; scharakteryzowanie spektroskopowe egzotycznych produktów ich fotolizy: $CH_2=PH$, $CH_2=AsH$, H-C≡As, CH_3-Sb i CD_3-Sb (Rozdział 4);
- uzyskanie nieznanej wcześniej cząsteczki H-C≡C-Sb (etynylostibinidyna, związek jednowartościowego antymonu) na drodze fotoodwodornienia etynylostibiny; przeprowadzono porównanie właściwości spektroskopowych HCCSb z właściwościami HCCN, HCCP i HCCAs; nowo odkryte pasma luminescencji przypisano wstępnie HCCAs i HCCSb (Rozdział 5);
- opisanie fotoodwodornienia propadienylofosfiny ($H_2C=C=CH-PH_2$) w zestalonym argonie jako wydajnej metody generowania astrochemicznie istotnej cząsteczki H-C≡C-C≡P (rozdział 6).

Przedstawiono perspektywy dalszego rozwoju kierunków badawczych zaprezentowanych w dysertacji.

Table of Contents

Chapter 1

Introduction

1. Introduction

For thousands of years, humans have been curious about the origin and nature of life. From unicellular to multicellular organisms, all life forms are composed of fundamental biomolecules like nucleic acids, proteins, and carbohydrates. Precursors to these biomolecules such as nitrogenous bases, amino acids and pentoses can be formed through chemical reactions involving simple molecules like methane, ammonia, phosphine, hydrogen, carbon dioxide, and water (Miller, 1953; Nina Hall, 2004; Smith et al., 2021). The elements found in all biomolecules are primarily hydrogen, carbon, nitrogen, oxygen, sulfur, and phosphorus.

Following the Big Bang, the Universe was extremely dense and hot, filled with a plasma of quarks, leptons, and bosons. As it expanded and cooled, hydrogen and helium atoms formed (Alpher et al., 1948). Heavier atoms, up to iron, can be synthesized through nuclear fusion in stars. Once the core of a massive star reaches iron, fusion ceases, leading to the star collapse and consequently to a supernova explosion (Janka et al., 2007). A wealth of heavy nuclei is produced during such events through the neutron or proton capture processes (Burbidge et al., 1957). Nucleosynthesis may also accompany cataclysmic neutron or black hole mergers (Curtis et al., 2023). The evolution of lower-mass stars ends with the ejection of their envelopes, rich in carbon, oxygen, and nitrogen, into the surrounding medium (Habing & Olofsson, 2004).

The formation mechanisms of molecules in diverse astrophysical environments remains an active research area (Corby et al., 2018; Yu et al., 2019). Many of these can certainly be formed in the interstellar medium via direct gas-phase reactions. Mineral dust grains, constituting approximately 1% of interstellar gas clouds by mass, are composed mostly of carbonaceous materials or silicates, with an admixture of elements like magnesium or iron, and serve as cold surfaces onto which molecules (first and foremost water) can be adsorbed. Icy layers coating dust grains facilitate chemical reactions, serving as a trap for atoms and molecules. Energetic photons and cosmic radiation particles can photolyze and/or ionize the trapped species, triggering processes which produce more complex compounds (Draine, 2003; Potapov et al., 2020). Once the dust grains are warmed, their icy layers evaporate and the liberated molecules enrich the interstellar medium. Their spectral signatures are detected mostly at radio frequencies (e.g. Green Bank Telescope, Atacama Large Millimeter Array), sometimes in infrared (e.g. James Webb Space Telescope), and occasionally in the visible region. To date, approximately 320 molecules have been identified in space.

1.1. Pnictogens

Elements of group-15 of the periodic table are called *pnictogens*. Nitrogen, the most electronegative member of this family, is followed by phosphorus, arsenic, antimony, bismuth, and moscovium. Some basic properties of pnictogen group atoms are listed in **Table 1-1**. Elements P, As, and Sb are the focus of this Thesis.

Table 1-1. Properties of pnictogen elements (source: https://pubchem.ncbi.nlm.nih.gov/periodic-table/)

Element	Atomic number	Atomic radius (pm)	Natural isotopic abundance (%)	Electronic configuration	Oxidation state	Ionization energy (eV)
N (non-metal)	7	65	^{14}N- 99.634 ^{15}N - 0.366	[He]2s^{2}2p^3	+5, +4, +3, +2, +1, -1, -2, -3	14.53
P (non-metal)	15	100	^{31}P - 100	[Ne]3s^{2}3p^3	+5, +3, -3	10.49
As (metalloid)	33	115	^{75}As - 100	[Ar]4s^{2}3d^{10}4p^3	+5, +3, -3	9.79
Sb (metalloid)	51	145	^{121}Sb – 57.21 ^{123}Sb – 42.79	[Kr]5s^{2}4d^{10}5p^3	+5, +3, -3	8.61
Bi (metal)	83	160	^{209}Bi – 100	[Xe]6s^{2}4f^{14}5d^{10}6p^3	+5, +3	7.29
Mc (metal)	115	187 (predicted)	No stable isotopes	[Rn]7s^{2}5f^{14}6d^{10}7p^3	Not available	Not available

Nitrogen is the 5th and phosphorus the 18th most abundant element in the Galaxy. In biological systems, however, P is the sixth most abundant. It is a crucial element in the backbone of nucleotides, phospholipids, and nucleic acids. Many nitrogen-containing chemical compounds, potential precursors to large biomolecules, have been extensively studied and widely detected in space. Only seven P-bearing compounds (CP, NCCP, CCP, HCP, PN, PO, and PH_3) have been identified in extraterrestrial environments, reflecting the fact that phosphorous is almost three orders of magnitude less abundant than nitrogen (Maciá-Barber, 2019). Arsenic, the next element of the group, has not yet been identified in the interstellar medium but has been found in the atmospheres of Jupiter and Saturn in the form of AsH_3 (Giles et al., 2017; Kim et al., 2001). A detailed review of the literature reveals significant gaps in knowledge of the photochemistry and spectroscopy of small oxygen-free molecules containing trivalent (let alone monovalent) pnictogen atoms heavier than N.

This dissertation focuses on pnictogen-bearing molecules, with emphasis given to astrophysically significant organophosphorus species, e.g. CP, HCP, CH_2PH, HCCP or HC_3P. The most important arsenic- and antimony-containing molecules explored here are CAs, HCAs, CH_2AsH, CH_3Sb, HCCAs, and HCCSb. Given their low kinetic stabilities, studies involving all of

these compounds pose significant experimental challenges. In this work, they have been investigated mostly in the cryogenic environment of a solidified rare gas (*matrix isolation* technique).

1.2. Spectroscopy

The most important energy levels of a molecule (see **Figure 1-1**) can be categorized as electronic, vibrational, and rotational. The simultaneous change in electronic and vibrational energy produces *vibronic* transitions; these were spectroscopically probed in the course of this doctoral work using the ultraviolet, optical, and infrared regions of electromagnetic radiation. Some basics of vibrational (IR absorption) and electronic (UV/Vis absorption and emission) spectroscopy are provided below.

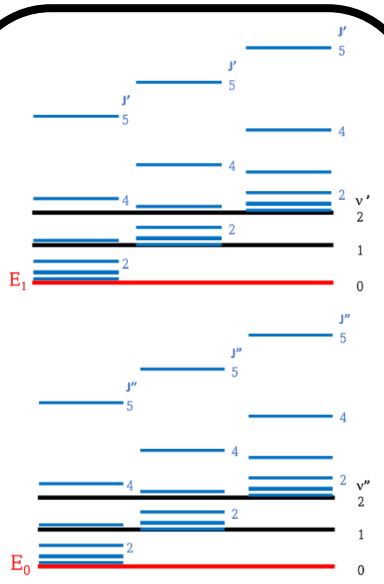

Figure 1-1. Electronic (red), vibrational (black), and rotational (blue) energy levels of a diatomic molecule.

1.2.1. Infrared absorption spectroscopy

The simplest approach to the phenomenon of molecular vibrations, which assumes that the force acting on oscillating atoms is directly proportional to their displacement, is known as the harmonic approximation. The blue parabola of **Figure 1-2** shows how the potential energy changes in a harmonically oscillating diatomic molecule. While conceptually useful, this description has severe limitations. Most importantly, it cannot describe the dissociation process. Still, the true potential energy curve (black in **Figure 1-2**) resembles a parabola at its bottom, that is for the smallest values (in particular: 0, 1) of the vibrational quantum number v, giving some rationale to low-level (harmonic approximation-based) theoretical predictions of vibrational frequencies.

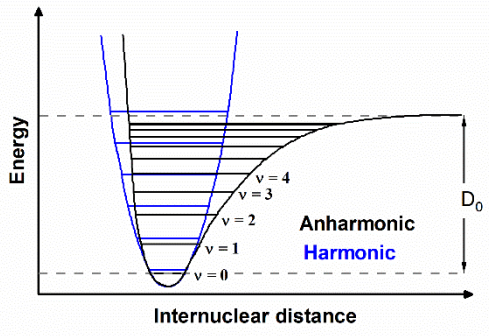

Figure 1-2. Potential energy of a quantum oscillator. D_0 is the dissociation energy.

The IR vibrational spectroscopy selection rule inherent to harmonic approximation, $\Delta v = 1$, becomes less stringent when the real (i.e. anharmonic) oscillators are considered. The *overtones* ($\Delta v = 2, 3, 4\ldots$) are then also allowed. As a rule, however, they are (just as are the *combination bands*, involving more than one vibrational mode), weaker than the corresponding fundamental bands (those due to the transitions from v=0 to v=1). An *N*-atomic molecule features 3*N*-6 modes of vibration (3*N*-5 when it is linear). Among these, one can distinguish bending (e.g. wagging, rocking, twisting, scissoring) and stretching vibrations. The critical condition for a vibrational band to appear in the absorption spectrum is that the electric dipole moment of a molecule should change during the respective molecular movement (more precisely: the gradient of electric dipole moment should have a non-zero value at the equilibrium position). Infrared absorption spectroscopy, usually combined with quantum chemical predictions of vibrational transitions, is the detection method of choice for the products of radiation-induced reactions in cryogenic matrices (see **Section 1.5**).

1.2.2. Electronic spectroscopy

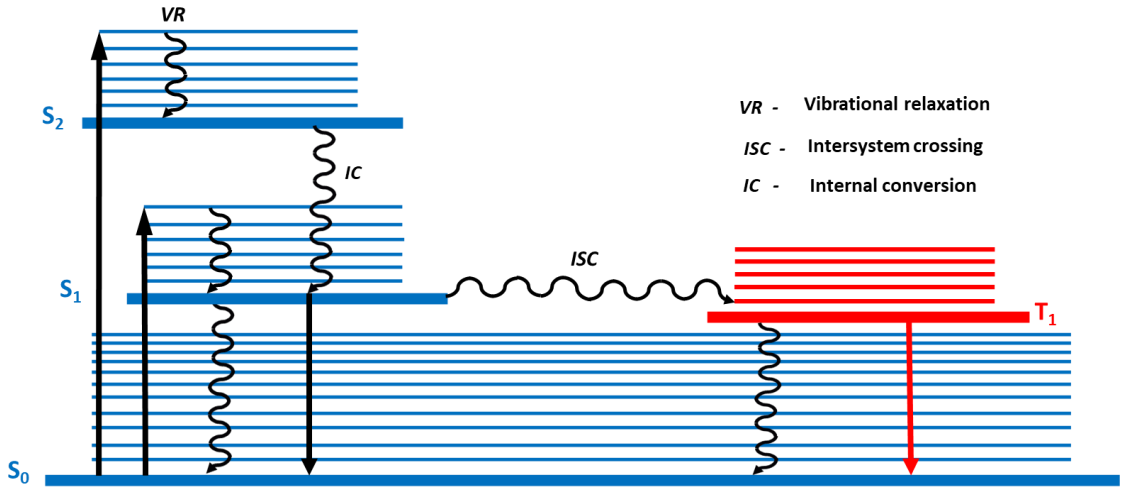

Figure 1-3. Jablonski diagram for a typical molecule featuring a singlet-multiplicity electronic ground state. Straight and wavy arrows represent radiative and nonradiative transitions, respectively. Singlet states are denoted by **S**, triplet by **T**.

Electronically excited molecules may undergo photophysical (radiative or non-radiative) transitions, as well as photochemical reactions. In the Jablonski diagram of **Figure 1-3**, the energy increases from the bottom to the top. Nonradiative pathways include vibrational relaxation, internal conversion, and intersystem crossing. Radiative relaxation (luminescence) is categorized as fluorescence or phosphorescence. A vibronic structure, often discernible in absorption and luminescence spectra, comes from the change of both electronic and vibrational excitation. It may

take the shape of a regular train of peaks. A *progression* is observed when either v' or v" does not change within the series (see **Figure 1-4**), while a *sequence* results from a constant value of Δv.

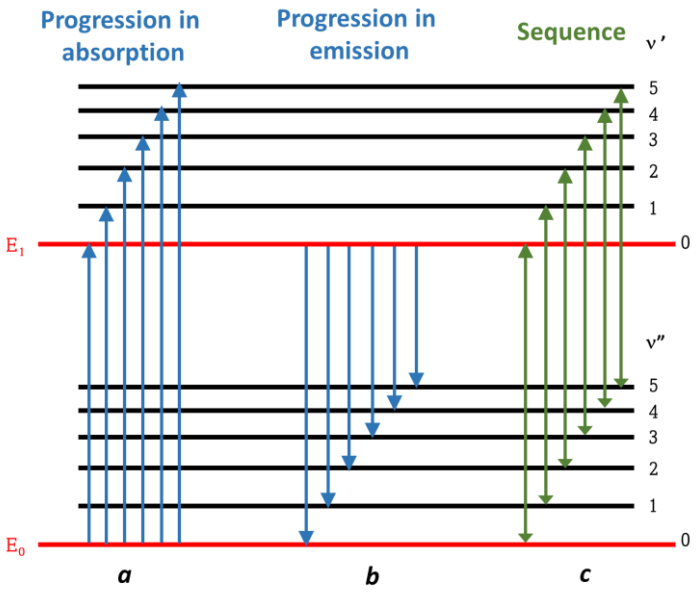

Figure 1-4. Diagrams illustrating the concept of vibronic progressions and sequences. Cases *a* and *b* correspond to the progressions observed in the electronic spectra of molecules isolated in low-temperature matrices: v"=0 in absorption and v'=0 in luminescence. Sequences (series of bands with constant Δv; case *c*) are not possible in cryogenic media.

For a molecule to undergo an allowed electronic transition, certain selection rules must be followed. The most important are those

- ***regarding spin****:* The total spin angular momentum of the electronic system should remain unchanged during the transition (ΔS=0). Therefore, phosphorescence (red arrow in **Figure 1-3**) is forbidden, as is absorption from a singlet electronic state to a triplet (e.g. Callomon & Davey 1963; Goodman & Kasha 1958; Jones et al. 1973; Kanda et al. 1964; Lewis & Kasha 1945; Marchetti & Kearns 1967; Meyer et al. 2017; Yuan et al. 2019);

- ***regarding symmetry:*** Specific rules depend on the point group. For linear molecules, the change of Λ (total orbital angular momentum quantum number) should be either 0 or ±1 and the wave function behaviour (symmetric or antisymmetric) with respect to reflection about the plane containing the internuclear axis should not change. Additionally (for all centrosymmetric molecules), the wavefunction parity (even, *g*, or odd, *u*) cannot be conserved in a transition. This rule about parity is also referred to as *Laporte's rule* and is strict, while the orbital angular momentum rule is rather easily violated.

- ***regarding the vibrational excitation change***: Δv=0, ±1, ±2, ±3, … The symmetry (see above) of a vibrational mode can be important when assessing the likelihood of a vibronic transition.

- regarding the rotational excitation change: For linear molecules, the allowed rotational quantum number (J) change is 0 or ±1 (however, ΔJ=0 is forbidden for those electronic+vibrational+rotational transitions which involve a stretching vibration).*

Violation of a selection rule usually implies low or very low transition probability. Accordingly, it may lead to spectroscopic signals that are weak or undetectable. Specific, dedicated techniques, involving e.g. very long path-lengths in absorption or ultrasensitive (photon-counting) detectors in emission spectroscopy may be needed in order to observe these less probable transitions.

Fluorescence occurs when an excited molecule radiatively relaxes to a lower electronic state without altering its total electronic spin. In **Figure 1-3**, this process is represented by downward-pointing straight arrows linking the excited singlet electronic states (S_1, S_2) with the ground state (S_0). In condensed phases, fluorescence rarely originates in an electronic state higher than S_1 (azulene being an example).

According to Kasha's rule, *the emitting level of a given multiplicity is the lowest excited level of that multiplicity* (del Valle & Catalán, 2019; Kasha, 1950).

The main reasons why polyatomic molecules present in condensed phases obey (with few exceptions) Kasha's rule are as follows:

i. a large number of vibrational levels, including those due to overtone and combination modes, result in a high density of states which promotes rapid nonradiative relaxation (IC between the excited electronic states, as well as VR);
ii. coupling to the vibrational modes of solvent molecules in a liquid or to the phonons (collective vibrations of a host crystal lattice) within solids.

When the Kasha's rule holds (and it generally does *not* in the gas phase), the vibronic structure of luminescence corresponds to a progression of bands originating in v'=0. This is the situation expected to occur in cryogenic matrices. Analysis of such a progression offers direct access to the energies of vibrational levels within the lower (usually: ground) electronic state involved in luminescence (**Figure 1-4**). This information often complements the data supplied by purely vibrational (i.e. IR or Raman) spectroscopy. Progressions of bands observed in electronic absorption spectra of low-temperature species originate in v"=0 of the ground state. According to the Boltzmann formula, the ratio of molecules in higher and lower thermally populated levels separated by the energy ΔE is given by:

$$N_{\text{higher}}/N_{\text{lower}} = g_{\text{higher}}/g_{\text{lower}} \exp(-\Delta E/kT) \qquad (1.1)$$

* With the exception of very special cases (e.g. diatomic hydrides), molecular rotations are effectively suppressed in cryogenic matrices.

where g_{higher}/g_{lower} is the ratio of the respective energetic degeneracies. Low temperatures reduce the population of higher levels. In the cryogenic conditions ($T \approx 10$ K) of matrix-isolation experiments presented in the Thesis, thermal population of all levels but the lowest vibrational level (v"=0) of the ground electronic state can be safely neglected. Consequently, all transitions start from v"=0. Intervals between the elements of a resultant progression are shaped by the distribution of vibrational levels within the excited electronic state (while the intensities of these vibronic bands depend on the overlap of v"=0 and v'=*n* vibrational wavefunctions).

Fluorescence lifetimes generally range from picoseconds to nanoseconds, depending on the competing processes.

Phosphorescence is another type of radiative relaxation, distinguished by a change in spin multiplicity between the initial and final (typically ground) electronic states (symbolized in **Figure 1-3** by a red arrow linking T_1 with S_0). This nonradiative photophysical process involves the *intersystem crossing* (ISC) between the excited electronic states of different multiplicities. Typically, phosphorescence can be discerned from fluorescence by its long lifetime (from milliseconds to seconds) and lower transition energy. For reasons explained in **Section 3.3.5**, phosphorescence of free radicals (a radiative quartet-doublet transition) is a very rare phenomenon.

1.3. Photochemistry

Photochemical processes are governed by two fundamental laws of photochemistry. The first of these, the Grotthuss-Draper law, states that only absorbed light can produce a photochemical transformation. According to the Stark-Einstein law, light absorption is a quantum process and, generally, one photon is absorbed by a single molecule. Photochemistry operates during the relaxation from an excited electronic state and may result in isomerization, dissociation and/or ionization.

The four basic types of photochemical reactions are listed below (Demtröder, 2018; Klán & Wirz, 2009; Peter Atkins & Julio de Paula, 2010).

a. Hot ground state reaction

When a reactant (A) reaches its excited electronic state (A^*), it can relax via various photophysical processes. Partly relaxed molecules may possess enough energy to populate the higher vibrational levels of their ground electronic state. Vibrationally excited molecules may cross a reaction barrier towards the ground electronic state of a product (B).

b. Adiabatic reaction

This one, typical for isomerization, proceeds entirely within the excited-state potential energy surface (PES). Following the excitation of *A* to *A**, the product is initially formed in its excited electronic state *B**, then relaxes to *B*.

c. Diabatic reaction

Here, *B* is formed directly from *A**. A *conical intersection*, i.e. certain point or a plane in the multidimensional space, makes a jump between the PESs of *A* and *B* possible.

d. Reaction via an intermediate

In this type of reaction, *A** relaxes to a shallow minimum which represents a short-lived intermediate species. Consequently, *B* is formed via the rearrangement of that species.

1.4. Organic intermediates

Reactive intermediates are species transiently formed during chemical reactions. Due to their kinetic instability, they are hard to detect under normal laboratory conditions. Some examples are shown in **Figure 1-5**. Among pnictogen-containing intermediates, *nitrenes*, species featuring monovalent nitrogen centers and triplet ground states, are well-known and widely studied because of their accessibility through photochemical or thermal decomposition of organic azides. While several stable carbenes and nitrenes have been isolated under typical laboratory conditions (Soleilhavoup & Bertrand, 2020), free molecules bearing a monovalent pnictogen atom heavier than N, i.e. *phosphinidenes*, *arsinidenes*, *stibinidenes*, or *bismuthinidenes* remain very poorly studied. Spectroscopy coupled with cryogenic isolation in inert matrices is an excellent tool for investigating such reactive species.

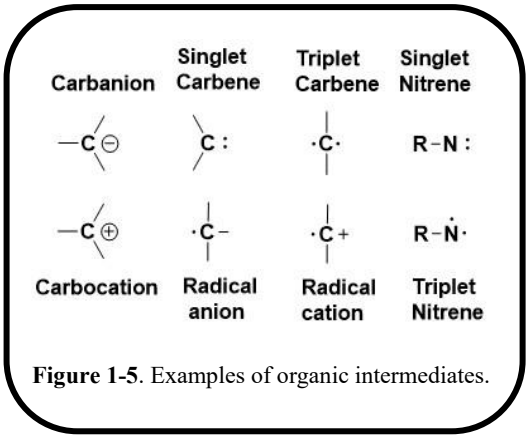

Figure 1-5. Examples of organic intermediates.

1.5. Matrix isolation technique

The cryogenic matrix isolation method provides an inert and stable environment where molecules, including very reactive species, can be trapped for further study. Trapping minimizes the influence of environmental factors such as intermolecular interactions. This low-temperature technique involves inert gas (*host*) atoms which are solidified (typically on a transparent substrate) along with the molecules of interest (*guest* species). The molar host-to-guest ratio is an important parameter, usually set within the range from several hundred to several thousand. True isolation is attained when guest molecules are separated from each other by host atoms. This greatly reduces the intermolecular interactions. Still, slight interactions with inert gas atoms remain, weakest for neon and much more pronounced for xenon. Argon is the most widely employed host in this technique. Outside of the noble gas family, N_2 and para-H_2 are also popular choices. Matrix isolation is typically used in conjunction with spectroscopic studies, in particular infrared absorption, Raman scattering, ultraviolet/visible absorption and luminescence. The restriction of rotational degrees of freedom and the absence of hot bands (i.e. those originating in $v'' > 1$) greatly reduces the number of vibrational or vibronic transitions and therefore simplifies the analysis of spectra.

Photolysis of molecules isolated in inert cryogenic matrices may generate reactive (i.e. typically very short-lived) intermediates. These can be trapped within the "cages" (voids between the host atoms), and remain stable unless decomposed by photochemical processes or quantum tunnelling. Guest species occupy substitutional sites (i.e. replacing one or more host atoms) and, occasionally, interstitial sites (between the host atoms). Once isolated, the guest species, particularly those larger in size and mass, are generally unable to move (diffuse) from one site to the other. Diffusion does occur, however, when the temperature is increased. *Annealing* is a commonly applied procedure involving a controlled, transient warm-up of the matrix sample. This can change the arrangement of isolated species and/or induce their chemical reactions.

1.6. Goal of the Thesis

The general aim of this dissertation was to advance the spectroscopy and photochemistry of small, kinetically unstable pnictogen-containing molecules. Specific objectives are listed below.

- Fine-tuning the preparative organic synthesis of pure HCP. If successful, description of the photochemistry of HCP in solid argon.

- Description of differences in photolyses of the methylpnictines CH_3PH_2, CH_3AsH_2, and CH_3SbH_2. How do these compare to methylamine, CH_3NH_2? Spectroscopic characterization of the respective photoproducts.
- Finding whether the ethynylstibinidene, HCCSb, can be obtained in a rare gas matrix following the photodehydrogenation route already explored for ethynylarsinidene, HCCAs, and ethynylphosphinidene, HCCP. If successful, spectroscopic (IR and UV/Vis absorption) characterization of HCCSb, as well as the search for electronic luminescence of HCCSb, HCCAs, and HCCP.
- Attempt to obtain phosphabutadiyne, HC_3P, by photodehydrogenation of a suitable precursor (reported spectroscopy of HC_3P being limited to the radio frequency range). If successful, spectroscopic characterization of this phosphorous-bearing analogue of cyanoacetylene.

1.7. The choice of precursor molecules

Precursors for the envisaged products of photochemical reactions, listed in the right column of **Table 1-2**, have been chosen based on the results of earlier matrix-isolation spectroscopic investigations carried out at the Institute of Physical Chemistry, PAS. These concerned the *in-situ* photochemical formation of HCCP via elimination of an H_2 molecule (or two hydrogen atoms) from either CH_3CP or $HCCPH_2$ (Lawzer et al., 2021). Additionally, the feasibility of double dehydrogenation was demonstrated e.g. by Mutunga & Anderson (2015) who found HCN as the product of matrix-isolated methylamine (CH_3NH_2,) photolysis.

Table 1-2. Precursors and plausible photoproducts

Precursors	Photoproducts
CH_3-XH_2 (methylpnictines), X standing for P, As, or Sb	Dehydrogenated: CH_2=XH, H-C≡X, •C≡X Isomeric: CH_2=XH_3 Originating in C-X cleavage: CH_4, •CH_3, CH_2, •CH, C, XH_3, •XH_2, XH, $X_{elemental}$
H-C≡C-SbH_2 (ethynylstibine)	Dehydrogenated, e.g.: H-C≡C-Sb, •CCSb Isomeric: CH_3-C≡Sb, CH_2=C(H)-Sb, CH_2=C=Sb-H Originating in C-Sb cleavage: C_2H_2, •C_2H, C_2, SbH_3, •SbH_2, SbH, $Sb_{elemental}$,
CH_2=C=CH-PH_2 (propadienylphosphine)	Dehydrogenated: H-C≡C-C≡P, CH_2=C(H)-C≡P, •C≡C-C≡P Isomeric: C_3H_5P species, e.g. CH_3-CH_2-C≡P Originating in C-P cleavage: CH_2=C=CH_2, CH_2=C=CH•, PH_3, •PH_2, PH, $P_{elemental}$ Originating in C-C cleavage, e.g.: CH_4, •CH_3, CH_2, •CH, H-C≡C-H, CH_2=CH_2, H-C≡C-P, H-C≡P, •C≡P

Chapter 2

Materials, tools, and procedures

2. Materials, tools, and procedures

2.1. Chemicals

Compounds listed in **Table 2-1** were synthesized by Prof. Jean-Claude Guillemin in the framework of collaboration between the Ecole Nationale Supériere de Chimie de Rennes (France) and IPC PAS. Most of these were stable at -60 ºC for at least several months. Ethynylstibine, however, had to be stored at the temperature of liquid N_2.

Table 2-1. Molecules - precursors of photochemical reactions isolated in cryogenic matrices in the course of this doctoral work.

Chemical compound	Name used in the Thesis
H-C≡P	phosphaethyne
$CHCl_2$-PH_2	α,α'-dicholromethylphosphine
CH_3-PH_2	methylphosphine
CH_3-AsH_2	methylarsine
CH_3-SbH_2	methylstibine
CD_3-SbH_2	deuterated methylstibine
H-C≡C-SbH_2	ethynylstibine
CH_2=CH-AsH_2	vinylarsine
CH_2=C=CH-PH_2	propadienylphosphine

The phosphaethyne (HCP) case was special. This extremely unstable substance had to be prepared before each experiment. The reaction involved elimination of two HCl molecules from α,α'-dichloromethylphosphine ($CHCl_2$-PH_2) with the help of a strong Lewis base, namely *DBU* (1,8-diazabicyclo[5.4.0]undec-7-ene), see **Scheme 2-1**. Dichloromethylphosphine, obtained from dichloromethylphosphonate by J.-C. Guillemin (the procedure has been reported; Mó et al., 2002) could be stored at -60 ºC, either in pure form or diluted in *diglyme* (diethylene glycol dibutyl ether). HCl elimination from $CHCl_2$-PH_2 was the critical step, optimized at IPC PAS. **Figure 2-1** illustrates the adopted setup, the main components of which include a 100 ml three-necked round-bottom flask, a U-shaped cold trap and a rotary pump. After the evacuation to 10^{-2} mbar, argon was introduced to the setup. The flask was filled with 40 ml of diglyme and 0.8 g of DBU, the solution was then purified from volatile contaminants by the triple application of the freeze-pump-thaw

procedure. Consequently, the flask was cooled down to -65 °C and dichloromethylphosphine (0.2 g), kept separately at -50 °C, was slowly added. The reaction is vigorous and exothermic. Once it was finished, the mixture was frozen using liq. N_2 and argon was pumped off. Then the flask was gradually warmed. After passing through a U-shaped trap maintained at -110°C (to remove the impurities less volatile than HCP), the final product was released to the metal manifold, where a standard gas mixture with Ar could be prepared for the matrix-isolation experiment.

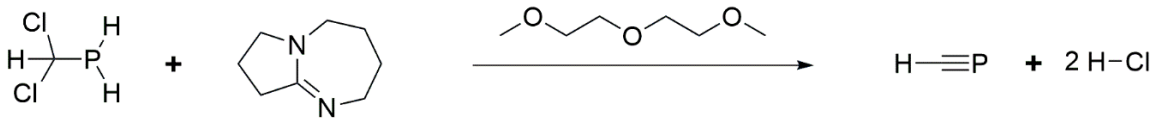

Scheme 2-1. Synthesis of HCP from α,α'-dichloromethylphosphine and DBU dissolved in diglyme.

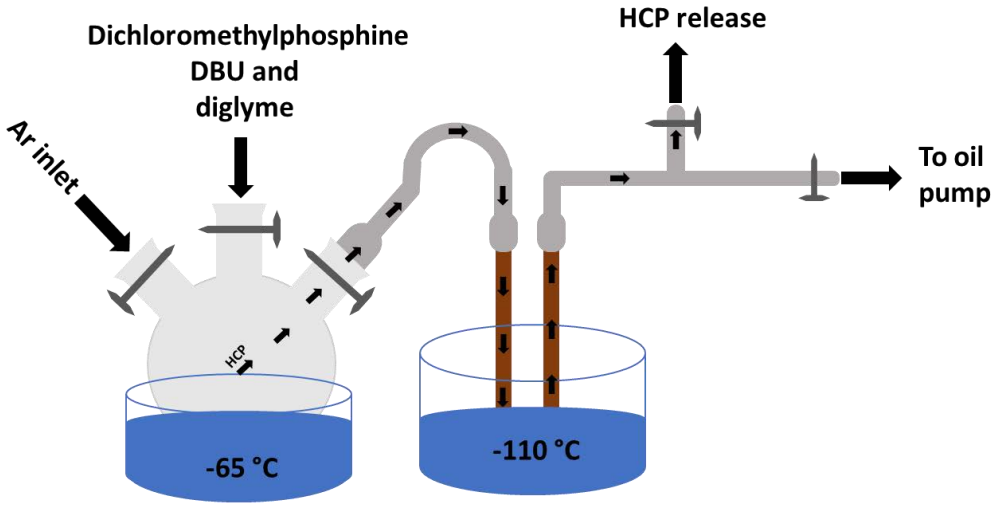

Figure 2-1.Schematic diagram of the HCP synthesis setup.

2.2. Preparation of cryogenic samples

Gas mixtures consisting of the molecules of interest (which usually served as the precursors of photochemical reactions) and of the host atoms (typically, 5.0-grade argon supplied by Multax was used) were prepared in a stainless-steel manifold (see **Figure 2-2**) before each matrix-isolation experiment. The manifold was previously evacuated to the pressure of not more than 2×10^{-6} mbar and the compound to be studied was purified using the *freeze-pump-thaw* procedure (a several times applied sequence involving solidification at 77 K, pumping, and warming up to the room temperature). Two MKS Baratron capacitance manometers (0–10 mbar, model 22-HA-00010BB,

and 1–1000 mbar, model 627BX13TOC1B) allowed to obtain the desired molar guest-to-host ratios (1:1000 or 1:500, most often). Once the mixture was ready, its flow towards the cryostat (on the order of 50 to 100 μmol/min) was regulated with a Granville-Phillips microleak valve. Inside the cryostat (closed cycle two-stage helium refrigerator; Advanced Research Systems model DE-202SE, ultimate temp. 6 K; see the **Appendix 9.1** for more technical details), after exiting the gas nozzle, the mixture was solidified onto a cold target window made of either caesium iodide or sapphire crystals (see the **Appendix 9.2** for the relevant transparency ranges). Temperature of the target window holder was measured with a silicon diode and regulated with a Lake Shore model 325 controller. Pumping station (serving both the cryostat and the gas manifold) comprised a membrane pump and a Pfeiffer Vacuum HIPace 80 turbomolecular pump (60 l/s).

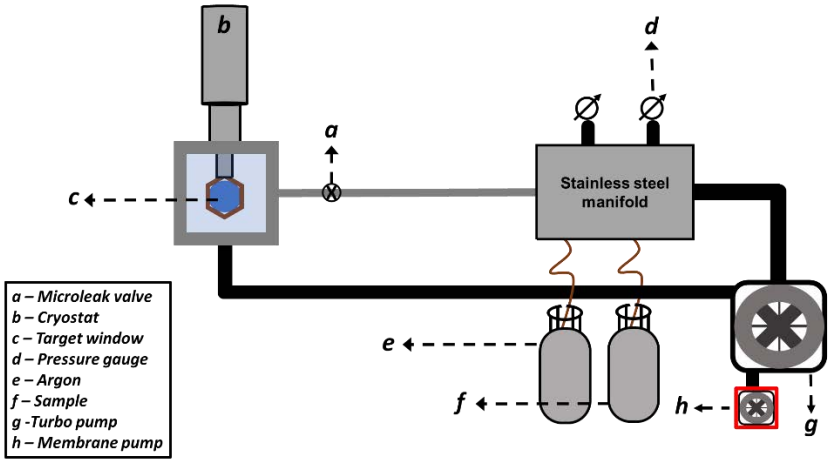

Figure 2-2. A schematic illustration showing the arrangement of the main elements of the matrix isolation setup.

2.3. Photolytic radiation sources

Either one of the two sources was used, depending on the needs of a specific photochemical experiment:

- microwave-driven xenon discharge lamp (Opthos Instrument Company, LLC) providing continuum vacuum-UV radiation (VUV), mostly within the 150-190 nm range;
- low pressure mercury lamp, (Philips UV-C, 11 Watt) dominated by resonance Hg emission at 254 nm.

The VUV lamp could be inserted into the cryostat via one of its side ports; to illuminate the sample directly from the distance of less than 4 cm. Alternatively, it was placed right in front of an external MgF_2 window of the vacuum shroud. The sample surface was typically oriented at 45° angle with respect to the irradiation direction, as shown in **Figure 2-3**. This allowed to monitor the photolysis progress via absorption spectroscopy without touching the experimental setup.

2.4. Spectroscopic measurements

The following instruments were employed for the acquisition of spectroscopic data.

1. **FTIR spectrometer** Vertex 70 (Bruker). Infrared absorption spectra were measured with a KBr beam splitter and a liquid N_2-cooled HgCdTe detector. Spectral resolution was usually set to 0.16 cm^{-1}. CsI-made windows were used both as the matrix substrate and for passing the IR beam through the vacuum shroud of the cryostat.
2. **UV/Vis spectrophotometer** 2401PC (Shimadzu Scientific Instruments). The resolution of 0.5 nm was typically applied. A sapphire window was used as the matrix substrate, external windows of the cryostat shroud (transmitting the UV/Vis beam) were made of quartz.
3. **Luminescence spectroscopy**

   Setup 1: Dispersed luminescence and luminescence excitation spectra of the CP radical were registered with an FS900CDT spectrofluorimeter (Edinburgh Instruments) equipped with an R955 photomultiplier (Hamamatsu) and a photon-counting system sensitive up to 800 nm. Wavelength calibration errors did not exceed 0.1 nm, the slit width used in the current experiments provided a resolution of 0.5 nm. A UV filter GG-13 placed before the detection-arm monochromator filtered out the excitation light. Vacuum shroud of the cryostat was fitted with two quartz windows set at right angles to each other (for the excitation and detection of luminescence) and with an MgF_2 window for the photolytic radiation. A sapphire window was used as the matrix substrate in all luminescence measurements (including those carried out with the setups described below).

   Setup 2: Luminescence was measured using an Omni-λ 300 spectrograph (Gilden, 600 grooves/mm grating) working in tandem with a gated CCD camera (Andor iStar DH734). An optical parametric oscillator (OPO; Opotek Radiant 355) featuring the tuning range of 210–2500 nm, 5 ns pulse width, and 10 Hz repetition rate was used as the excitation source. A digital delay generator DG535 (Stanford Research) triggered OPO and the CCD camera, while a fast oscilloscope (Yokogawa, DL9140) was used to verify the timing. Luminescence of ethynylstibinidene and ethynylarsinidene was investigated with this setup.

   Setup 3: Luminescence, excited with the focused radiation of a light-emitting diode (peak intensity at 340 nm, bandwidth of approx. 20 nm) and collected with a lens, was fed via an optical fibre, either (i) to an Omni-λ 300 spectrograph (Gilden, 600 grooves/mm grating) working in tandem with an Andor iStar DH734 camera or (ii) to a compact spectrograph (Mightex Systems; spectral resolution of approx. 1 nm) equipped with a CCD matrix detector and a fixed grating.

Setup 4: (*Setup 3 modified for the needs of phosphorescence lifetime measurements*). Phosphorescence spectra dispersed with an Omni-λ spectrograph and detected with the Andor iStar camera were recorded at various delay times (gate pulse width of 10 ms and step of 10 ms) with respect to the shut-off of the 340 nm LED used for the excitation. Alternatively, undispersed phosphorescence was collected with a cooled photomultiplier (Hamamatsu R955), the output of which was recorded by a digital oscilloscope (Lecroy WaveAce 2032).

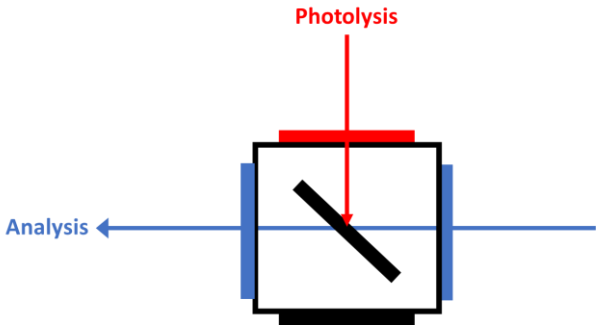

Figure 2-3. Schematic cross-section showing the analyzing beam of an FTIR spectrometer (or UV/Vis spectrophotometer) and the photolyzing UV beam, both incident on the sample inside the cryostat. The outer windows of the cryostat are matched to the wavelength ranges of both beams.

2.5. Quantum chemical calculations

Geometry optimization, as well as electronic energy and vibrational frequency predictions were accomplished making use of density functional theory, as implemented in Gaussian 16 Revision B.01 suite of programs (Frisch et al. 2016). B3LYP functional was combined with either aug-cc-pVTZ (for P- and As-containing molecules; Dunning 1989; Kendall et al. 1992) or def2-TZVP (for Sb-containing ones; Weigend 2006; Weigend & Ahlrichs 2005) as the basis sets. Avogadro and ChimeraX software (Goddard et al. 2018; Meng et al. 2023; Pettersen et al. 2021) were used to visualize the vibrational modes. More advanced ab initio calculations cited in the Thesis, pertaining to the excited electronic states of HCCAs and HCCSb, were accomplished by Dr. Marcin Gronowski (Lawzer et al., 2023).

Chapter 3

Phosphaethyne (HCP) and phosphaethynyl radical (CP)

3 Phosphaethyne (HCP) and phosphaethynyl radical (CP)

3.1 HCP - a literature overview

The spectroscopy of gas-phase phosphaethyne (HCP), the simplest phosphalkyne, has been thoroughly studied despite the low kinetic stability of this compound. It was originally generated by discharging phosphine (PH_3) between graphite electrodes and detected with mass spectrometry and infrared absorption spectroscopy (Gier, 1961). The microwave spectroscopy of HCP and its isotopologues DCP, $H^{13}CP$ and $D^{13}CP$ was subsequently investigated (Tyler, 1964). Both an IR spectrum (Johns et al. 1969) and UV absorption spectrum of HCP and DCP were also measured, revealing rovibrational transitions for ν_1, ν_2, $2\nu_2$, and ν_3 as well as energies of seven excited electronic states. More precise measurements of rovibrational bands and the associated spectroscopic constants were subsequently carried out (Cabana et al., 1982; Garneau & Cabana, 1978, 1980). Numerous studies have been aimed at the description of these states (Hartford et al., 1972; Hartford et al., 1973; Ishikawa et al., 1997; Ishikawa, et al., 1999; 1999a; 1999b; Lehmann et al., 1985; Mason & Lehmann, 1993; Moehlmann et al., 1972; Namai et al., 2009). The ionisation potentials of HCP are 10.79 ± 0.01 eV ($X^2\Pi$) and 12.86 ± 0.01 eV ($A^2\Sigma$), as found with photoelectron spectroscopy (Frost et al., 1973).

Apart from gas-phase discharges, HCP can be produced through pyrolysis (at ~1000 °C) from methyldichlorophosphine (Hopkinson et al., 1976a). The gas-phase Raman spectrum was measured following such a pyrolytic generation (Kalasinsky & Pechsiri, 1985). The procedure was subsequently modified by introducing two cold traps following the pyrolysis oven (Chen et al., 1990). The first of these traps contained KOH maintained at 200 K to remove HCl and other impurities while a trap at 77 K collected HCP. The same research group later reported stimulated emission pumping spectra of vibrationally excited HCP, and the high-resolution Fourier transform rovibrational spectrum (Ishikawa et al., 1996, 1997; Jung et al., 1997). The procedure for production of HCP was slightly modified in the study by Jung et al. by using triazine as a base for HCl removal rather than KOH. For rotational (millimetre-wave) spectroscopy, HCP was generated by pyrolyzing a gaseous mixture of chloroform and PH_3 (Bizzocchi et al., 2005).

Numerous quantum chemical studies have explored the spectroscopic properties of HCP (Beck et al., 2000; Botschwina et al., 1975; Bredenbeck et al., 2000; Farantos et al., 1996; Jacobson & Child, 2001; Joyeux, 1998; Joyeux et al., 1998; Koput, 1996; Koput & Carter, 1997; Lehmann et al., 1985; Nanbu et al., 2000; Peterson & Woods, 1989). Several theoretical investigations were devoted to intermolecular complexes, dimers, and trimers of HCP (Craw & de Almeida, 1991;

Hammami et al., 2008; Hofmann et al., 1999; Höltzl et al., 2006; Kollman et al., 1975; Lucas et al., 2008; Nguyen et al., 1993; Slanina, 1992; Slanina et al., 1992). Recently, an HCl:HCP complex arising from the photolysis of 1-chlorophosphaethene (CH_2PCl) or dichloromethylphosphine (CH_3PCl_2) in solid argon was reported (Jiang et al., 2023); HCP behaved there as a hydrogen bond acceptor.

HCP is considered to be a prebiotic molecule. Its presence in the protoplanetary nebula CRL 2688, in the envelope of the evolved carbon star IRC +10216 (Agúndez et al., 2007; Milam et al., 2008), as well as in diffuse and translucent interstellar medium (Chantzos et al., 2020) has been confirmed. To the best of Author's knowledge, the photochemistry of HCP has not yet been studied. This chapter is devoted mostly to the application of cryogenically isolated HCP as a photochemical precursor for CP radicals and to the spectroscopy of CP.

3.2 Infrared spectroscopy of HCP isolated in solid argon

Although the infrared spectrum of HCP has been thoroughly studied in the gas phase, no published reports pertain to pure HCP isolated in a rare gas matrix. Pyrolysis experiments of Jiang et al. (2023) produced a matrix-isolated mixture of HCP and HCl, but the concentration of free HCP was low compared to that of the H-bonded species HCP:HCl. Two fundamental bands of uncomplexed HCP were, however, reported. In the current study, following the preparative synthesis (see the details provided in **Section 2.1**), practically pure HCP, containing only small amounts of residual water, was isolated in an argon matrix.

The resultant fundamental vibrational frequencies of HCP are listed in **Table 3-1**, and compared with literature values. Some differences can be noted. For instance, the CH bending mode of HCP was previously reported as a single sharp peak at 672.9 cm^{-1} (Jiang et al., 2023). In the current study, three distinct peaks: at 672.8, 676.6, and 688.0 cm^{-1} are observed. **Figure 3-1** illustrates the splitting observed in the infrared bands of HCP. It may arise from dissimilar microenvironments (matrix "sites") around the trapped molecules. While only two IR bands of matrix-isolated HCP (representing CH bending and CH stretching fundamental vibrations) were previously reported (Jiang et al., 2023), this study reveals all fundamentals and an overtone band assigned with the aid of available gas-phase values.

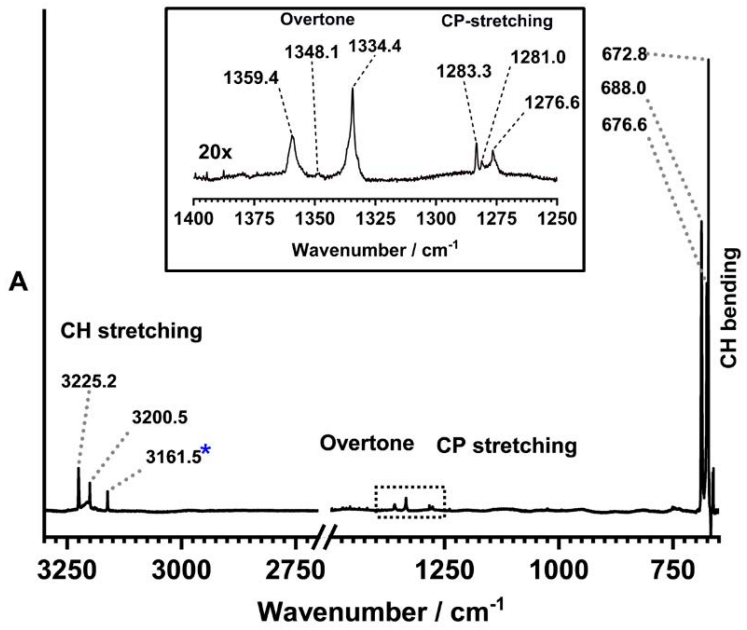

Figure 3-1. Infrared spectrum of HCP isolated in solid argon. Figure 3-2 suggests a correlation between the asterisked band intensity and the content of water (present as an impurity).

A sharp and distinct infrared feature appears at 3161.5 cm^{-1} (marked with an asterisk in **Figure 3-1**). Given its large shift from the identified C-H stretching bands of HCP (cf. **Table 3-2**), its origin is unlikely to be from a matrix site. Further experiments and detailed analysis indicated that the feature was not correlated with HCP. Atmospheric impurities such as water and carbon dioxide are common in matrix-isolation experiments. As shown in **Figure 3-2**, the peak at 3161.5 cm^{-1} is most probably related to water molecules contained in the sample.

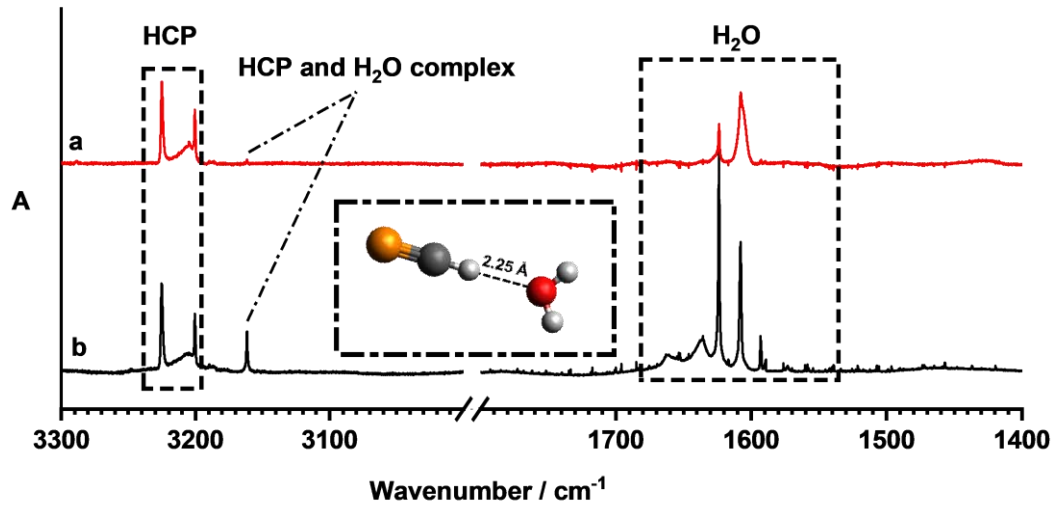

Figure 3-2. Infrared spectra for similar concentrations of HCP in solid argon, but different content of matrix-isolated water (low in **a**, high in **b**). The C_{2v} geometry of a DFT-predicted HCP:H_2O complex is shown in the inset.

Table 3-1. Measured infrared absorption band frequencies (cm^{-1}) of HCP along with values reported in the literature.

Mode	Literature		This work (Ar, 5 K)
	Gas phase (Cabana et al., 1982)	**In solid Ar** (Jiang et al., 2023)	
ν_1	3216.88952	3200.5	3225.2
			3201.0
$2\nu_2$	1355.16	-	1359.4
			1348.1
			1334.4
ν_3	1278.2798	-	1283.3
			1281.0
			1276.6
ν_2	674.6999	672.9	688.0
			676.6
			672.8

Table 3-2. B3LYP/aug-cc-pvTZ prediction for IR transitions of HCP, H_2O, and the intermolecular complex HCP:H_2O.

Mode	Theory				In solid Ar Frequency / cm^{-1}			
	Free H_2O freq. in cm^{-1} (absolute intensity in km/mol)	**Free HCP freq. in cm^{-1} (absolute intensity in km/mol)**	**H_2O: HCP complex freq. in cm^{-1} (absolute intensity in km/mol)**	**Complex-monomer frequency shift in cm^{-1}**	**Complex-monomer frequency shift in cm^{-1}**	**Free H_2O [a]**	**Free HCP**	**HCP-H_2O complex (this work)**
H-O-H asymmetric stretching (H_2O)	3743 (63)		3744 (74)	-1	-	-	-	-
H-O-H symmetric stretching (H_2O)	3644 (4.6)		3646 (10)	-2	-	-	-	-
C-H stretching (HCP)		3216 (77)	3165 (162)	51	63.7	-	3225.2	3161.5 (s)
					39	-	3200.5	
H-O-H scissoring (H_2O)	1562 (76)		1564 (72)	-2	-	1625 1608	-	-
C-P stretching (HCP)		1285 (0)	1279 (7)	6	-	-	1283.3	-
					-	-	1281.0	
					-	-	1276.6	
C-H in-plane bending (HCP)			768 (75)	-84	-64	-	688.0	752 (w)
C-H out-of-plane bending (HCP)		684 (77)	750.7 (69)	-66.7	-71.4	-	676.6	748 (w)
					-75.2		672.8	

a) Based on Table 4 of Forney et al. (1993).

DFT calculations predict that H_2O and HCP form a stable intermolecular complex (see the inset in **Figure 3-2**) with a strong IR band at 3165 cm^{-1} (**Table 3-2**). HCP acts there as a hydrogen

donor. Because of the complexation, its C-H bond becomes weaker and therefore the respective vibrational frequency decreases (for free HCP, the C-H stretching appears at 3200.5 and 3225.2 cm^{-1}). These calculations, together with our IR measurements, offer strong support for the assignment of the observed 3161.5 cm^{-1} band to the HCP:H_2O complex. IR features of the complex located in the "water region" of the spectrum are hard to discern due to their low intensities, small complexation-induced shifts, and the presence of water oligomers.

3.3 Photochemical generation of CP radical from HCP

3.3.1 Photochemistry of HCP

The photolysis of matrix-isolated HCP was conducted using broadband (150 – 190 nm) radiation generated by a xenon microwave discharge lamp. Photochemical changes were monitored over time with FT-IR spectroscopy. The decomposition of HCP was evident, but the IR spectrum did not show any vibrational bands of photoproducts. Separate experiments were therefore dedicated to the study of UV/Vis absorption. A clear vibronic progression with a spacing of approx. 800 cm^{-1} was uncovered between 34 000 cm^{-1} and 29 000 cm^{-1} (**Figure 3-3**) and assigned to CP, based on the reported gas-phase fluorescence (Bärwald et al., 1934). The detailed description of this spectrum and its comparison with literature data are given in **Section 3.3.3**. No evidence of CP could be found using IR spectroscopy due to the intrinsic weakness of the respective vibrational transition (DFT-predicted infrared absorption intensity is only 0.9 km/mol).

3.3.2 Phosphaethynyl radical, CP – a literature overview

The CP radical can be viewed as the simplest organophosphorus species. Its first laboratory detection and spectroscopic characterization via electronic fluorescence (Herzberg, 1930) was accomplished when the radical accidentally appeared in experiments aimed at the generation of P_2. Pure phosphorus vapor was discharged in argon, but the contamination from tap grease and sealing wax acted as a source of carbon. Consequently, Herzberg and his collaborators published a detailed interpretation of CP fluorescence detected within the range 2900 – 5000 Å (34 480 - 20 000 cm^{-1}) and provided molecular constants for the ground $X^2\Sigma^+$ and two lowest excited states, namely $B^2\Sigma^+$, $A^2\Pi_i$. They also analyzed the rotational structure within the observed (3,0), (2,0), (0,1), and (0,3) emission bands of the $B^2\Sigma^+$-$X\ ^2\Sigma^+$ system (Bärwald et al., 1934). The 0-0 band of $B^2\Sigma^+$-$A^2\Pi_i$ was

analyzed by Chaudhury & Upadhya (1969). Following this work, the 0-0 and 1-1 bands of $B^2\Sigma^+$-$A^2\Pi_i$ system were reinvestigated, leading to more accurate predictions of molecular constants. Further research resulted in more precise measurements. One notable finding was the determination of the spin-splitting constant for the $X\ ^2\Sigma^+$ state of CP which was initially assumed to be negative (Bärwald et al., 1934) but later found to be positive (Tripathi et al., 1981). A near-IR $A^2\Pi_i - X\ ^2\Sigma^+$ fluorescence analogous to the red system of CN was investigated with high-resolution Fourier transform spectroscopy (Ram et al., 1992; Ram & Bernath, 1987). Ground-state rotational levels of CP were studied using microwave spectroscopy, which aided in detecting the radical in astrophysical environments (Saito et al., 1989).

While the ground and excited doublet electronic states of CP have been extensively explored, no experimental evidence of the high-spin electronic states of CP has been found. However, the respective theoretical studies existed. Molecular constants and potential energy curves (PECs) of thirteen electronic states, including three quartets, were predicted using ab initio multi-reference single and double-excitation (MRD-CI) calculations (Gu et al., 1994). Gu et al. also computed the energies of the first five vibrational levels for the six lowest electronic states of CP (among them the quartets). Another theoretical study employed the complete active space self-consistent field (CASSCF) method followed by the multi-reference configuration interaction (MRCI) approach with Davidson correction (MRCI+Q) to predict spectroscopic parameters (including spin-orbital coupling constants) and PECs for various doublet, quartet and sextet electronic states (Shi et al., 2012). The coupled cluster approach and MRCI along with large basis sets (up to aug-cc-pV5Z and complete basis set exploration) supplied even more accurate predictions of spectroscopic parameters for the doublet, quartet, and sextet states (Abbiche et al., 2014). The ab initio valence internally contracted multireference configuration interaction (icMRCI) method, which incorporates Davidson correction, core-valence and scalar relativistic corrections, and basis-set extrapolation, has also been applied to investigate the PECs and spectroscopic parameters for as many as sixteen low-lying electronic states (Qin et al., 2019), although spin-orbit coupling effects were not included. More recently, PECs of the electronic states and the associated transition dipole moments (with the inclusion of spin-orbit coupling) were computed using the CASSCF method followed by the icMRCI approach (Zhang & Zhu, 2021). The large basis sets applied for the phosphorus atom were aug-cc-pV(5 + d)Z and aug-cc-pV(6 + d)Z, and for the carbon atom aug-cc-pV5Z and aug-cc-pV6Z.

With calculations describing the high-spin states of CP, but no experiments showing their existence, there was an important gap in the spectroscopic description of these diatomic radicals.

3.3.3 Electronic absorption spectroscopy of CP

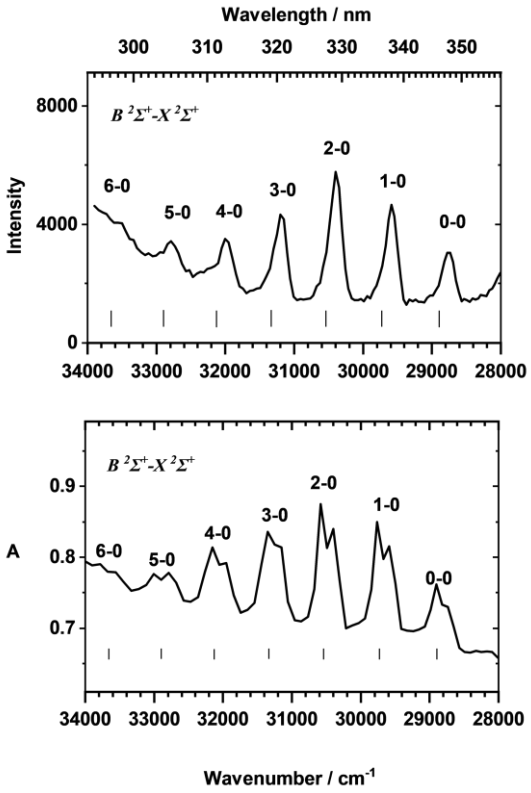

Figure 3-3. Bottom panel: UV absorption spectrum of CP in solid argon. **Top panel:** Luminescence excitation spectrum measured by monitoring the intensity of an emission band observed at 560 nm (17 840 cm^{-1})**.** Markings at the bottom of each plot show the gas-phase locations of bands constituting the [v'=n → v"=0] progression in $B^2\Sigma^+$-$X^2\Sigma^+$ fluorescence (Bärwald et al. 1934).

No electronic absorption measurements have been published for CP until the research reported here for matrix isolated CP. Gas-phase fluorescence band frequencies measured for the CP transitions originating from vibrationally excited levels within the excited electronic state (Bärwald et al., 1934) could, however, be used to interpret our UV absorption measurements. These bands are clearly related, with small gas-to-matrix shifts, to the emission bands reported for the [v'=n → v"=0] progression in $B^2\Sigma^+$-$X^2\Sigma^+$ fluorescence of CP (see **Figure 3-3** and **Table 3-3**).

The absorption peaks have double maxima, likely due to the matrix-site splitting. The presence of dissimilar matrix sites was also visible in the infrared spectrum of HCP (**Section 3.2**). Upon annealing the matrix at 20 K, the absorption peaks coalesced into single bands. A discussion of such thermally induced effects is provided in **Section 3.3.5.1**. According to Qin et al. (2019), the $B^2\Sigma^+$-$X^2\Sigma^+$ transition is mostly due to the promotion of an electron from the highest occupied molecular orbital (HOMO) to the lowest unoccupied molecular orbital (LUMO).

Table 3-3: Vibronic transition frequencies (cm^{-1}) for the B $^2\Sigma^+$-X $^2\Sigma^+$ system of CP.

Band (v'-v")	Absorption, solid Ar	Fluorescence, gas phase [a]
0-0	28 900	28 900
1-0	29 760	29 722
2-0	30 580	30 538
3-0	31 350	31 337
4-0	32 150	32 126
5-0	33 000	32 900
6-0	33 790	33 671

a- Values taken from Table 2 of the paper by Bärwald et al. (1934)

3.3.4 Luminescence of CP

3.3.4.1 Preliminary Measurements

The first measurements of CP luminescence in a previously photolyzed Ar:HCP matrix sample were accomplished with a setup comprised of a light-emitting diode (LED), lens, and low-resolution CCD spectrograph (Mightex) fed via an optical fiber (details regarding the setup are given in **Section 2.4**). The LED emitted broadly in the region extending approx. from 320 nm to 360 nm, with a maximum at 340 nm. A lens focused that near-UV radiation onto the sample. The resultant intense bluish-white luminescence, analyzed at a right angle with respect to the excitation beam, revealed the vibronic structure shown in **Figure 3-4**. When the excitation source was blocked, the emission took a sizable fraction of a second to decay, suggesting the presence of phosphorescence (see **Section 3.3.5.2**. for emission lifetime measurements).

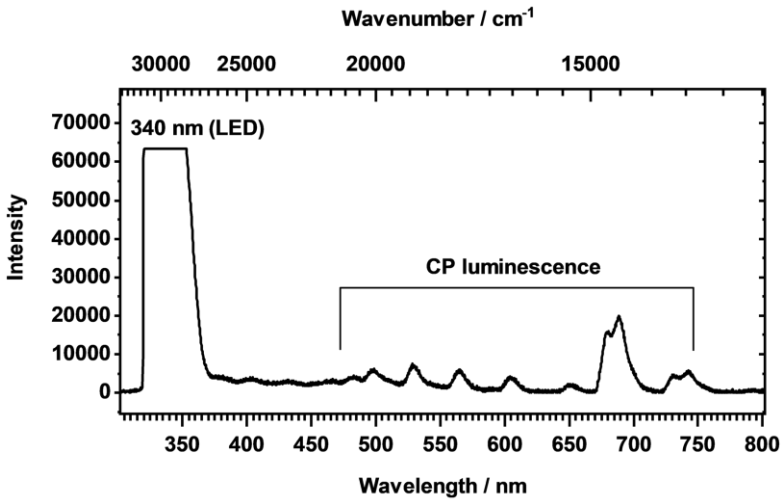

Figure 3-4. Luminescence of CP produced by photolysis of Ar matrix-isolated HCP, as measured with a low-resolution spectrograph. Excitation source: 340 nm LED.

3.3.4.2 Fluorescence of CP

More advanced measurements of dispersed luminescence and luminescence excitation spectra were carried out using an FS900CDT spectrofluorimeter (Edinburgh Instruments, details are given in **Section 2.4**). **Figure 3-5** presents a 3-dimensional map where the intensity of CP radical luminescence is plotted as a function of both emission and excitation wavelengths. Two series of contours marked with yellow-dotted ovals are not due to CP. The diagonal one is due to "ghosts" caused by optical imperfections of the monochromator, while the vertical one, generated by the excitation at 310 nm, comes from an unrecognized impurity (which did not show up in IR or UV/Vis absorption spectra).

Figure 3-6 displays the interpreted fluorescence spectrum of CP. Band positions observed in the current work are close to the previously reported gas-phase values (**Table 3-4**). Two emission systems were detected: $B^2\Sigma^+$- $X^2\Sigma^+$ (ca. 29 000 to 22 500 cm^{-1}) and $B^2\Sigma^+$ - $A^2\Pi_i$ (ca. 22 500 to 19 500 cm^{-1}). The signal-to-noise ratio of their vibronic features presented in **Figure 3-6** is high, with the exception of the *0-0* band of $B^2\Sigma^+$-$A^2\Pi_i$ (see the inset) which is not easily discernible, indicating a low Franck-Condon factor. All detected bands of the $B^2\Sigma^+$- $A^2\Pi_i$ system show double maxima due to the spin-orbit coupling in $A^2\Pi_i$. The reported value of this splitting is 157.87 cm^{-1} (Tripathi et al., 1981), while our measurements give a value of ~150 ± 10 cm^{-1}.

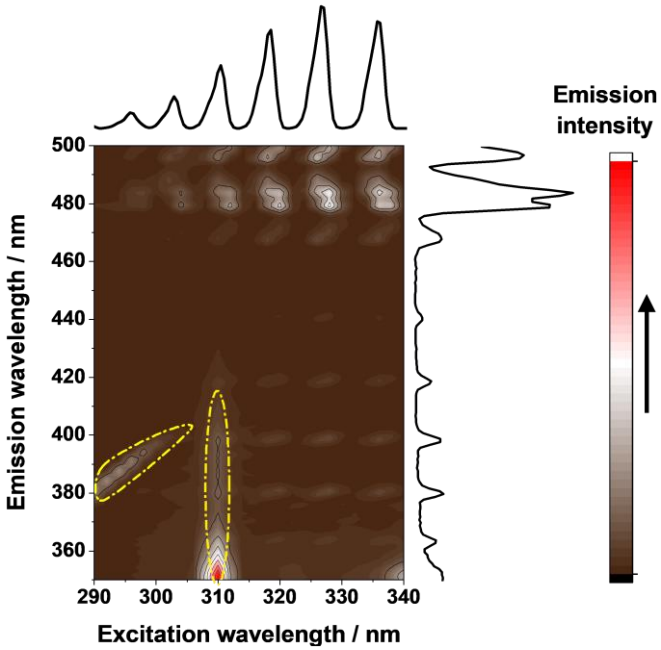

Figure 3-5. Excitation-emission map of luminescence intensity observed for CP radicals photoproduced in solid Ar. Trace at the top represents a fluorescence excitation spectrum obtained by monitoring the emission at 483 nm. Vertical trace represents a dispersed fluorescence spectrum produced by the excitation at 336 nm. See the text for the discussion of spectral features encircled with yellow ovals.

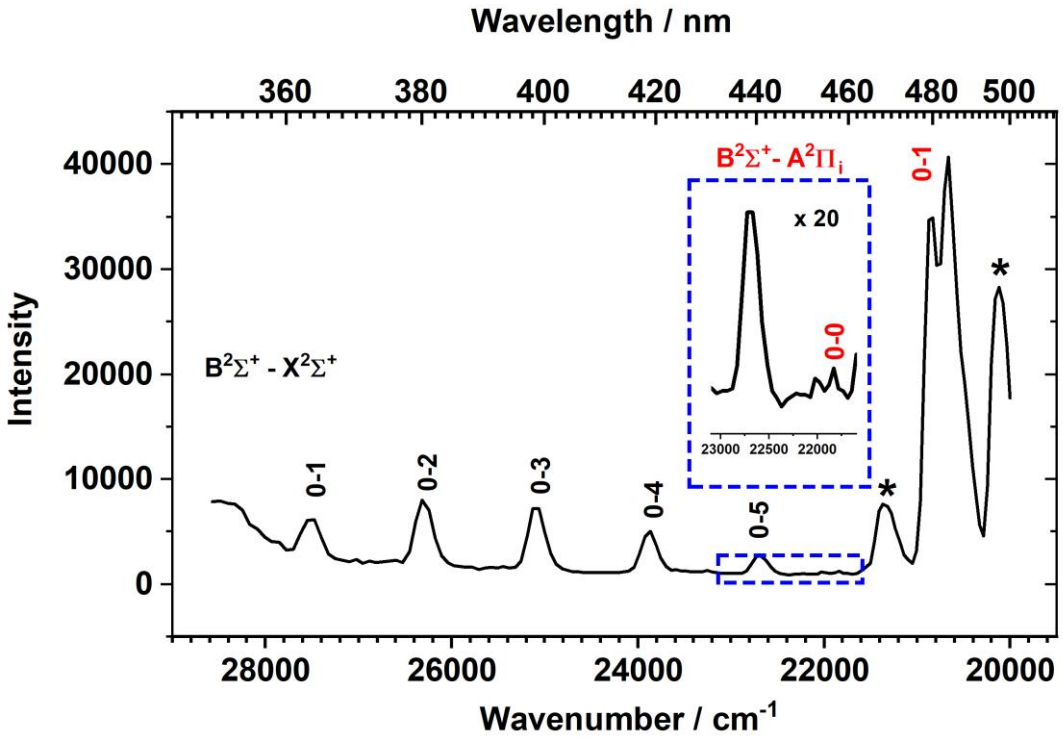

Figure 3-6. Luminescence of CP in solid argon (high frequency region), λ_{exc} = 336 nm. Asterisked bands are due to phosphorescence (see Section 3.3.4.3).

Table 3-4. Wavenumbers of fluorescence bands observed for Ar matrix-isolated CP, compared to the gas-phase values.

Transition	Ar matrix /cm^{-1}	Gas phase [a] / cm^{-1}
$B^2\Sigma^+$ to $X^2\Sigma^+$		
0-0	28 900	28 900
0-1	27 520	27 675
0-2	26 360	26 462
0-3	25 140	25 264
0-4	23 910	24 079
0-5	22 750	--
$B^2\Sigma^+$ to $A^2\Pi_i$		
0-0	22 040 21 870	22 095 21 937
0-1	20 890 20 720	21 046 20 887
0-2	19 850 19 660	--

a - Values taken from Table 2 of the Barwald et al. (1934) paper.

3.3.4.3 Phosphorescence of CP

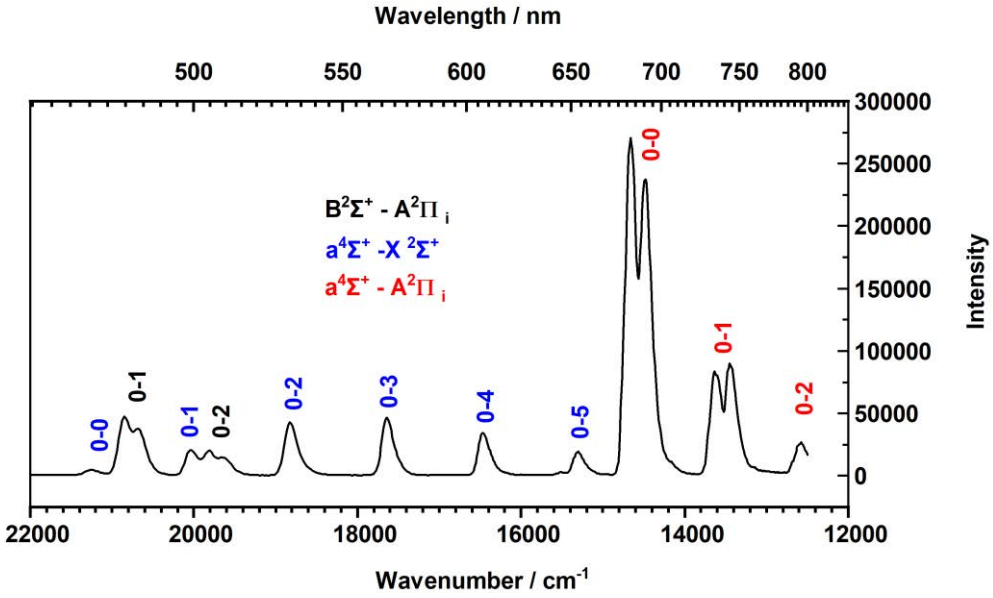

Figure 3-7. Luminescence of CP in solid argon (low frequency region), λ_{exc} = 328 nm (see **Figure 3-8**).

Apart from $B^2\Sigma^+$- $X^2\Sigma^+$ and $B^2\Sigma^+$- $A^2\Pi_i$ fluorescence, a new emission system is observed (**Figure 3-7**) upon exciting CP to its $B^2\Sigma^+$ state. The associated luminescence excitation spectrum (obtained by taking a horizontal cross-section of the map in **Figure 3-8**) shown in the top panel of **Figure 3-3**, matches the excitation pattern of $B^2\Sigma^+$- $X^2\Sigma^+$ fluorescence (**Figure 3-5**). These matching excitation spectra are evidence that the new luminescence can be attributed to CP and not some other species. A vibronic progression starting at 21 430 cm^{-1} and extending down to 15 420 cm^{-1} is currently assigned to the new electronic system: $a^4\Sigma^+$-$X^2\Sigma^+$. Its spacing (1235 cm^{-1} to 1170 cm^{-1}), consistent with that observed in $B^2\Sigma^+$- $X^2\Sigma^+$ fluorescence (cf. **section 3.3.4.2**), reflects the intervals between the vibrational levels of the $X^2\Sigma^+$ state.

Yet another luminescence system, observed at lower energies, i.e. between 15 000 cm^{-1} and 12 000 cm^{-1}, can be identified as $a^4\Sigma^+$ - $A^2\Pi_i$. An intense, sharp emission band marks its origin at 14 490 cm^{-1}. This is in agreement with theory (Zhang & Zhu, 2021) which predicts $a^4\Sigma^+$ and $A^2\Pi_i$ to be separated by 14 600 cm^{-1}. The 0-1 and 0-0 bands of this system are spaced by ~1057 ± 10 cm^{-1} (the reported gas-phase value is 1062.5 cm^{-1}; Ram et al. 1992). Bands of the $a^4\Sigma^+$ - $A^2\Pi_i$ system are doubled, indicative of spin-orbit coupling in the $A^2\Pi_i$ state (the presence of sublevels $A^2\Pi_{1/2}$ and $A^2\Pi_{3/2}$). The magnitude of this splitting is approximately 150 ± 10 cm^{-1}, in harmony with the analogous phenomenon observed in $B^2\Sigma^+$-$A^2\Pi_i$ fluorescence bands (cf. **Section 3.3.4.2**). Frequencies and assignments are summarized in **Table 3-5** for all observed phosphorescence bands.

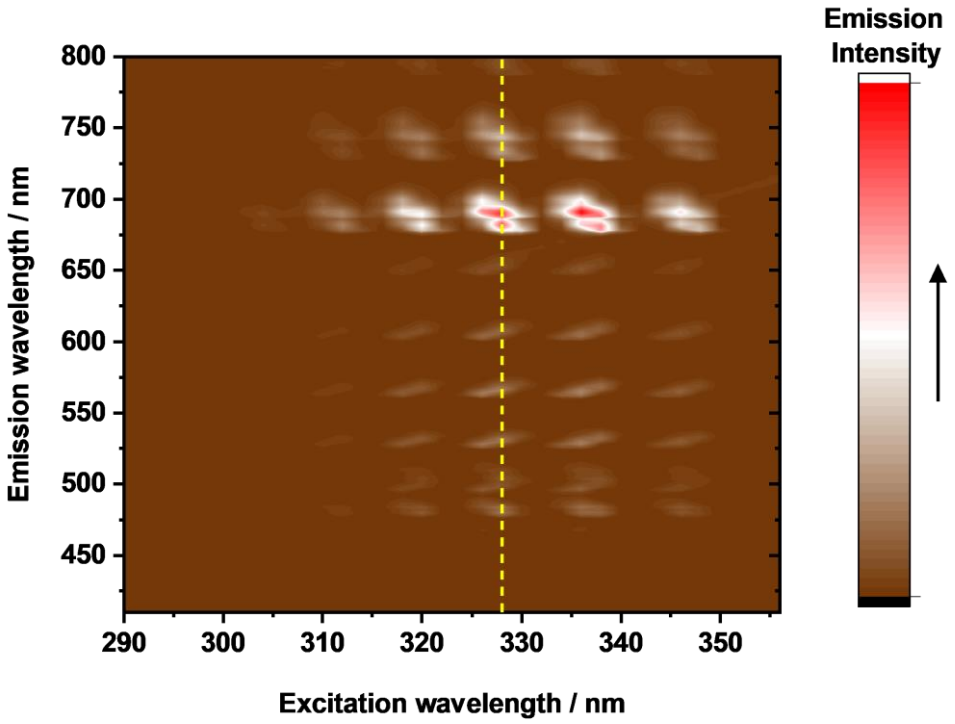

Figure 3-8. Excitation-emission map of luminescence intensity observed for CP radicals photoproduced in solid Ar. Dashed line corresponds to the spectrum depicted in **Figure 3-7.**

Table 3-5. Vibronic band frequencies (cm^{-1}) for the CP radical phosphorescence in solid argon.

Transition	Ar matrix	Vibronic spacing
$a^4\Sigma^+$- X $^2\Sigma^+$		
0-0	21 430	-
0-1	20 195	1235
0-2	18 970	1225
0-3	17 770	1200
0-4	16 590	1180
0-5	15 420	1170
$a^4\Sigma^+$ - $A^2\Pi_i$		
0-0	14 490 14 335	--
0-1	13 445 13 285	1045 1050
0-2	12 560 --	885 --

3.3.5 Why does CP phosphoresce?

For closed-shell molecules, application of Hund's rule (maximization of the total spin) results in triplet multiplicity of the lowest excited state (**Figure 3-9**, case *a*).

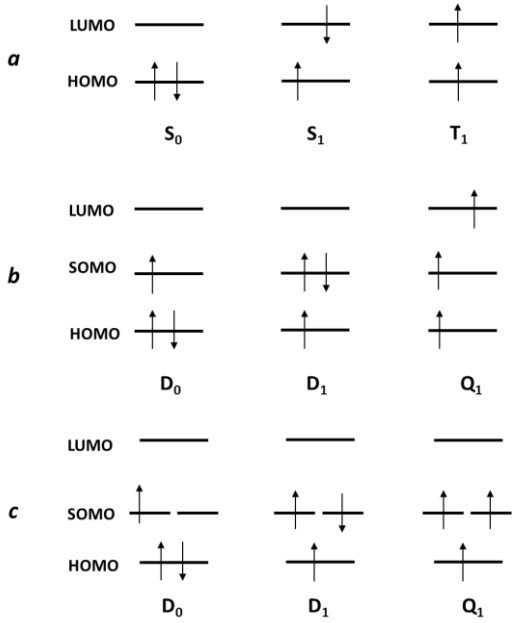

Figure 3-9. Simplified schemes of electronic orbital configurations depicted for: (*a*) the lowest singlet and triplet states of a closed-shell molecule; (*b*) the lowest doublet and quartet states of a free radical; and (*c*) the lowest states of a free radical with a degenerate ground state (e.g. NO). HOMO, SOMO, and LUMO refer to the highest occupied, singly occupied, and lowest unoccupied molecular orbitals, respectively. The Hund's rule (maximization of multiplicity) dictates that the lowest excited electronic state is: T_1 for (*a*), D_1 for (*b*), and Q_1 for (*c*). Typically, the electronic configuration of free radicals is that shown in (*b*).

For radicals, however, a similar pattern i.e. a higher-spin (quartet) state lying below the first exited doublet state is generally not expected and quartet-doublet phosphorescence remains a rare phenomenon. A few exceptions occur for radicals with degenerate ground states (case *c* of **Figure 3-9**), such as NO, BiO (Frosch & Robinson, 1964; Shestakov et al., 1998). The location of the lowest quartet state $a^4\Sigma^+$ of CP has to be typical, i.e. it lies above the lowest excited doublet. Its population via a nonradiative transition from $A^2\Pi_i$ is therefore unlikely. However, theoretical studies (Abbiche et al., 2014; Qin et al., 2019; Zhang & Zhu, 2021) provide a clue as to why CP phosphoresces. The key feature is that the second quartet electronic state $1^4\Delta$ (3.55 eV; 28 600 cm^{-1}) is predicted to lie just below or almost coincident with the second excited doublet $B^2\Sigma^+$ (3.58 eV, 28 900 cm^{-1}) across a broad range of interatomic distances. Such a coincidence likely facilitates sizable ISC from the photoexcited $B^2\Sigma^+$ to the $1^4\Delta$ state, **Figure 3-10**. This is followed by fast IC to the $a^4\Sigma^+$ state. As expected, no luminescence originating directly from $1^4\Delta$ has been observed. Excitation to $B^2\Sigma^+$ resulted in luminescence beginning at 21 430 cm^{-1}, which aligns very well with

the theoretically predicted energy gap (T_e= 21 500 cm^{-1}) between the ground doublet state ($X^2\Sigma^+$) and the lowest quartet state ($a^4\Sigma^+$) of CP (Zhang & Zhu, 2021).

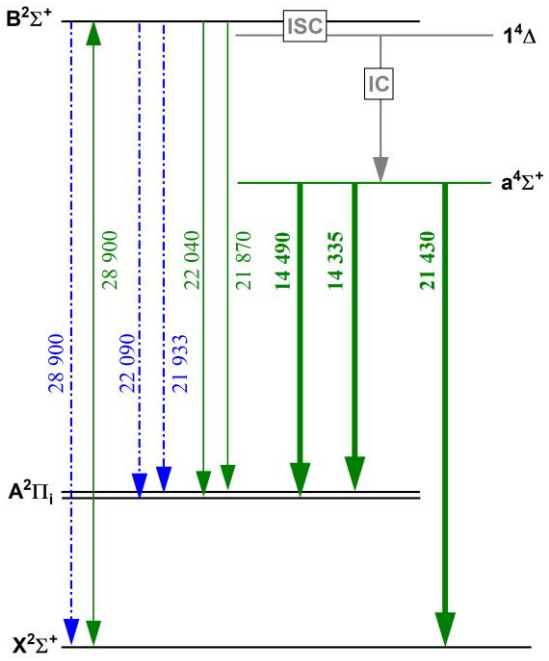

Figure 3-10. Electronic transitions of the CP radical. Numbers provide the system origin frequencies (cm^{-1}). Dashed blue arrows symbolize all gas-phase transitions reported by Bärwald et al. (1934), Ram et al. (2014), and Tripathi et al. (1981). Solid green arrows correspond to the transitions observed here in solid argon (bold denotes phosphorescence). ISC and IC stand for intersystem crossing and internal conversion, respectively.

3.3.5.1 Effect of annealing

As mentioned earlier, double maxima observed in UV absorption and emission bands of CP can be attributed to matrix sites, i.e. to disparate, slightly different microenvironments. This was proven by annealing the matrix. Upon warm-up, the matrix softens, allowing the radicals to occupy a more stable position within their native sites. Following the annealing, the doublet UV absorption peaks of CP coalesced into singlets (**Figure 3-11**). The feature enlarged in **Figure 3-12** is due to the origin band of the $a^4\Sigma^+$-$A^2\Pi_i$ system. As many as four maxima (marked with black dotted circles) can be discerned there because the matrix-induced splitting is accompanied by the doubling caused by the presence of $A^2\Pi_{1/2}$ and $A^2\Pi_{3/2}$ sublevels (**Section 3.3.4.3**). After the annealing, maxima due to one matrix site grew at the expense of another.

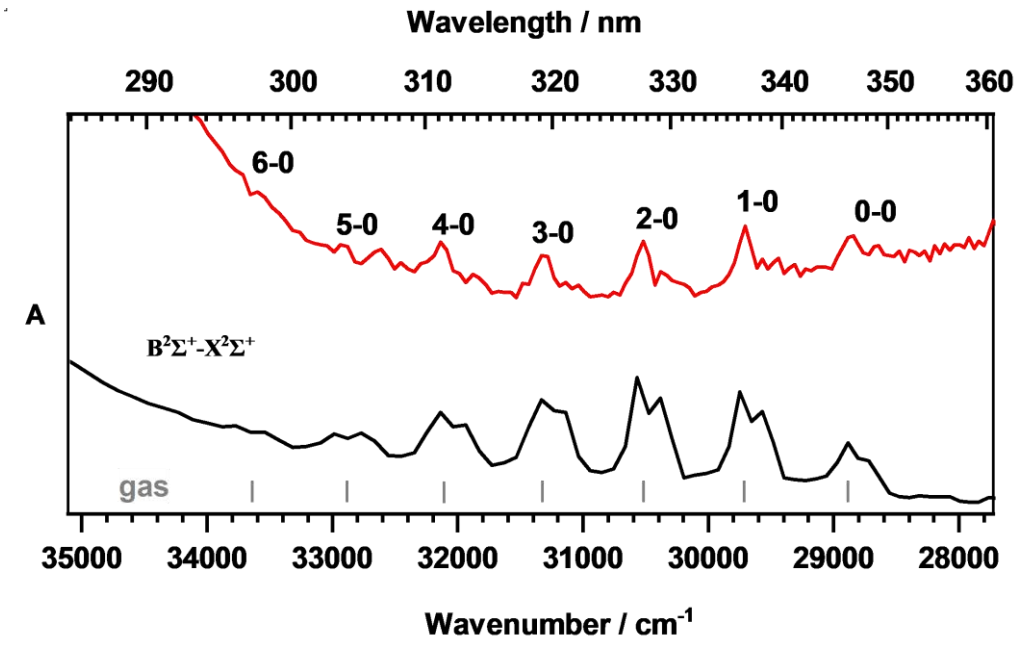

Figure 3-11. UV absorption spectrum of CP radical in solid argon before (**bottom**) and after (**top**) annealing.

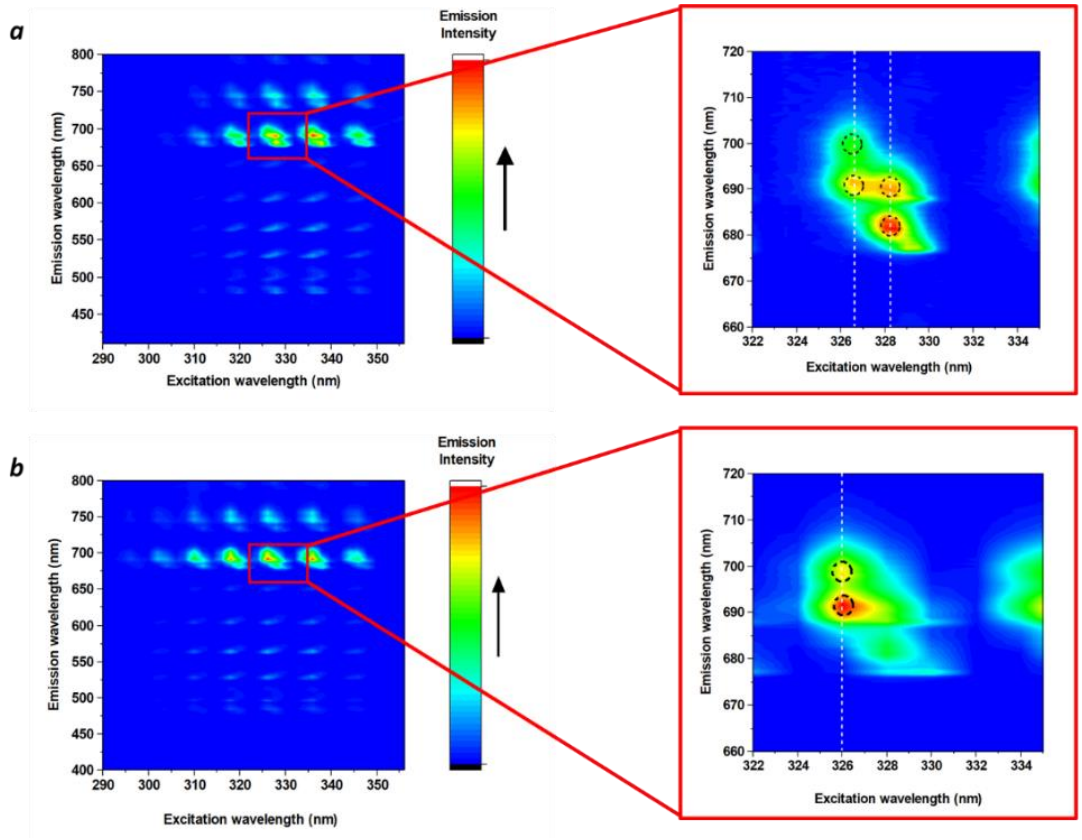

Figure 3-12. Excitation-emission map of luminescence intensity observed for CP radicals photoproduced in solid Ar, as measured (**a**) before annealing and (**b**) after annealing to 20 K. The enlarged fragment corresponds to the origin band of the $a^4\Sigma^+$-$X^2\Sigma^+$ system excited by the (2,0) transition of $B^2\Sigma^+$-$X^2\Sigma^+$.

3.3.5.2 Lifetime of Phosphorescence

Two different methods and detectors were applied to measure the phosphorescence lifetime. One of these involved monitoring the decay of undispersed phosphorescence using a cooled photomultiplier, its output being recorded by an oscilloscope. The second method employed a gated CCD camera coupled to a monochromator for measuring the dispersed emission intensity as a function of time elapsed from switching off the excitation UV light. In both methods, a 340 nm LED was used as the UV source (all details related to the setups are provided in **Section-2.4**). Least square fitting to the traces presented in **Figure 3-13** yields 0.1 s as the monoexponential decay time, independent of the method. Importantly, lifetimes measured for the $a^4\Sigma^+$-$X\ ^2\Sigma^+$ and $a^4\Sigma^+$-$A^2\Pi_i$ transitions were, within the experimental error, the same, as expected for the emissions sharing the same initial state (cf. right panel of **Figure 3-13**).

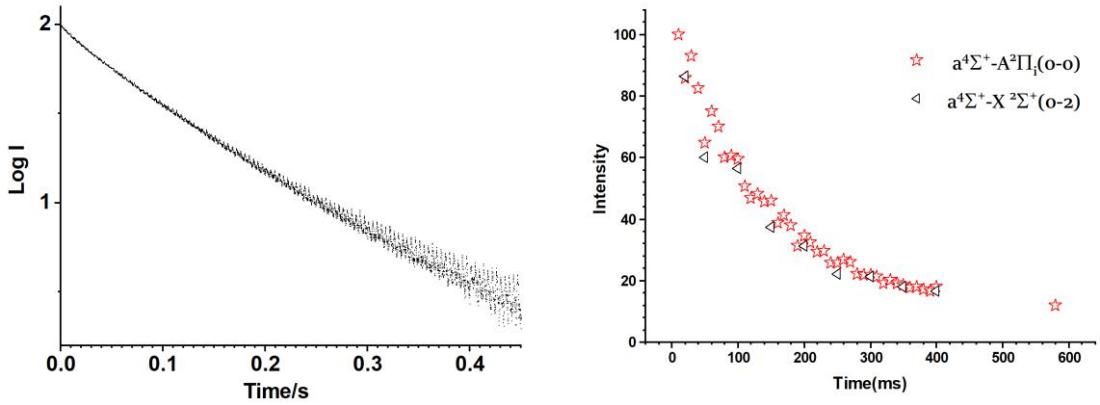

Figure 3-13. Left: phosphorescence decay of undispersed phosphorescence measured with a photomultiplier connected to a digital oscilloscope (logarithm of relative intensity vs. time). **Right:** dispersed phosphorescence intensity (initial value normalized to 100) measured using a monochromator coupled with a CCD camera. Red stars correspond to $a^4\Sigma^+$-$A^2\Pi_i$ and black triangles to $a^4\Sigma^+$-$X\ ^2\Sigma^+$ transitions. Time zero corresponds to switching off the excitation light (340 nm LED).

3.4 Conclusions

HCP, the heavier analogue of hydrogen cyanide, was successfully synthesized and its infrared spectroscopy was studied in solid argon. A spectral signature of the previously unexplored hydrogen bond between HCP and water (present as a trace impurity) was found in IR absorption. UV photolysis of HCP, monitored with both vibrational and electronic spectroscopy, revealed the CP radical as the only detectable product of UV irradiations. This paved the way for spectroscopic investigations of cryogenically isolated CP that had never been possible before. Apart from the $B^2\Sigma^+$—$X^2\Sigma^+$ system detected in absorption, $B^2\Sigma^+$—$X^2\Sigma^+$ and $B^2\Sigma^+$— $A^2\Pi_i$ fluorescence emissions were analyzed. Most importantly, the phosphorescence of CP was discovered. It is shaped by the

new electronic systems: $a^4\Sigma^+$—$X^2\Sigma^+$ and $a^4\Sigma^+$—$A^2\Pi_i$. These unusual cases of quartet–doublet phosphorescence were thoroughly analyzed and published in Angewandte Chemie (Ganesan et al., 2022). A plausible photophysical mechanism (suggested by recent theoretical studies) was proposed.

Chapter 4

Photochemistry of methylpnictines

(CH_3XH_2, X= P, As, Sb)

4. Photochemistry of methylpnictines (CH_3XH_2, X= P, As, Sb)

4.1. Methylpnictines – a literature overview

The photochemistry of gaseous methylamine in the wavelength range 190 - 240 nm has been very well studied. Radical fragments CH_3NH, CH_3, NH_2, and CN along with the closed-shell molecules methane (CH_4), methylene imine (CH_2NH_2), and hydrogen cyanide (HCN) appeared as the irradiation products (Ahn et al., 2008, 2012; Ashfold et al., 1997; Cachón et al., 2023; Epshtein et al., 2015; Gardner & McNesby, 1982; Michael & Noyes, 1963; Nishi et al., 1980; Recio et al., 2023; Reed et al., 1996; Waschewsky et al., 1995). The photo-oxidized species, methylene imine (CH_2=NH), was formed at a very low yield compared to the methylamino radical, CH_3NH (Gardner & McNesby, 1982; Michael & Noyes, 1963). A recent theoretical study suggests that the presence of a conical intersection between the first excited state and the ground state of the [CH_3NH + H] system favors the formation of CH_3NH (Recio et al., 2023). The photochemistry of methylamine at 184.9 nm studied by electron spin resonance spectroscopy also revealed the formation of methylamino radical and proved the hydrogen atom cleavage from the amino group (Hadley & Volman, 1967). In these studies, homolytic cleavage involving H-atom dissociation from methylamine was a major photodissociation pathway while loss of molecular hydrogen was minor (Gardner & McNesby, 1982; Michael & Noyes, 1963; Recio et al., 2023). At higher irradiation energies (147 nm and 123.6 nm), H_2 formation prevailed over the homolytic cleavage (Gardner & McNesby, 1982; Magenheimer et al., 1969). Depending on the irradiation wavelength, H_2 elimination was proposed to happen via two different photochemical routes, i.e. either by the recombination of separately detached H atoms or direct elimination of H_2 from methylamine. These routes were postulated on the basis of experiments with free radical scavengers NO, O_2, and acetylene. In the presence of NO and O_2, the quantum yield of H_2 at 185 nm was close to zero which suggests that H_2 was formed through the recombination of atoms. High-energy VUV radiation (147 or 124 nm) produced hydrogen molecules in significant quantities even when H atom scavengers were present (Gardner & McNesby, 1982), suggesting that H_2 was formed directly from methylamine prior to the appearance of radicals. **Scheme 4-1** summarizes the reported gas-phase photochemical reactions of methylamine.

The photochemistry of methylamine has also been studied in solid parahydrogen at the irradiation wavelength of 193 nm. The major photoproducts were those formed by H_2-elimination

(such as CH_2NH and HCN). The only radical product, tentatively identified, was CH_3NH (Mutunga & Anderson, 2015). The cage effect was proposed as a crucial contributor to this change in the photochemistry of methylamine in solid p-H_2.

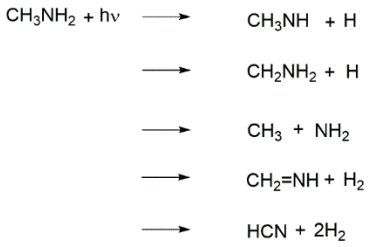

Scheme 4-1. Gas-phase photochemistry of methylamine.

Recently, photochemical investigations on ethynylphosphine, ethynylarsine and ethynylstibine in inert gas matrices revealed UV-induced H_2 elimination leading to triplet pnictinidenes (Lawzer et al., 2021, 2023). Theoretical reports on the H_2-elimination route in methylpnictines are scarce (Viana, 2017; Viana & da Silva, 2014). To the best of Author's knowledge, no experimental studies devoted to photochemistry of either CH_3PH_2, CH_3AsH_2, or CH_3SbH_2 have ever been reported.

Radiation-induced molecular rearrangements are *a priori* likely to occur in a rare gas matrix, one can then possibly expect the appearance of the elusive species $CH_2{=}XH_3$ (X = P, As, Sb). No spectroscopic measurements have been reported for such methylpnictine isomers, even though a neutralization-reionization mass-spectrometric experiment confirmed the existence of $CH_2{=}PH_3$ (Keck et al., 1992).

This work focuses on elucidating the photochemistry of methylphosphine, methylarsine and methylstibine in argon matrices and on the characterization of photolysis products with infrared and UV/Vis spectroscopy.

The expected products fall into two categories:

1. ***Open shell*** - CH_3-XH, CH_2-XH_2, triplet CH_3-X, triplet HC-XH_2, CH_2=X, HC=XH, C≡X, H
2. ***Closed shell*** - $CH_2{=}XH_3$, CH_2XH, singlet CH_3-X, singlet HC-XH_2, HC≡X, H_2.

For some of these, neither experimentally measured nor theoretically predicted spectroscopic characteristics could be found in the literature. For phosphorous- and arsenic-bearing molecules, DFT computations of molecular geometry, electronic energy and vibrational frequencies made use of the B3LYP functional with the aug-cc-pVTZ basis set. For the derivatives of antimony, the Karlsruhe basis set, def2-TZVP was better suited for the calculation. The results of these calculations are collected in the **Table 9-2**, **Table 9-4** and **Table 9-6**.

4.2. Methylphosphine

4.2.1. Spectroscopy of methylphosphine

All methylpnictines are C_s point group molecules with 15 fundamental modes of vibration. Among these modes, 9 belong to the A' and 6 to the A" representation (A' and A" refer to the symmetric and antisymmetric behavior with respect to reflection through a mirror plane). IR bands due to diverse vibrational modes of methylphosphine are shown in **Figure 4-1**. All these, together with the combination and overtone bands (not shown in the Figure), are listed in **Table 4-3**. A weak, broad band at 941.3 cm^{-1}, not reported previously, is tentatively assigned to the combination band $\nu_8+\nu_{15}$.

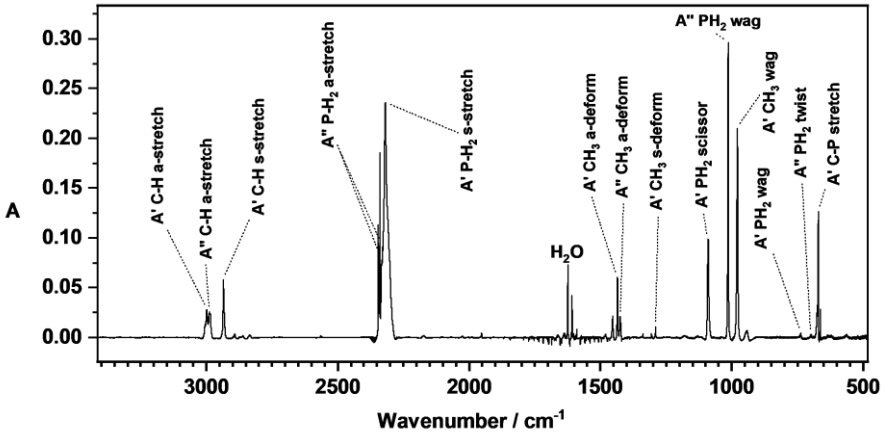

Figure 4-1. IR absorption spectrum of methylphosphine isolated in a cryogenic argon matrix (guest-to-host molar ratio of 1:1000).

Prior to the current work, the only available electronic absorption spectrum of methylphosphine was the one reported by Halmann (1963). Our own measurement of Ar matrix isolated methylphosphine is shown in (**Figure 4-2**), nominally corrected for strong scattering by crystalline Ar. Neither our spectrum nor that of Halmann (1963) provide evidence for UV transitions in the vicinity of 254 nm. Nevertheless, resonance Hg radiation produces a photolytic effect, indicating UV light absorption. This might be due to a band centered in the gas phase at 202 nm and red-shifted by the matrix (TD-DFT calculations, pertaining to gaseous molecules, point to a weak electronic transition in the vicinity of 220 nm (5.7 eV), oscillator strength 0.04; see **Table 4-1**).

Table 4-1. Theoretically predicted (TD-B3LYP/aug-cc-pVTZ) vertical excitation energies (eV) and oscillator strength values for the lowest electronic transitions of methylphosphine, CH_3PH_2.

Energy of excitation from the ground state	Oscillator strength
5.66	0.04
6.18	0.07
6.65	0.03

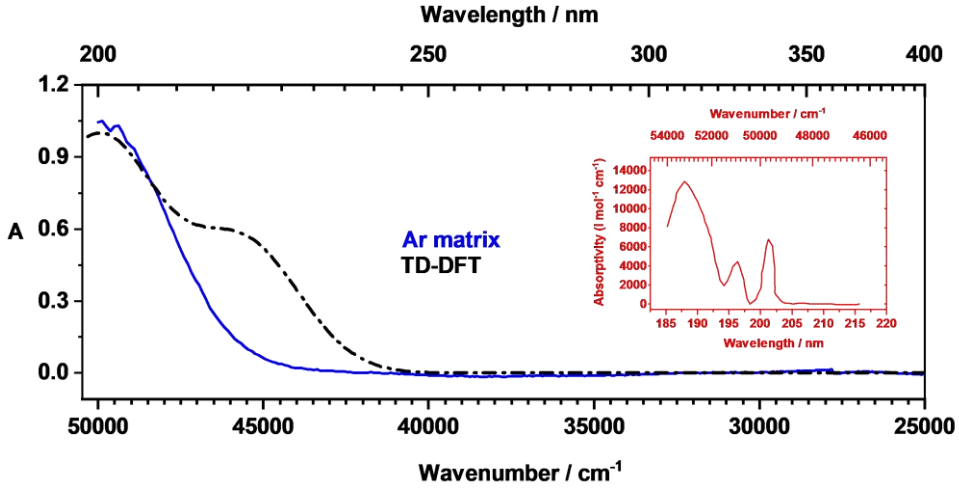

Figure 4-2. Experimental and TD-DFT-predicted UV absorption spectra of methylphosphine. The theoretical spectrum is broadened by convoluting with a Gaussian function, FWHM = 4033 cm^{-1} (0.5 eV) (for illustrative purposes only). Experimental data are corrected for radiation scattering by assuming its linear dependance on $1/\lambda$. No absorption was detected in the visible range. **Inset spectrum:** Gas-phase absorption, based on Halmann's (1963) data.

4.2.2. Photochemistry of methylphosphine

Analysis of our photochemical experiments benefited from the vibrational frequencies previously measured for CH_2PH and HCP (Johns et al., 1969; Pellerin et al., 1987), as well as from the theoretical predictions of harmonic and anharmonic vibrations available for CH_2PH_2, $HC{=}PH_2$ (singlet and triplet), CH_3P (singlet and triplet), $CH_2{=}P$, and HC=PH (Rey-Villaverde et al., 2013).

Three kinds of experiments were performed. The molar ratio of methylphosphine to argon was maintained at a constant level of 1:1000.

Exp1 – *Low-pressure Hg lamp (254 nm) as the photolyzing source;*
Exp2 – *Broadband Xe microwave discharge lamp (ca. 150-190 nm) as the photolyzing source;*
Exp3 –*Xe lamp irradiation followed by Hg lamp irradiation.*

The results of Exp1 revealed CH_4 and HCP as the photolysis products (see also **Sections 4.2.2.2** and **4.2.2.4** below). **Figure 4-3** and **Figure 4-4** show the identification of methane by its fundamental vibrational bands at 1304 cm^{-1} and 3025 cm^{-1}, in agreement with the values reported for an argon matrix (Cabana et al., 1963; Govender & Ford, 2000; L. H. Jones et al., 1986) and of HCP (based on the spectrum of pure HCP, cf. **Section 3.2**), respectively. Exp2 produced more photoproducts than Exp1, including CH_2PH, HCP, CP, methane, and PH. These results are similar to what was observed for CH_3NH_2 photolysis (193 nm, in solid *p*-H_2) reported by Mutunga & Anderson (2015), where CH_2NH, HCN and methane were observed. No evidence was found for photo-rearranged products. Details, grouped by each product, are given in the subsections below.

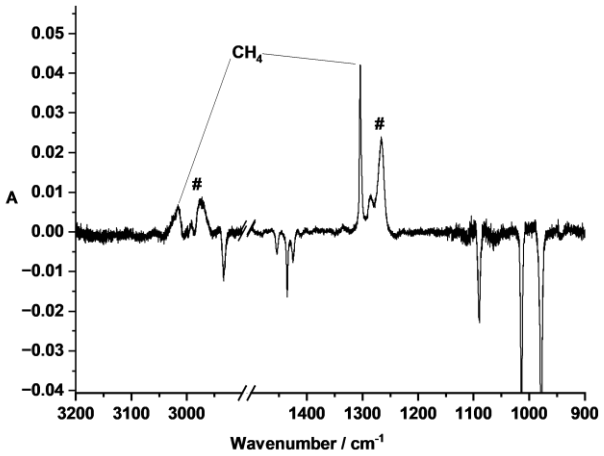

Figure 4-3. Baseline corrected difference spectrum (after-minus-before photolysis) showing the net effect of 9-day Hg-lamp photolysis of methylphosphine isolated in solid argon. Bands marked with # are most likely due to unspecified long-chain (polymeric) structures. Bands pointing downwards illustrate the decay of the precursor compound.

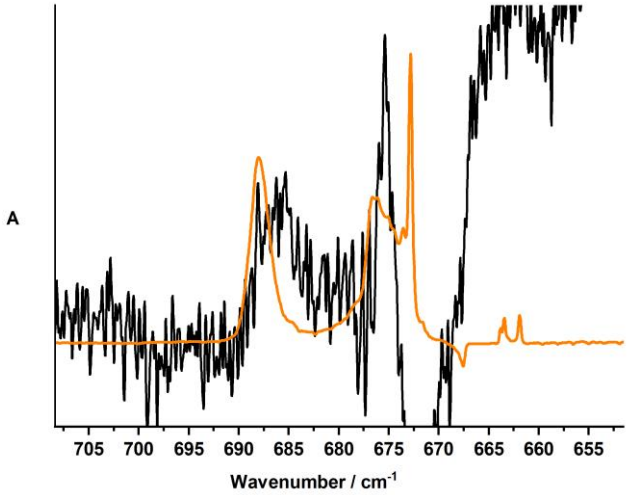

Figure 4-4. Black: difference spectrum (after-minus-before photolysis) showing the net effect of 9-day Hg-lamp photolysis of methylphosphine isolated in solid Ar. **Orange:** spectrum showing the bands of pure HCP isolated in solid Ar.

4.2.2.1. Phosphaethene (CH_2=PH)

Theoretical predictions of the ground state equilibrium geometry, electric dipole moment, charge distribution, vertical excitation energies to low-lying electronic states, ionization potential, spin rotational constants, and several other molecular properties of CH_2=PH have already been obtained by various methods (Bruna et al., 1985; Kim et al., 1993; Lemierre et al., 2005; Pang et al., 2017; Rey-Villaverde et al., 2013; Rozhenko et al., 1999; Watts et al., 1989; Woon & Herbst, 2009).

Phosphaethene is a highly unstable compound. It was first obtained by pyrolyzing either $(CH_3)_2PH$, CH_3PH_2 or $Si(CH_3)_3CH_2PH_2$, which gave access to the microwave spectrum, and therefore to the rotational constants, the quartic centrifugal distortion coefficients, and the electric dipole moment (Hopkinson et al., 1976b; Kroto et al., 1980, 1981b). The synthetic routes were further improved. By obtaining phosphaethene from chloromethylphosphine, two infrared bands were tentatively identified in a KBr pellet at 77 K (Pellerin et al., 1987), namely at 2260 cm^{-1} and 850 cm^{-1}. Using a similar synthetic procedure, the vertical ionization potentials (10.3 and 10.7 eV) were subsequently supplied by photoelectron spectroscopy (Lacombe et al., 1988). Quite recently, an adiabatic ionization energy ($X^2A^+ \leftarrow X^1A'$) of 10.07 eV has been measured (Mukhopadhyay et al., 2022) using synchrotron radiation-based double imaging photoelectron-photoion coincidence (i^2PEPICO) spectroscopy.

In the course of this doctoral work, following the photolysis (Exp2) of methylphosphine in solid Ar, five mutually correlated IR absorption bands of phosphaethene were observed (**Figure 4-5**, **Table 4-2**). The weakness of the 1414 cm^{-1} feature makes its assignment tentative.

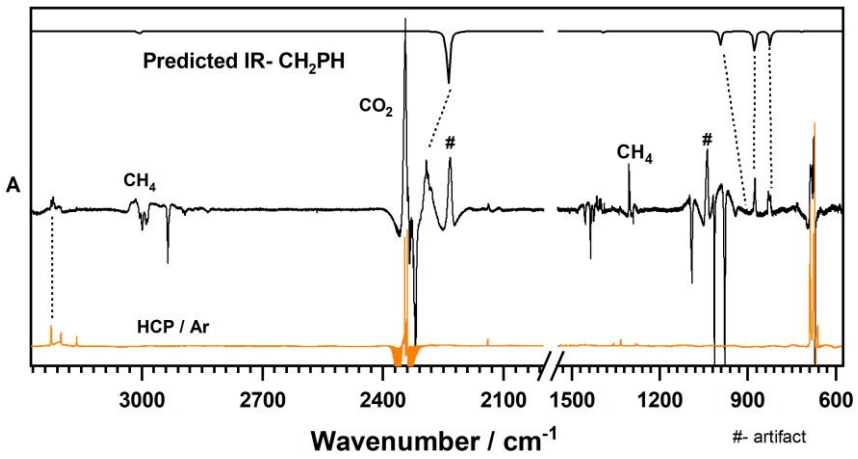

Figure 4-5. Middle: Difference spectrum (after-minus-before photolysis) showing the net effect of 4-hour VUV xenon lamp irradiation for methylphosphine isolated in solid argon. **Top:** (inverted intensity scale): B3LYP/aug-cc-pVTZ (harmonic approximation, scaling factor 0.96) prediction for CH_2PH. **Bottom:** Authentic HCP isolated in solid argon. The '#' marked peaks are due to artifacts.

Table 4-2. Infrared absorption bands of CH_2=PH.

Mode of vibration	RCCSD(T) (Rey-Villaverde et al., 2013)		B3LYP /aug-cc-pVTZ Scaling- 0.96		This work In Ar, 6 K		KBr pellet, 77 K, tentative assignments by Pellerin et al., (1987)
	harmonic cm^{-1}	anharm. cm^{-1}	cm^{-1}	km/mol	cm^{-1}	Relative intensity	cm^{-1}
ν_1 (a') CH asym. stretch.	3151	3100	3085	0.5	--	--	--
ν_2 (a') CH sym. stretch.	3063	3009	3007	4.4	--	--	--
ν_3 (a') PH stretching	2282	2279	2237	94	2287* 2292*	2	2260
ν_4 (a') HCH bending	1430	1411	1395	2.4	1414 *a*	1	
ν_5 (a') CPH bending	1017	1020	994	23	903	2	
ν_6 (a') CP stretching	976	976	961	1.9			
ν_7 (a') CH_2 rocking	723	741	718	0.7			
ν_8 (a") CH_2 wagging	891	881	878	44	875	10	860 (broad)
ν_9 (a") out-of-plane	839	831	826	24	830	10	

*) Site-splitting.
a) Tentative assignment.

4.2.2.2. Phosphaethyne (HCP)

While CH_2=PH appears following the photo-detachment of two hydrogen atoms (or an H_2 molecule) from methylphosphine, the elimination of four H atoms leads to another observed product: H-C≡P. A detailed literature review pertaining to this molecule and an account of the presently explored IR spectroscopy of the pure matrix-isolated substance was given in **Section 3.2**. Based on these measurements, HCP could be unambiguously identified among the photolysis products. This can be seen in the spectra of **Figure 4-4** and **Figure 4-6** produced by irradiating methylphosphine with Hg (Exp1) and Xe (Exp2) lamps, respectively. In **Figure 4-6**, differences in the matrix site-induced structure of the IR bands observed for pure HCP and for the photochemically obtained compound can be observed.

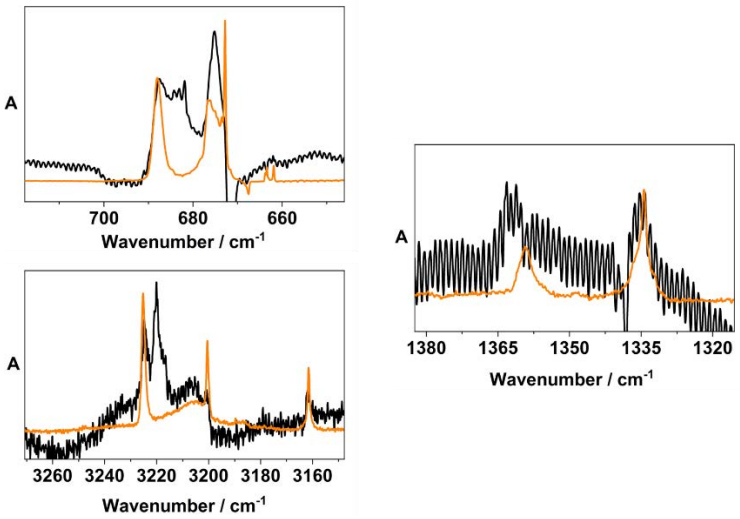

Figure 4-6. IR spectra of pure (**orange trace**) and photolytically derived (VUV Xe lamp irradiations, **black trace**) HCP isolated in argon matrices.

4.2.2.3. Phosphaethynyl radical, CP

No infrared absorption of C≡P could be detected in these experiments due to the low intensity of its single vibration which has a DFT-predicted absolute IR intensity of only 0.9 km/mol. However, the radical could be easily identified via UV absorption due to the characteristic vibronic progression of the $B^2\Sigma^+$-$X^2\Sigma^+$ system (see **Section 3.3.3**). **Figure 4-7** shows a comparison of the electronic absorption spectra observed following Exp2 and after the photolysis of pure HCP isolated in an argon matrix using the same Xe lamp. It unambiguously proves the presence of CP as one of the photoproducts. The size of the methylphosphine precursor molecule (and therefore the volume and shape of a native cage for the photoproduced CP) is significantly different from that of HCP, which is reflected in the appearance of a clear site-splitting when pure HCP is used as a precursor.

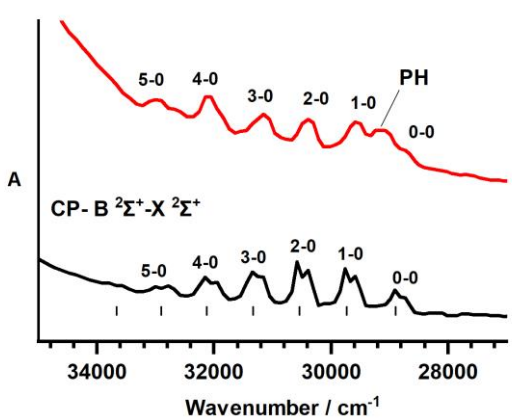

Figure 4-7. UV absorption spectra of the CP radical photochemically generated in solid argon from methylphosphine (**top**) and HCP (**bottom**). Vertical bars mark the location of respective transitions observed in fluorescence of gas-phase CP (Bärwald et al. 1934).

4.2.2.4. Phosphinidene (PH) and methane

Two fundamental bands of methane, 1304 cm^{-1} (strong) and 3025 cm^{-1} (weak), are observed upon photolysis in both Exp1 and Exp2. Their assignment, based on the published spectra of the Ar matrix-isolated compound (Cabana et al., 1963; Joneset al., 1986) was straightforward. Formation of CH_4 was also observed in a study of the photolysis of methylamine in solid p-H_2 (Mutunga & Anderson, 2015). In addition to methane, phosphinidene (the diatomic molecule PH featuring a triplet ground electronic state)* has been found with UV absorption spectroscopy (see **Figure 4-7**). The location of its broad band at 343 nm (29 150 cm^{-1}), close to the origin of the $B^2\Sigma^+$-$X^2\Sigma^+$ system of CP, coincides with that reported for PH trapped in solid argon (Harrison & Williamson, 2005).

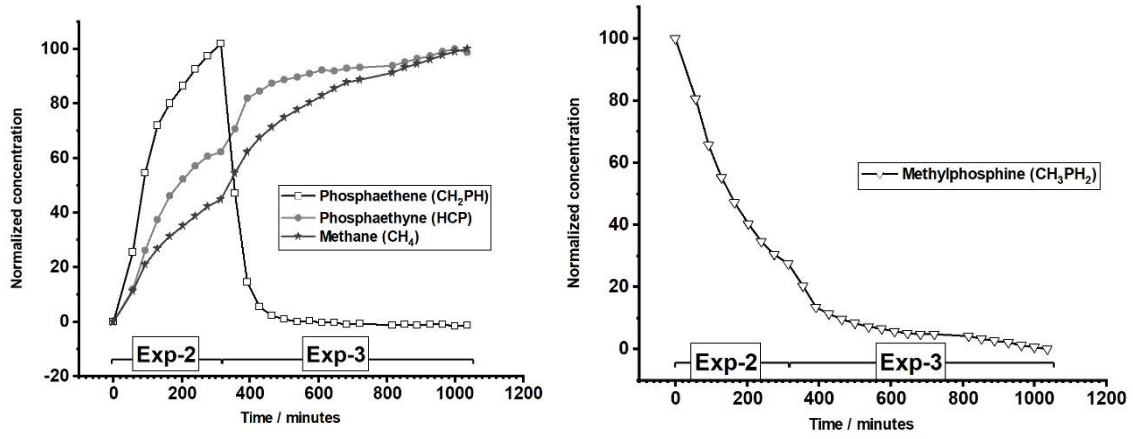

Figure 4-8. Left: Time evolution of photoproduct concentrations over primary (VUV source) and secondary (254 nm) irradiations of methylphosphine. **Right:** the corresponding decay of methylphosphine. Concentrations monitored by measuring the intensities of IR absorption bands at 1013.4, 875, 673, and 1304 cm^{-1} for methylphosphine, phosphaethene, phosphaethyne, and methane, respectively.

Figure 4-8 illustrates Exp3 by showing the precursor and photoproduct time evolution curves. All product concentrations increased until the Xe lamp (a VUV source) was replaced with the Hg lamp (254 nm). From that point on, the concentration of CH_2PH began to decrease abruptly and a sudden increase in HCP was observed, suggesting that dehydrogenation was the important decay channel for CH_2PH irradiated at 254 nm. An increase in methane concentration, related to the onset of 254-nm photolysis, can be associated with the parallel concentration jump observed for CH_3PH_2 (right panel of **Figure 4-8**).

* The same name applies also to the whole family of molecules bearing a monovalent phosphorous atom.

Table 4-3. IR absorption bands of methylphosphine and of its two photodehydrogenation products, as measured in solid Ar.

Wavenumber (cm^{-1})			Assignment		
This work Ar, 6K	Literature		CH_3PH_2	CH_2PH	HCP
	gas or theory	solid [b]			
3225.0	3216.9[a]				ν_1
3220.1					
3005.2	3002.8[b]	2981.0	ν_1		
2998.7	2989.8[b]				
2988.4 2985.1	2989.8[b]	2972.7	ν_{10}		
2935.1	2936.4[b]	2917.7	ν_2		
2892.4		2890.2	$^{13}C\ \nu_2$		
2860.8	2866.7[b]	2853.5	$\nu_4+\nu_{12}$		
2835.8	2848.6[b]	2824.3	$2\nu_4$		
2722.2		2702.8	$\nu_5+\nu_{12}$		
2564.7	2526.4[b]		$2\nu_6$		
2328.5	2309.0[b]	2303.2	ν_{11}		
2333.0	2304.6[b]		ν_3		
2319.8 2321.5					
2288.0	2237 [c]			ν_3	
2292.5					
1952.6	1965.6[b]	1950.1	$\nu_5+\nu_9$		
1453.7		1450.7	$\nu_8+\nu_{14}$		
1435.3	1435.2[b]	1422.0	ν_4		
1425.7	1428.6[b]		ν_{12}		
1414.5	1395.0[c]			ν_4	
1403.9					
1400.0					
1338.3	1349.1[b]	1347.0	$2\nu_9$		
1334.5	1335.0[a]				$2\nu_2$
1291.1	1296.2[b]	1276.0	ν_5		
1090.3	1091.9[b]	1077.4	ν_6		
1014.0	1016.9[b]	1009.6	ν_{13}		
978.3	977.6[b]	982.7	ν_7		
941.3			$\nu_8+\nu_{15}$		
903.5	994[c]			ν_5	
875.4	878[c]	850		ν_8	
829.9	826[c]			ν_9	
738.2	729.5[b]	736.4	ν_8		
698.6		695.9	ν_{14}		
688.2 675.2	674.0[a]				ν_2
671.3	675.7[b]	675.5	ν_9		

(***a***) Measured by Jung et al. (1997); (***b***) measured by Lannon & Nixon (1967); (***c***) B3LYP/aug-cc-pVTZ prediction (this work).

4.3. Methylarsine

4.3.1. Spectroscopy of methylarsine

The microwave spectroscopy of methylarsine is known (Milovanović & Mitić 2020). Infrared absorption, both in the gas-phase and the bulk solid, was studied by Harvey & Wilson (1966), whose analysis served as a guide for interpreting our own IR spectrum of the Ar matrix-isolated compound. The spectrum (**Figure 4-9**) is similar to that of methylphosphine although there are some qualitative differences. In methylarsine, the asymmetric methyl group deformations appear as a single sharp peak (1430.1 cm^{-1}, assigned to *a*", ν_4). For methylphosphine, the asymmetric methyl group deformations produce two bands, *a*' (1425.7 cm^{-1}) and *a*" (1435.3 cm^{-1}). No *a*' band was observed for methylarsine. Also, there is considerable ambiguity concerning the assignment of weak, closely spaced AsH_2 *a*" twisting (650.7 cm^{-1}, ν_{14}) and *a*' wagging (678.8 cm^{-1}, ν_8) vibrations. As expected, given the huge difference of pnictogen atom masses, the separation of asymmetric methylarsine stretching frequency (ν_3 at 2125.5 cm^{-1}) from that of methylphosphine (2328.5 cm^{-1}) is large. A detailed interpretation of infrared bands, along with overtones and combination bands, is detailed in **Table 4-8**.

To the best of the Author's knowledge, the electronic spectroscopy of methylarsine has never been examined. TD-DFT calculations (**Table 4-4**) were employed to predict the vertical excitation energies along with the respective oscillator strengths. **Figure 4-10** gives the comparison of calculated and measured spectra.

Table 4-4. Theoretically predicted (TD-B3LYP/aug-cc-pVTZ) vertical excitation energies (eV) and oscillator strength values for the lowest electronic transitions of methylarsine, CH_3AsH_2.

Energy of excitation from the ground state	Oscillator strength
5.68	0.06
6.15	0.10
6.82	0.00

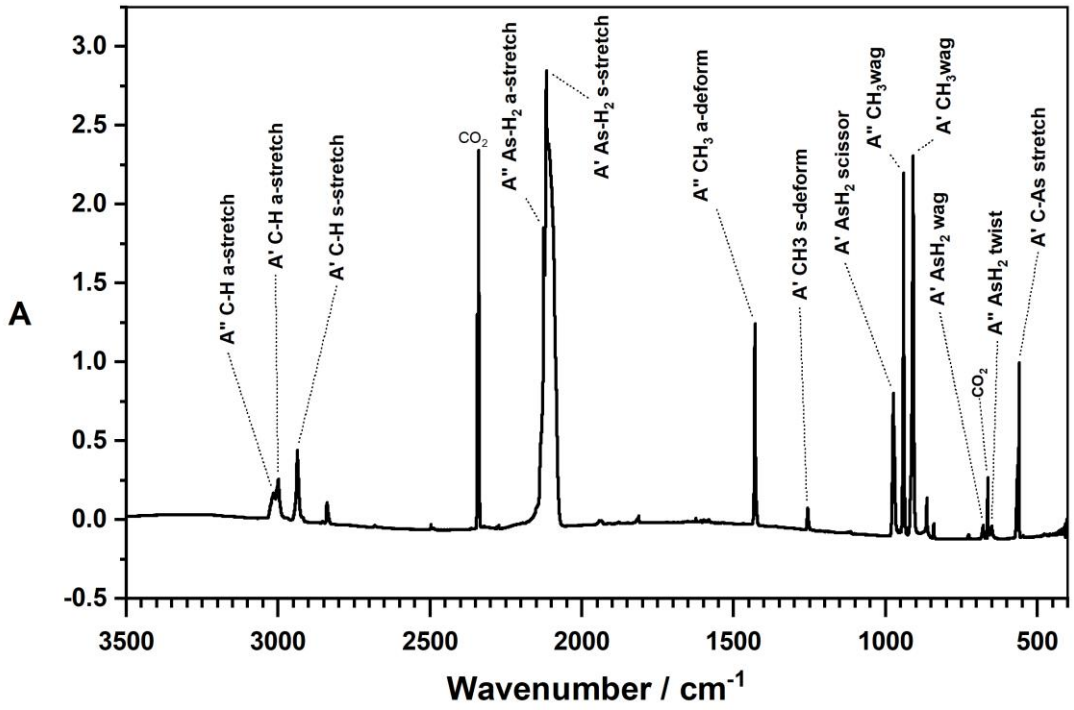

Figure 4-9. Infrared absorption spectrum of methylarsine isolated in solid argon at 10 K.

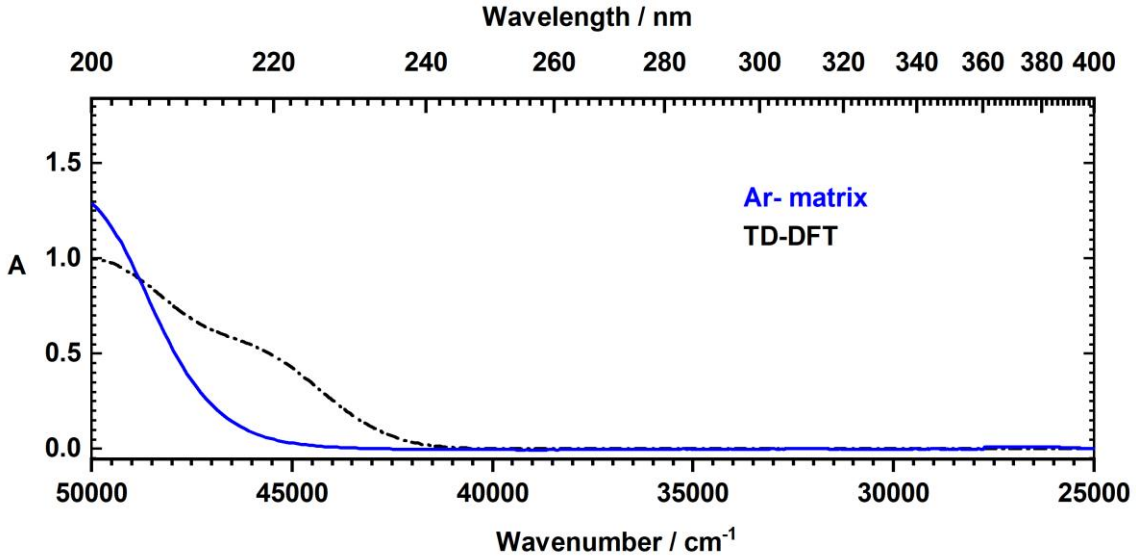

Figure 4-10. Experimental and TD-DFT predicted UV absorption spectra of methylarsine. The theoretical spectrum is broadened by convoluting with a Gaussian function, FWHM = 0.5 eV (for illustrative purposes only). No absorption was detected in the visible range.

4.3.2. Photochemistry of methylarsine

No experimental spectroscopic data are available for any of the probable products of methylarsine photolysis. Theoretically predicted vibrational frequencies were reported only for CH_2=AsH and H-C≡As (Marchal et al. 2010). Therefore, prior to the planned experiments, geometries, energies, and IR spectra of CH_3-AsH, CH_2-AsH_2, CH_3-As (triplet and singlet), HC-AsH_2 (triplet and singlet), CH_2=As, HC=AsH and C≡As were computed here using the same approach as for methylphosphine-related products. These theoretical results are collected in the **Table 9-4**.

Just as in the case of methylphosphine, three kinds of experiments were performed:

Exp1 - *Low-pressure Hg lamp (254 nm) as the photolyzing source;*
Exp2 - *Broadband Xe microwave discharge lamp (ca. 150-190 nm) as the photolyzing source;*
Exp3 - *Combination of Xe lamp irradiation followed by Hg lamp irradiation.*

The guest-to-host ratio was typically maintained at 1:1000. Photolysis progress was monitored with infrared and UV/Vis absorption spectroscopy. Photoproducts were similar to those obtained with methylphosphine. Exp1 led to production of HCAs (**Figure 4-13**) and CH_4 (**Figure 4-15**), while CH_2AsH, HCAs, CAs, CH_4, and AsH were formed in Exp2. No isomers of the precursor molecule were detected. The time evolution of precursor and products concentrations, as indicated with the integrated intensities of relevant IR absorption bands, is presented in **Figure 4-11**.

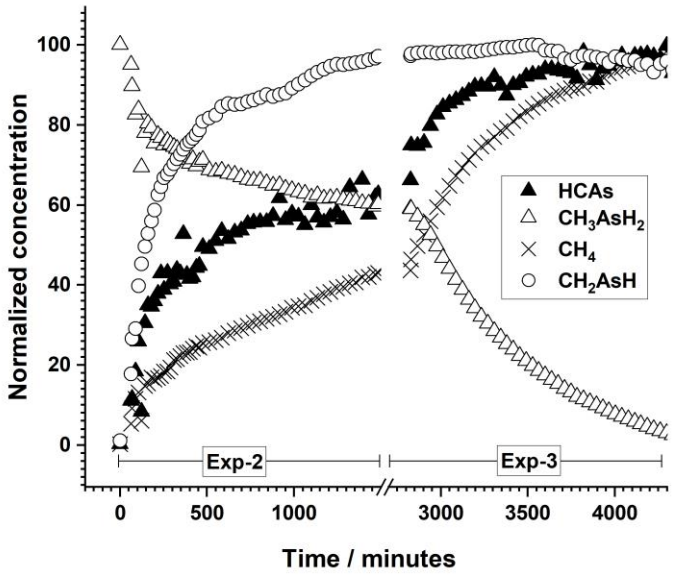

Figure 4-11. Time evolution of precursor and photoproduct concentrations over primary (VUV source) and secondary (254 nm) irradiations methylarsine, as monitored with IR bands at 934, 771, 612, and 1304 cm^{-1} for CH_2AsH_2, CH_2AsH, HCAs, and CH_4, respectively.

4.3.2.1. Arsaethene (CH_2AsH)

Arsaethene was first synthesized in 2004 for UV-photoelectron spectroscopy measurements (Chrostowska et al. 2004, 2010). More recently, the synchrotron radiation-based threshold photoelectron spectroscopy of CH_2AsH was investigated with vibronic resolution and an ionization potential of 9.61 eV was measured (Karaev et al., 2023). Anharmonic infrared spectra have been predicted at the DFT level (Marchal et al., 2010). Theoretical approaches also included an analysis of H_2 elimination from methylarsine to produce arsaethene (Viana, 2017) and a study on the reactivity of arsaethene with H^+ and Cu^+ cations (Luna et al., 2000). A study on its reactivity with H^+ and Cu^+ cations demonstrated that the carbon atom of CH_2AsH is more electronegative than arsenic.

No experimental reports on the infrared spectroscopy of CH_2AsH can be found in the literature. The comparison of DFT-predicted IR frequencies with the values measured during our own investigations is detailed in **Table 4-5**. The outcome of Exp3 indicates clearly that the concentration of CH_2AsH increases throughout the Xe lamp irradiation. During the secondary (Hg lamp) photolysis, its concentration quickly plateaus (cf. **Figure 4-11**). This saturation likely reflects an equilibrium between photodestruction of the compound and its creation via dehydrogenation of methylarsine. Five infrared absorption bands of this exotic molecule were observed, their spectral assignments are listed in **Figure 4-12**.

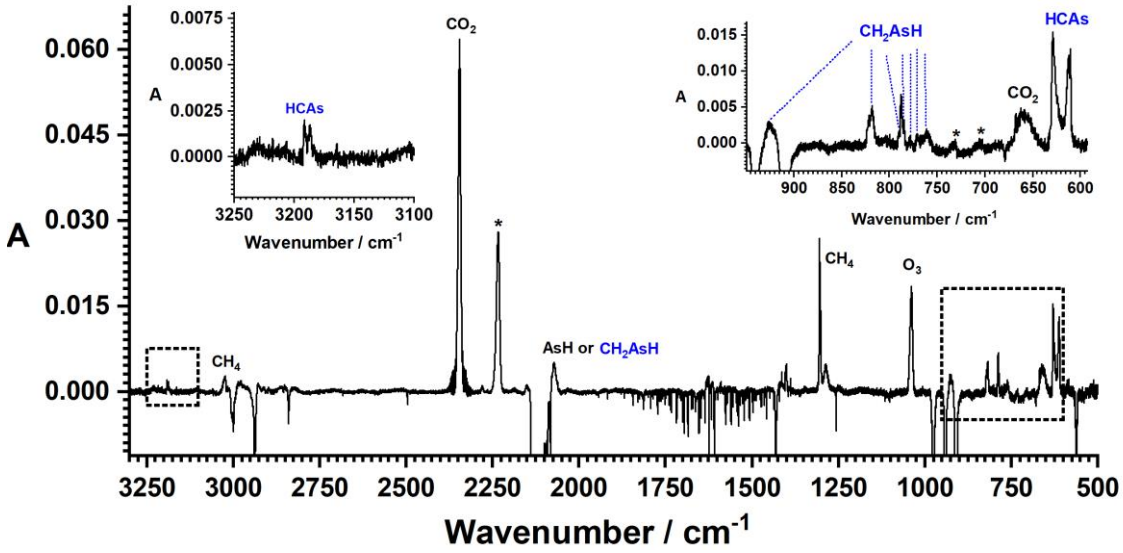

Figure 4-12. Difference spectrum (after-minus-before photolysis) showing the net effect of 6 hours of VUV irradiation of methylarsine isolated in solid argon. Weak bands are enlarged in the insets.

Table 4-5. Comparison of predicted and observed IR absorption bands of arsaethene.

Mode of vibration	Former theoretical prediction (anharmonic), by Marchal et al. 2010 cm^{-1} (km/mol)	This work cm^{-1} (km/mol)	
		B3LYP/aug-cc-pVTZ scaling factor- 0.96	Ar matrix, 6 K
ν_1, CH asym str. (a')	3114 (0.4)	3103.6 (0.1)	-
ν_2, CH sym str. (a')	3035 (2.1)	3011.0 (2.7)	-
ν_3, AsH str. (a')	2104 (147.6)	2060.0 (100)	2071.4 (100)
ν_4, HCH bend (a')	1395 (1.2)	1371.9 (0.8)	-
ν_5, CAsH bend (a')	931 (21.9)	906.4 (15.3)	927.7 (3.7)
ν_6, C=As str. (a')	840 (63.5)	830.1 (38.9)	817.9 822.3 (4.6)
ν_7, CH_2 rock (a')	679 (0.6)	659.3 (1)	-
ν_8, CH_2 wag (a'')	834 (3.4)	801.9 (2.2)	804.7 (0.2)
ν_9, out-of-plane (a'')	779 (22.5)	768.1 (14.7)	771.3 (2.7)

4.3.2.2. Arsaethyne (HCAs)

There is currently only one published experimental account concerning H-C≡As. UV-photoelectron spectroscopy and mass spectrometry measurements demonstrated the existence of this hydrogen cyanide analogue (Guillemin et al., 2008).

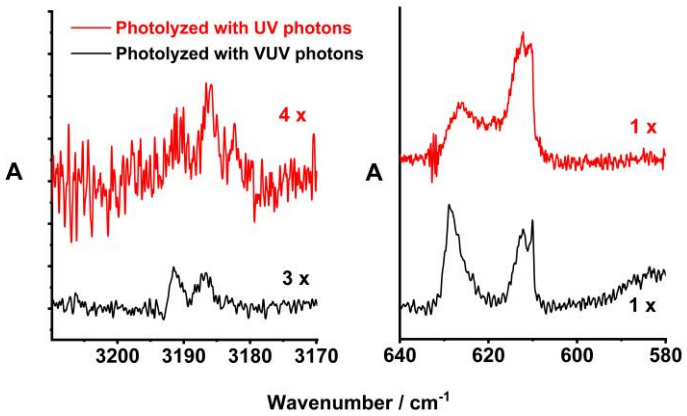

Figure 4-13. Fragments of IR absorption difference spectra (after-minus-before photolysis) showing the C-H stretching (**left panel**) and bending (**right panel**) bands of HCAs resulting from UV (254 nm) and VUV (150-190 nm) irradiation of methylarsine in argon matrices.

Presently, following the photolysis of methylarsine in solid argon at the guest-to-host ratio of 1:1000, C-H bending band of HCAs could be clearly identified in the IR absorption spectrum. Increasing the concentration to 1:500 allowed detecting the associated weak C-H stretching band (**Figure 4-13**). The two bands were assigned (cf. **Table 4-6**) based on anharmonic DFT predictions

of vibrational transitions (Marchal et al., 2010). The decay of CH_2AsH at the onset of secondary photolysis (254 nm; Exp3, see **Figure 4-11**) may be accompanied to an increase of the HCAs concentration, suggesting that arsaethene might act as the direct precursor for arsaethyne.

Table 4-6. Observed IR absorption bands of HCAs in solid argon compared to theoretical predictions (frequency values in cm^{-1}, relative intensity given as a percentage with respect to the strongest band).

Mode	B3LYP/aug-cc-pvtz, harmonic		DFT, anharmonic (Marchal et al., 2010)	In solid Ar, 5 K	
	Frequency, scaling factor 0.96	Relative Intensity	Frequency	Frequency	Relative Intensity
H-C≡As (stretching)	3184.1 (15.8)	16	3249	3187.0 3191.2	5.6
C≡As (stretching)	1065.2 (2.0)	2	1104	--	--
C-H (deformation)	632.9	100	646	628.4 612.1 610.2	100

4.3.2.3. Arsaethynyl radical, AsC

The gas-phase fluorescence excitation spectrum of AsC (Yang & Clouthier, 2011) revealed the presence of absorption in the UV region. A theoretical study devoted to the relevant electronic states appeared in the same year (de Lima Batista et al., 2011). Both these reports were helpful in the interpretation of UV/Vis absorption data. As noted by Yang & Clouthier, the v"-0 progression of the $B^2\Sigma^+ - X^2\Sigma^+$ system features irregular spacing, but the exact cause of that perturbation has not been identified. The same characteristic progression appeared here for VUV-irradiated methylarsine isolated in solid argon (**Figure 4-14**, **Table 4-7**).

Table 4-7. Vibronic bands frequencies (cm^{-1}) of the $B\ ^2\Sigma^+ - X\ ^2\Sigma^+$ system of CAs.

Band $B\ ^2\Sigma^+ - X\ ^2\Sigma^+$	Gas phase (Yang & Clouthier, 2011)	This work Argon matrix (cm^{-1})	Gas-to-matrix shift *
0-0	26 067.9	25 980	-90
1-0	26 651.3	26 560	-90
2-0	26 851.7	26 810	-40
3-0	27 365.4	27 290	-80
4-0	27 509.5	27 430	-80
5-0	28 072.9	28 010	-60
6-0	28 717.2	28 653	-60
7-0	29 376.2	29 330	-50

* Estimated error: 40 cm^{-1}.

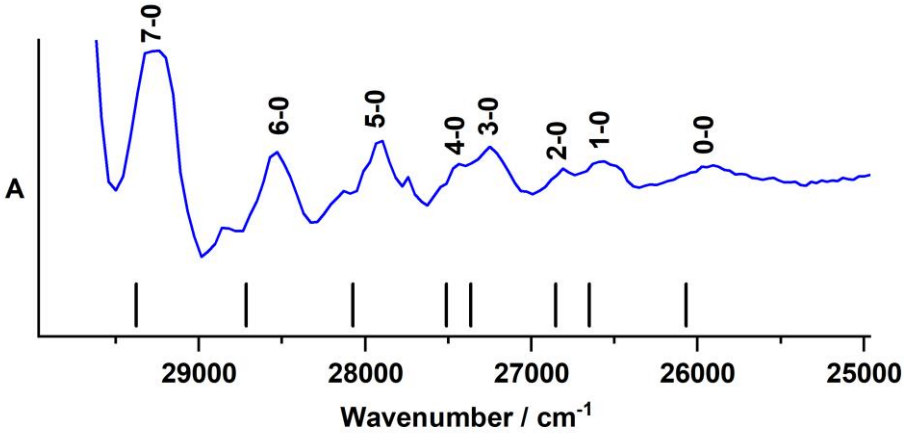

Figure 4-14. UV/Vis absorption spectrum of AsC generated by photolyzing Ar matrix-isolated methylarsine with a VUV xenon lamp. The reported (Yang & Clouthier 2011) gas-phase positions of $B^2\Sigma^+$ - $X^2\Sigma^+$ vibronic band maxima are marked by vertical bars.

4.3.2.4. Arsinidene (AsH) and methane

Methane was detected following the photolysis of matrix-isolated methylarsine irrespective of the radiation source applied (i.e. with either Hg lamp or VUV Xe lamp) via the IR bands of the fundamental modes observed at 1304 and 3025 cm^{-1}. The band at 2071.4 cm^{-1} might be attributed to AsH or CH_2AsH. We have tentatively attributed this feature to AsH due to its proximity to the reported gas-phase value is 2076.93 cm^{-1} (Hensel et al., 1995), as well as prominent appearance of AsH in the electronic spectrum. The UV band for matrix-isolated AsH was observed at 29 820 cm^{-1} (see **Figure 4-16**), implying a gas-to-matrix shift of ca. -140 cm^{-1} with respect to the position reported (Dixon et al., 1966) for the origin of the $A^3\Pi$ - $X^3\Sigma^-$ system of AsH: 29 959 cm^{-1}.

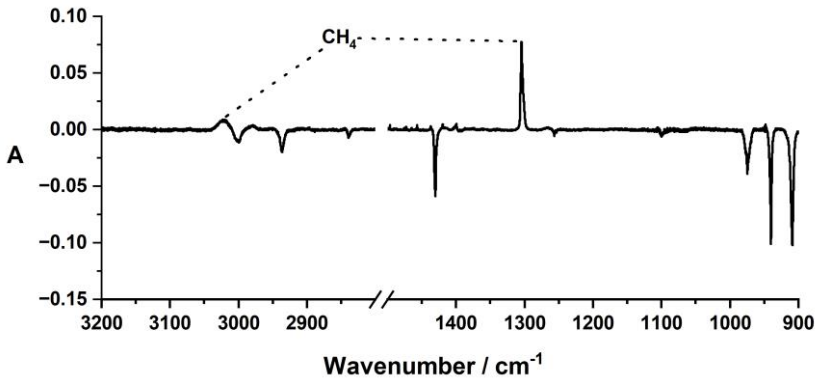

Figure 4-15. IR absorption difference spectrum (after-minus-before photolysis) showing the net effect of 31 hours of Hg-lamp irradiation for methylarsine isolated in solid argon. Precursor bands point downwards.

The presence of CH_4 and AsH indicates C-As bond breaking. Unfortunately, given that the IR band tentatively assigned to AsH partly overlaps the decreasing peak of the precursor, it was difficult to compare the time evolution curves of these two photoproducts. Exp1 and (see **Figure 4-11** and **Figure 4-15**) Exp3 show that formation of methane is particularly efficient in the course of Hg lamp photolysis. Methylarsine seems to be the direct precursor in this process. Throughout the experiment, its concentration decreased without reaching a plateau, mirroring the increase of CH_4

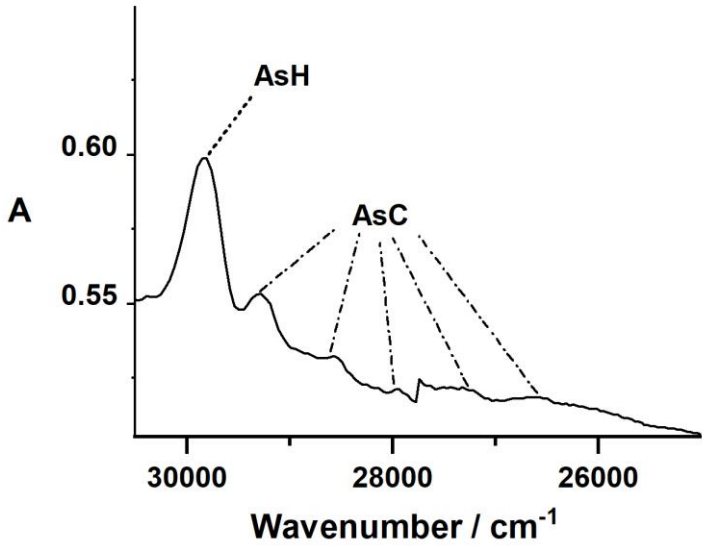

Figure 4-16. UV/Vis absorption spectrum measured for Ar matrix-isolated methylarsine after 4 hours of Xe lamp irradiations.

Table 4-8. IR bands of methylarsine and of its two photodehydrogenation products isolated in solid Ar.

Wavenumber (cm^{-1})			Assignment		
Ar matrix (this work)	Literature		CH_3AsH_2	CH_2AsH	HCAs
	Gas phase or theory	solid[a]			
3191.2 3187.0	3184[b]	--			ν_1
3024.7	3033[a]	3005	ν_{10}		
3014.2 2999.0	3018[a]	2987	ν_1		
2936.9	2945[a]	2916	ν_2		
2839.7 2854.7	2847[a]	2813	$2\nu_4$		
-	2742[a]	-	$\nu_{11}+\nu_{14}$		
2682.6	2658[a]	-	$\nu_9+\nu_3$		
2496.3	2510[a]	-	$2\nu_5$		
-		2290	$\nu_4+\nu_7$		
2125.5 2116.9	2102[a]	2075	ν_3		
2089.9 2081.8	2102[a]	2075	ν_{11}		
2071.4	2060[b]			ν_3	
1943.0	1919[a]	1918	$2\nu_6$		
1813.0	1823[a]	-	$2\nu_7$		
-	1443[a]	1421	ν_{12}		
1430.1	1435[a]	1412	ν_4		
1256.4	1263[a]	1247	ν_5		
1235.5	-	1248	$\nu_9+\nu_8$		
1114.9	1121[a]	1126	$2\nu_9$		
974.7	973[a]	960	ν_6		
940.1	934[a]	932	ν_{13}		
927.7	906[b]			ν_5	
908.8	905[a]	901	ν_7		
840.9	833[a]	843	$\nu_2-\nu_3$		
822.3 817.9	830[b]			ν_6	
804.7	802[b]			ν_7	
771.3	768[b]			ν_8	
678.8	674[a]	668	ν_8		
650.7	654[a]	644	ν_{14}		
628.4 612.1 610.2	633[b]				ν_3
560.2	563[a]	565	ν_9		

a) Harvey & Wilson (1966)
b) Marchal et al. (2010)

4.4. Methylstibine

4.4.1. Spectroscopy of methylstibine

The infrared absorption spectrum of methylstibine has been reported (Carey et al., 1968) but the authors considered their assignments to be tentative. I have analyzed this spectrum in more detail with the assistance of DFT-based calculations and based on analogies with IR absorption of matrix-isolated methylphosphine and methylarsine.

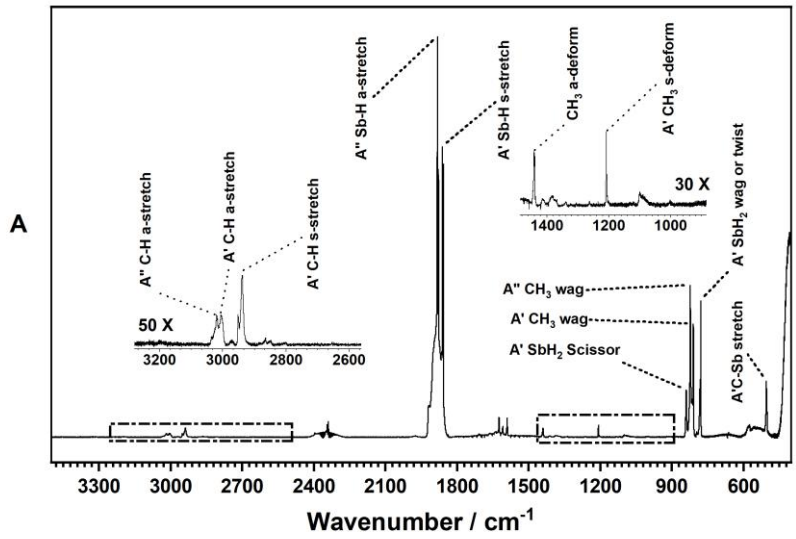

Figure 4-17. Infrared absorption spectrum of methylstibine isolated in solid argon at 10 K (guest-to-host ratio of 1:1000). Dotted regions are presented in more detail as insets.

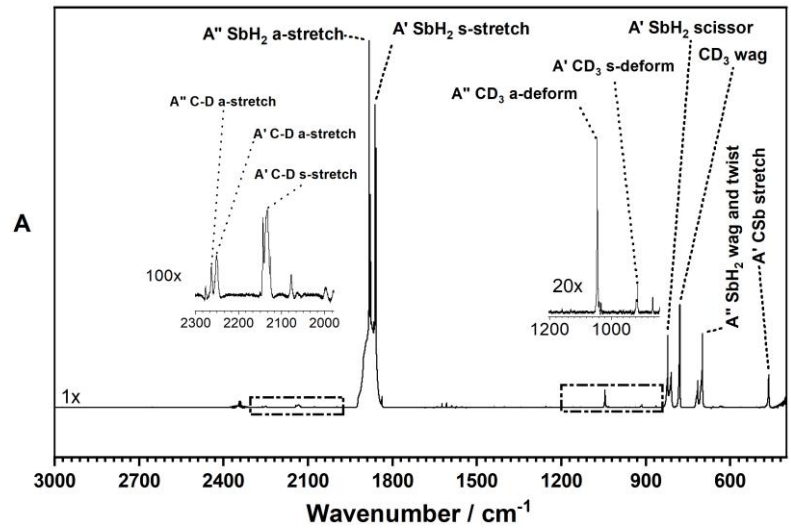

Figure 4-18. Infrared spectrum of methyl-deuterated methylstibine (CD_3SbH_2) isolated in solid argon at 10 K (guest-to-host ratio of 1:1000). Dotted regions are presented in more detail as insets.

The infrared spectrum of methylstibine isolated in solid argon (**Figure 4-17**) is similar to the spectra of methylphosphine and methylarsine but with all bands shifted to lower frequencies. This shift is particularly large for the modes explicitly involving the heavy atom (Sb-H asymmetric stretching at 1882.5 cm^{-1}, symmetric stretching at 1861.1 cm^{-1}, SbH_2 scissoring at 839.9 cm^{-1}, SbH_2 waging or twisting at 779.1 cm^{-1}, C-Sb stretching at 504.1 cm^{-1}). **Table 4-9** provides assignments for CH_3SbH_2, including overtone and combination bands. For comparison, the IR spectrum (**Figure 4-18**) and band assignments (**Table 4-9**) for methyl-deuterated methylstibine (CD_3SbH_2), also employed as a photochemical precursor during our experiments, are provided. Although the predicted IR transitions of CD_3SbH_2 were reported (Kim et al., 2009), no experimental spectrum has ever been measured. Particularly large isotopic shifts are observed for the CD_3 wagging, symmetric and asymmetric deformations, as well as for the C-D symmetric and asymmetric stretchings.

The electronic spectroscopy of methylsibine has not been studied before. The current UV absorption spectrum (**Figure 4-19**) is consistent with the TD-DFT-based predictions provided in **Table 4-10**. Just as for the P- and As-bearing analogues, the first electronic transition is expected around 220 nm (excitation energy of ca. 0.5 eV).

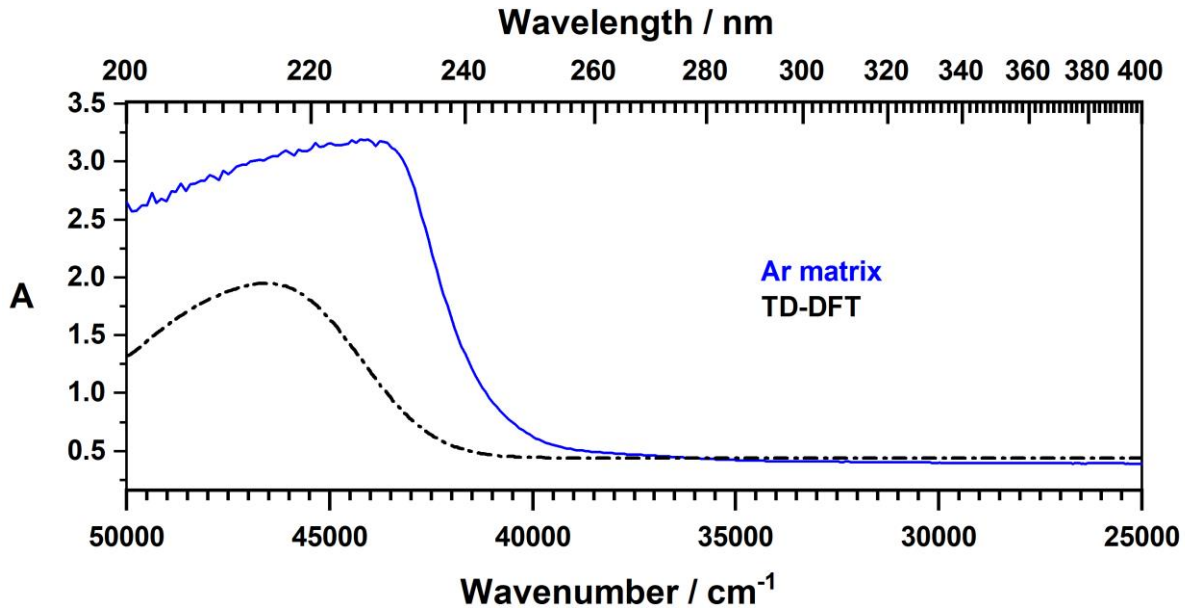

Figure 4-19. Experimental (**blue**) and TD-DFT-predicted (**dash-dot black**) UV absorption spectra of methylstibine. The theoretical spectrum is broadened by convoluting with a Gaussian function, FWHM = 0.5 eV (for illustrative purposes only). No absorption was detected in the visible range.

Table 4-9. Theoretically predicted and experimentally observed IR absorption bands of methylstibine, CH_3SbH_2 and partly deuterated methylstibine, CD_3SbH_2.

Vibrational frequencies / cm^{-1}					Assignment
CH_3SbH_2 Ar matrix (this work)	**CD_3SbH_2 Ar matrix (this work)**	**Gas phase [a]**	**CH_3SbH_2 Theory [b]**	**CD_3SbH_2 Theory [b]**	
3035.0	2276.1	2991	3156.9	2340.7	ν_{10}
3018.7	2264.2				
3004.8	2251.4	2991	3138.2	2325.2	ν_1
2951.6	2143.6	2956	3055.8	2187.0	ν_2
2939.1	2133.8	2929			
2864.2 2847.2	2077.5 2063.3	2869			$2\nu_4$
2802.6					$\nu_{11}+\nu_{14}$
2396.0		2409			$2\nu_5$
2150.9		2150			$\nu_4+\nu_7$
1882.5 1877.9	1882.5 1877.9	1874	1920.6	1920.6	ν_3
1861.1 1857.7	1861.1 1857.7	1863	1915.9	1915.9	ν_{11}
1708.6		1734			$2\nu_6$
1440.1	1044.8	1438	1467.5	1061.7	ν_4
	1401.2				
1208.0	1033.0	1205	1239.6	1063.3	ν_5
1100.6	914.0	1143			$\nu_{8+}\nu_9$
1003.4	863.3	933 922 909			$2\nu_9$
839.9	822.4 809.9	834	853.1	834.8	ν_6
822.4 809.9	779.1	821	837.4	723.7	ν_{13}
779.1	715.8 698.7		831.9	707.4	ν_7
580.0	473.8		571.0	500.2	ν_8
504.1	463.9	503	494.2	454.4	ν_9

a) Carey et al. 1968

b) B3LYP/def2-TZVP, this work.

Table 4-10. Theoretically predicted (TD-B3LYP/def2-TZVP) vertical excitation energies (eV) and oscillator strength values for the lowest electronic transitions of methylstibine, CH_3SbH_2.

Energy of excitation from the ground state	Oscillator strength
5.68	0.08
6.72	0.13
7.30	0.001

4.4.2. Photochemistry of methylstibine

Published reports concerning the spectroscopy of potential methylstibine photolysis products are scarce. The infrared spectroscopy of the Ar matrix-isolated radical species CH_3SbH and its isotope CD_3SbD have been investigated (Cho & Andrews, 2012a). In the same study, DFT-predicted vibrational frequencies were provided for the CH_2SbH_2 radical. To the best of Author's knowledge, no theoretical nor experimental spectroscopic data have been reported for any of the other expected photoproducts: $CH_2{=}SbH_3$, $CH_2{=}SbH$, CH_3-Sb, HC-SbH_2, $CH_2{=}Sb$, HC=SbH, HC≡Sb or C≡Sb. Results of the respective, presently performed quantum calculations are collected in the **Table 9-6**.

Two kinds of photolysis experiments were performed using CH_3SbH_2 as a precursor:
Exp1 - *Low-pressure Hg lamp (254 nm) as the photolyzing source;*
Exp2 - *Broadband Xe microwave discharge lamp (ca. 150-190 nm) as the photolyzing source.*

Both Exp1 and Exp2 resulted in production of methylstibinidene (CH_3Sb), diatomic stibinidene (SbH), and methane. The Hg lamp was much more effective in photolyzing CH_3SbH_2 than in analogous irradiations of CH_3PH_2 or CH_3AsH_2. Indeed, as illustrated by **Figure 4-19**, the electronic absorption at 254 nm is in the case of methylstibine higher than for the other two methylpnictines. Details pertaining to the identification of photoproducts are given in the following sections.

4.4.2.1. Stibinidene (SbH) and methane

Methylstibine yields methane when irradiated with a mercury lamp (**Figure 4-20**). The efficiency of such a production of CH_4 from methylpnictines increases in the series: CH_3PH_2 < CH_3AsH_2 < CH_3SbH_2. The presence of SbH was confirmed by its infrared band which appeared at 1840 cm^{-1}, in agreement with a former matrix-isolation study on laser ablation of antimony in presence of hydrogen (Wang et al., 2003).

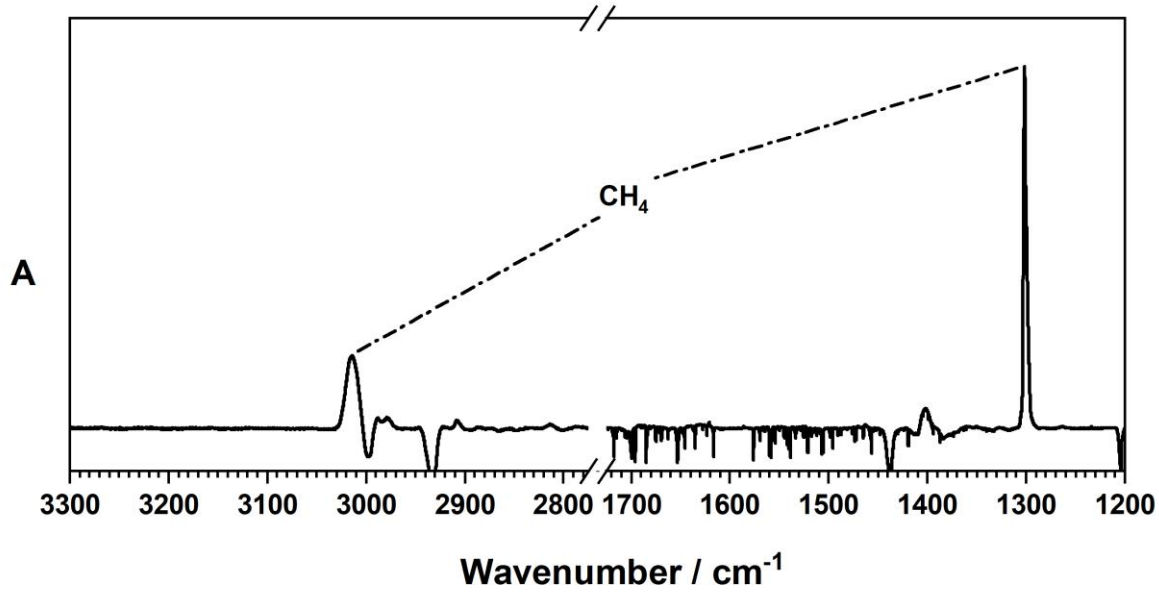

Figure 4-20. IR absorption difference spectrum (after-minus-before photolysis) showing the net effect of 21 hours of 254 nm irradiation for methylstibine isolated in solid argon.

4.4.2.2. Methylstibinidene (CH_3Sb)

Weak but sharp infrared peaks at 497.5, 1182.2, 1190.8, and 1199.5 cm^{-1} were observed upon Hg lamp (254 nm) irradiation of matrix-isolated methylstibine. Based on our theoretical predictions, these features cannot be assigned to CH_2SbH, HCSb, or CSb which might be expected as products based on what we observed in photolyses of methylphosphine and methylarsine. This can be at least partly explained with the results of a theoretical study by Schoeller et al., (1997). It was found there that the π-bond strength decreases in $H_2C{=}XH$ compounds with the increasing mass of the pnictine atom X. The dehydrogenation product CH_2SbH is therefore less stable (and thus more prone to the carbon-pnictogen bond cleavage) compared to the P- and As-bearing analogues.

Since the IR bands mentioned above were very weak, another experiment was performed with the guest-to-host ratio increased from 1:1000 to 1:300 and an Hg lamp applied for the photolysis. Additional peaks at 2913.3 and 2993.9 cm^{-1} (i.e. in the C-H stretching region) appeared (**Figure 4-21**). Together, these spectral features match the theoretical predictions for methylstibinidene, a chemical compound belonging to the group of pnictinidenes (see **Section 5.1**). Further confirmation of the assignment was obtained by the isotopic labelling experiment, using CD_3SbH_2 (**Figure 4-22**). The deuteration-induced spectral shifts reasonably matched the predicted ones (see **Table 4-11**). This exotic compound of monovalent antimony, CH_3-Sb, features a triplet-multiplicity ground electronic state (DFT calculations locate the lowest singlet 25 kcal/mol or 1.1 eV above the ground state). Although the ionization potential and spin-orbit splitting of methylstibinidene have very

recently been supplied by threshold photoelectron spectroscopy (Karaev et al., 2023), our own experiment provides the first IR spectrum of this species.

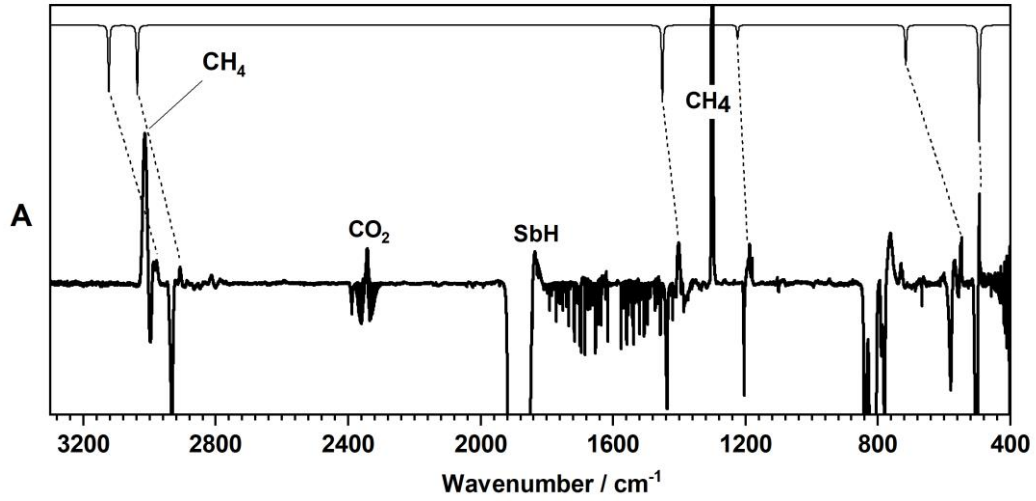

Figure 4-21. Bottom: IR absorption difference spectrum (after-minus-before photolysis) showing the net effect of 21 hours of Hg-lamp irradiation for methylstibine isolated in solid argon. **Top:** theoretically predicted IR spectrum of CH_3Sb with absorbance scale reversed to facilitate the comparison.

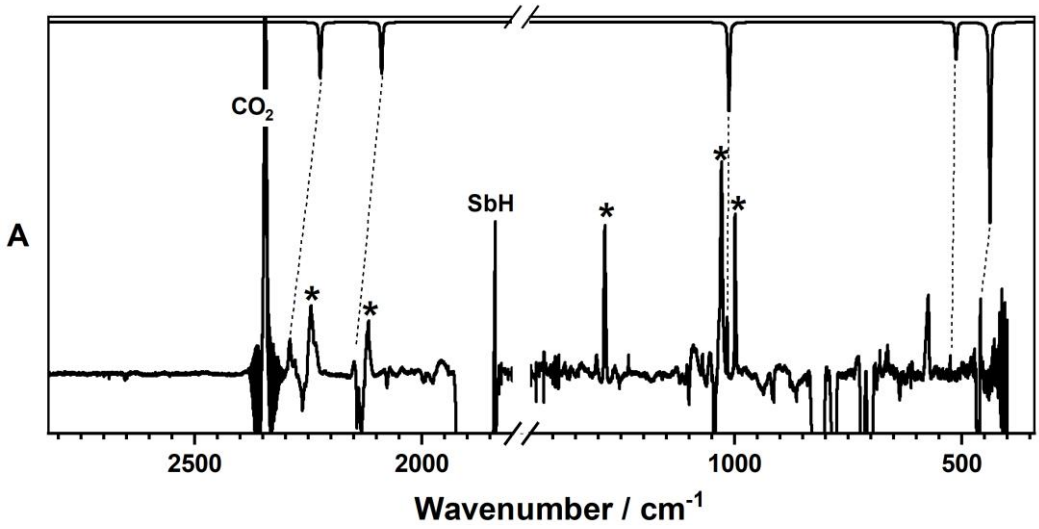

Figure 4-22. **Bottom:** IR absorption difference spectrum (after-minus-before photolysis) showing the net effect of 15 hours of Hg-lamp irradiation for partly deuterated methylstibine (CD_3SbH_2) isolated in solid argon. **Top:** theoretically predicted IR spectrum of CD_3Sb with absorbance scale reversed to facilitate the. Asterisked bands are due to partly deuterated methane, CD_3H.

Table 4-11. Theoretically predicted and experimentally observed IR absorption bands of CH_3Sb and CD_3Sb.

Mode	B3LYP/def2-TZVP cm^{-1} (km/mol)			In solid Ar [a] cm^{-1}			
	CH_3-Sb	CD_3-Sb	Isotopic shift	Isotopic shift	CH_3-Sb		CD_3-Sb
C-H asym. stretch (E)	2999 (5.6)	2222 (2.4)	-777	-715.2	2993.9 (w)		2278.7 (m) [b]
C-H sym. stretch (A)	2918 (11.6)	2087 (4.4)	-831	-842.9	2913.3 (w)		2070.4 (w) [b]
C-H scissor (E)	1394 (6.4)	1011 (3.7)	-383	-331.1	1402.1 (m)		1071.0 (m)
C-H bend (A)	1175 (2.4)	898 (0.0)	-277	-	1182.2 1190.8 1199.5	m	-
C-H bend (E)	688 (3.4)	511 (1.6)	-176	-127.8	653.9 (w)		526.1 (w)
C-Sb stretch (A)	475 (19.5)	437 (16.9)	-38	-38.5	497.5 (s)		459.1 (s)

a) s - strong, m - medium, w - weak;

b) Shift with two CD stretching could only be identified tentatively because it falls within congested regions of the spectrum.

4.5. Conclusions

The photochemistry of CH_3XH_2 (X=P, As, Sb) species isolated in solid Ar and irradiated by a mercury lamp (254 nm), a Xe microwave discharge lamp (ca. 150-190 nm), or the combination a Xe lamp followed by a Hg lamp is summarized in **Scheme 4-2**. Photoproducts arising from CH_3PH_2 and CH_3AsH_2 are similar and include the P- and As-analogues of CH_2XH, HCX, CX, and XH, as well as CH_4 (**Scheme 4-2**, top panel). Once produced, CH_2=PH and CH_2=AsH could be further photolyzed using 254 nm radiation of a Hg lamp. No CH_3-P or CH_3-As methylpnictinidenes could be detected in these experiments and no evidence of the isomeric species CH_3XH_2 or isomers of the identified photoproducts could be found.

For methylstibine (CH_3SbH_2), the dehydrogenation channel produces only methylstibinidene, CH_3-Sb (a triplet-multiplicity species), at the photolysis wavelengths tested, and does not produce any observable CH_2=SbH. No evidence for an analogous CH_3-X product was found in photolyses of CH_3PH_2 or CH_3AsH_2. The breakage of the C-Sb bond followed by formation of SbH and CH_4 proceeds more easily for Sb- than for the P- or As-analogues.

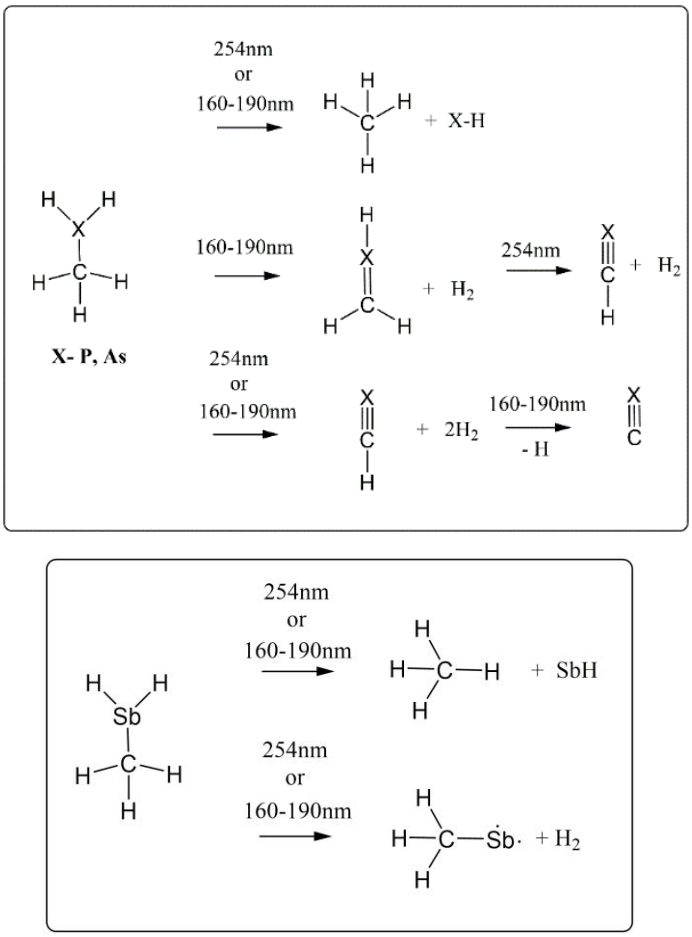

Scheme 4-2. Photochemical reactions observed for methylphosphine, methylarsine, and methylstibine isolated in solid argon.

This research gave access, for the first time, to the vibrational spectroscopy of CH_2=AsH, HC≡As, and CH_3-Sb, refinement of the vibrational spectroscopy of CH_2=PH, and allowed first measurements of electronic spectroscopy of CH_3-AsH_2, and CH_3-SbH_2.

Chapter-5

Ethynylstibinidene

and ethynylarsinidene

5. Ethynylstibinidene and ethynylarsinidene

5.1. Pnictinidenes- an overview

Molecules containing monovalent pnictogen atoms (N, P, As, Sb, Bi) in the +1-oxidation state are known as *pnictinidenes*. They are highly reactive and generally unstable due to the high electron deficiency at the pnictogen center; see **Figure 5-1** (Lu & Zeng, 2024; Qian et al., 2024; Wu, et al., 2023b). Stabilization can be achieved through electron-donating groups or by steric effects introduced with suitable substituents. For example, the singlet form of a phosphino-phosphinidene was observed at room temperature, its stability being achieved by π–donation from the phosphinyl center to the vacant *p* orbital on the terminal phosphorus atom (Liu et al., 2016). A recent paper reported on a triplet stibinidene (**Figure 5-2**) stabilized by bulky hydrindacene ligands (Wu, et al., 2023b). Synthesizing and characterizing free pnictinidenes bearing no appropriate substituents is challenging, as they tend, under standard laboratory conditions, to form the dipnictenes (molecules with a double bond between pnictogen atoms) or higher oligomers (Liu et al., 2016). Among the pnictinidenes, nitrenes have been quite extensively investigated (Wentrup 2018). However, studies on such molecules bearing a pnictogen atom heavier than N are very limited (Lu & Zeng 2024). Excluding several diatomics (hydrides and halides), the only published reports, prior to the current doctoral work, are those on mesitylphosphinidene (Akimov et al., 2017; Li et al., 1994), phenylphosphinidene (Mardyukov et al., 2017; Mardyukov & Niedek, 2018), CH_3As, CH_3Sb, stibinidene with a hydrindacene ligand (Cho & Andrews, 2012b; Karaev et al., 2023; Mukhopadhyay et al., 2020; Wu, Li, et al., 2023b) BiX (X=Me, $AlCl_4$) (Corbett & Lynde 1971; Cubicciotti 1960; Mukhopadhyay et al. 2020), and sterically protected bismuthinidene (Wu, et al., 2023a).

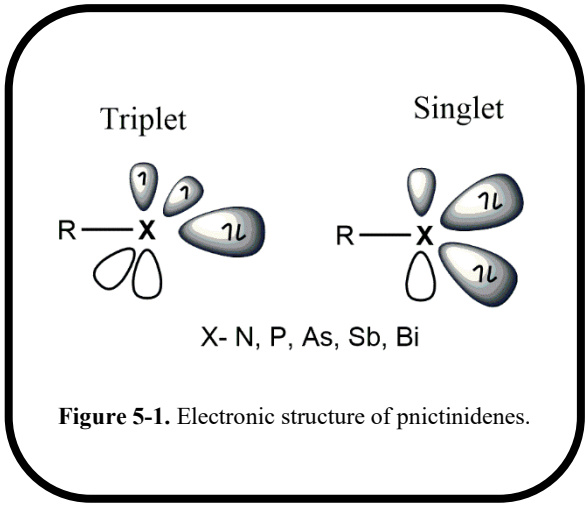

Figure 5-1. Electronic structure of pnictinidenes.

Recently, Lawzer at al. (2021) reported on an efficient photochemical route to ethynylphosphinidene (HCCP) from phosphapropyne (CH_3CP) in rare gas matrices.

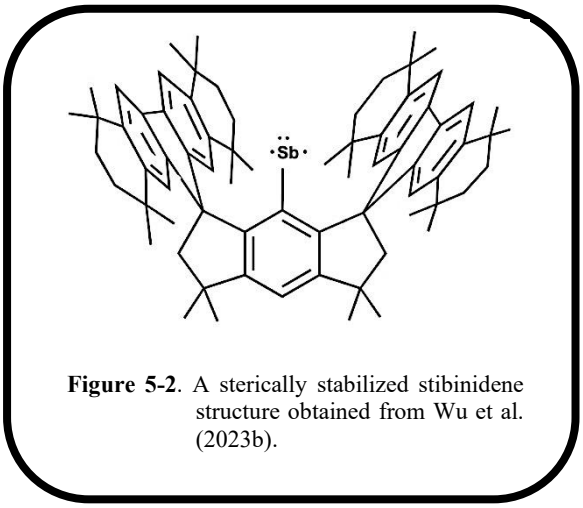

Figure 5-2. A sterically stabilized stibinidene structure obtained from Wu et al. (2023b).

Photochemistry of ethynylphosphine ($HCCPH_2$) was investigated within the same study and, again, HCCP appeared as the major product following UV irradiation.

It seemed promising to attempt, along the similar lines, the generation of unknown species: ethynylarsinidene (HCCAs) and ethynylstibinidene (HCCSb) using ethynylarsine, $HCCAsH_2$ (or vinylarsine, $H_2CCHAsH_2$), and ethynylstibine, $HCCSbH_2$, as the respective precursors.

Below, the Author gives a full description of the part of this research dealing with the formation of HCCSb from $HCCSbH_2$. Omitted are some of the details pertaining to the spectroscopy and photochemistry of $HCCAsH_2$ which were carried out by the Author's colleague Dr. Arun-Libertsen Lawzer (Lawzer et al. 2023). However, the Author's studies on luminescence of HCCAs are described in Section 5.3 and a comparison of ethynylpnictinidenes, including HCCAs, based on all available data, is presented in **Section 5.2.2.2**.

5.2. Photolysis of ethynylstibine ($HCCSbH_2$)

5.2.1. Spectroscopy of the precursor

To generate ethynylstibinidene (H-C≡C-Sb), ethynylstibine (H-C≡C-SbH_2) was used as a precursor. Since the IR spectroscopy of $HCCSbH_2$ has not been previously studied, assignments of the detected bands relied on B3LYP/def2TZVP predictions (see **Figure 5-3** and **Table 5-1**). The identified impurities, coming from the preparative synthesis, were acetylene and stibine (SbH_3)*. One of the C-H stretching bands of $HCCSbH_2$ could not be reliably measured because of an overlapping acetylene band.

TD-DFT calculations were used to predict the electronic transitions of $HCCSbH_2$ in the UV region (see **Table 5-2**). The experimental spectrum (**Figure 5-4**) shows a broad, structureless absorption with an onset at approximately 250 nm (40 000 cm^{-1}), blended with UV scattering.

* The general name "stibine" refers also to all molecules bearing an -SbH_2 group.

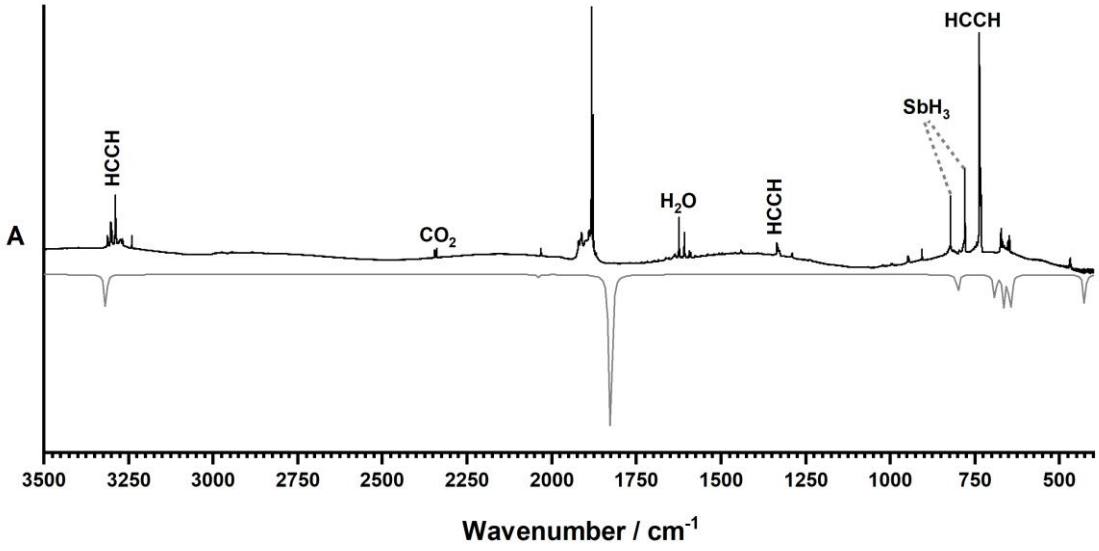

Figure 5-3. Top: IR absorption spectrum of $HCCSbH_2$ isolated in argon matrix at 10 K. **Bottom**: predicted (B3LYP/def2-TZVP) spectrum with its absorbance scale inverted.

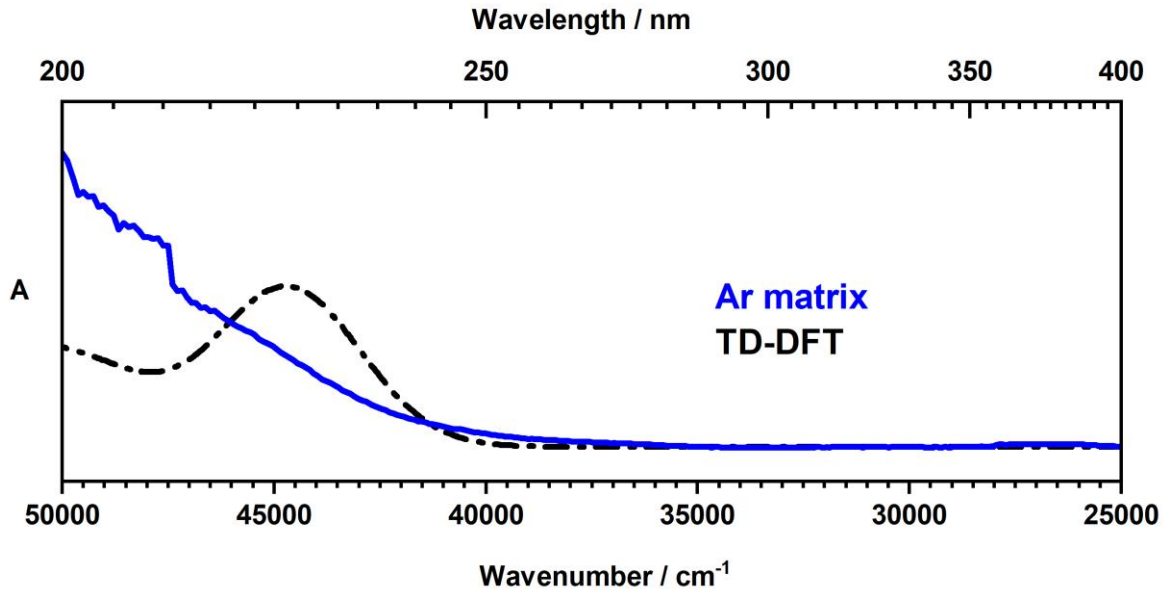

Figure 5-4. Experimental and TD-DFT-predicted UV absorption of ethynylstibine. The theoretical spectrum is broadened by convoluting with a Gaussian function (FWHM = 0.5 eV, for illustrative purposes only). No absorption was detected in the visible range. Experimental data are corrected for radiation scattering by assuming its linear dependence on $1/\lambda$.

Table 5-1. IR spectroscopy of $HCCSbH_2$: theory and experiment.

Mode		B3LYP/def2-TZVP		In solid argon	
		Frequency [a] **(cm^{-1})**	**Absolute Intensity (km mol^{-1})**	**Frequency (cm^{-1})**	**Relative Intensity (%)**
ν_1	C-H stretching	3315.7	55.5	3311.7 3298.5 3267.2	31.5 --[b] 11.0
ν_2	C-C stretching	2040.6	5.3	2031.7	11.2
ν_3	SbH_2 antisym. stretching	1833.8	163.0	1915.8 1911.9 1873.1 1867	- 94.9 7.6 4
ν_4	SbH_2 sym. stretching	1828.6	153.5		
ν_{10} + ν_5	-	-	-	1289.3	22.9
ν_5	SbH_2 scissoring	803.1	30.9	811.8	28.7
ν_6	C-C-H out-of-plane bending	681.5	45.1	672.4	100
ν_7	C-C-H in-plane bending	654.4	67.5	667.6	37.9
ν_8	SbH_2 wagging	647.2	43.2	651.8	34.2
ν_9	SbH_2 twisting	640.4	7.5	647.7	53.73
ν_{10}	C-Sb stretching	427.5	45.1	468.6	50.1
ν_{11}	C-C-Sb in-plane bending	212.3	11.3	out of detection range	
ν_{12}	C-C-Sb out-of-plane bending	200.9	9.7		

a) Scaling factor 0.96.

b) Overlap with an acetylene band.

Table 5-2. DFT (B3LYP/def2-TZVP) predictions for the vertical excitations from the ground state to the four lowest excited singlet electronic states of ethynylstibine ($HCCSbH_2$).

Excitation energy (eV)	Oscillator strength
5.52	0.025
5.54	0.05
5.99	0.001
6.18	0.04

5.2.2. Photolysis products

5.2.2.1. Time evolution and IR spectroscopy

$HCCSbH_2$ was irradiated in solid argon with an Hg lamp (254 nm). **Figure 5-5** shows how the crucial peaks, monitored via IR absorption, evolved over time. Most of the precursor compound was decomposed within the first 2 hours. IR bands at 474 cm^{-1}, 635 cm^{-1}, and 1956 cm^{-1} appeared early. All three featured the same (within experimental errors) growth curves, suggesting a single carrier. Based on the DFT predictions, these can be assigned to, respectively, C-Sb stretching, C-C-H bending, and C-C stretching vibrational modes of triplet ethynylstibinidene (HCCSb). The triplet multiplicity of the ground electronic state of HCCSb and location of the lowest singlet approx. 0.95 eV (7700 cm^{-1}) higher were confirmed with TD-DFT computations. The HCCSb concentration grows during the first 2 hours of irradiation and slightly decreases later on, as depicted by **Figure 5-5**. An infrared spectrum measured for a photolyzed $HCCSbH_2$/Ar sample, alongside the calculated spectrum of HCCSb, is displayed in **Figure 5-6**. The respective band frequencies and intensities can be found in the last columns of **Table 5-3**.

Apart from HCCSb, decomposition of $HCCSbH_2$ creates HCCH, SbH and CCSb. Vibrational frequencies of HCCH (Jovan Jose et al., 2007; Krajewska et al., 2002) and SbH (Wang et al., 2003) in solid argon have been reported previously. The IR spectrum of CCSb, however, has not been measured until the present work. Open-shell coupled cluster RCCSD(T) calculations by Milovanović & Jerosimić (2013) suggest that CCSb is linear and features an IR band at 1765 cm^{-1} (harmonic approximation), close to the currently observed frequency of 1751 cm^{-1}.

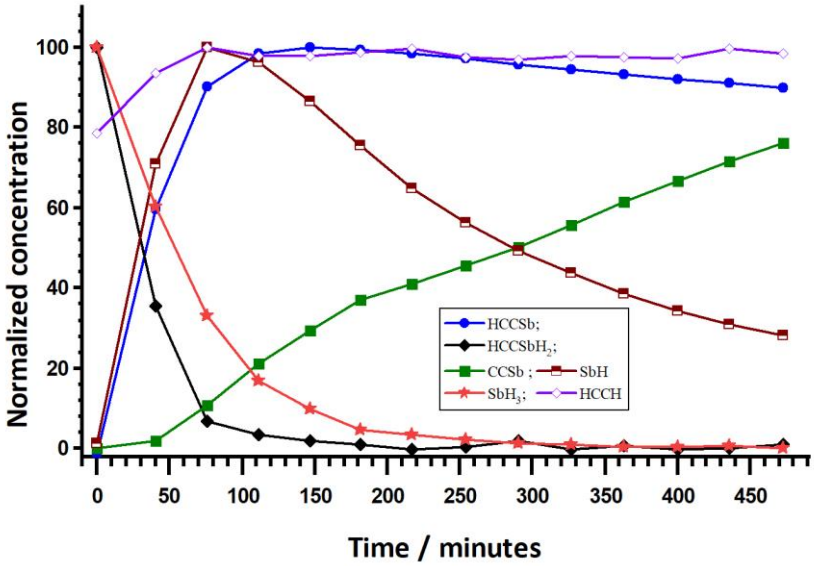

Figure 5-5. Evolution of the normalized IR band intensities for the precursor ($HCCSbH_2$) and photoproducts isolated in solid argon, as monitored during UV (254 nm) irradiation. Also shown is the evolution of impurities (SbH_3 and HCCH) present in the $HCCSbH_2$ sample. Wavenumbers of the monitored bands are 468.6, 635.1, 1751, 1840, 822.3, and 736.8 cm^{-1} for $HCCSbH_2$, HCCSb, CCSb, SbH, SbH_3, and HCCH, respectively.

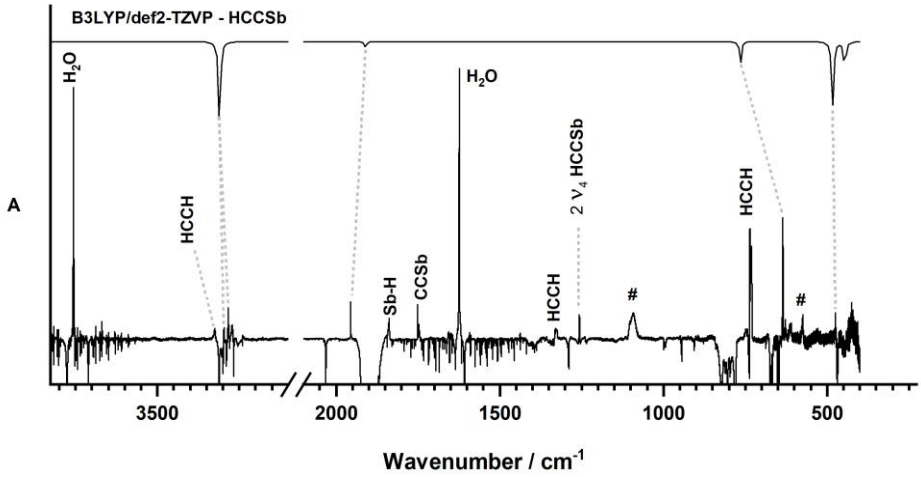

Figure 5-6. Bottom: baseline-corrected difference spectrum (after-minus-before irradiation) for Ar matrix-isolated $HCCSbH_2$ subjected to the 254 nm photolysis. **Top:** predicted (B3LYP/def2-TZVP) spectrum of triplet HCCSb (absorbance scale is reversed to ease the comparison).

The time evolutions of HCCH and SbH_3 impurities contained in the $HCCSbH_2$ sample (cf. spectrum in **Figure 5-3**) were also monitored. As depicted by **Figure 5-5**, the concentration of HCCH increased until $HCCSbH_2$ was completely destroyed. Acetylene, therefore, appeared as both an impurity and a photoproduct. On the other hand, SbH_3 was not created during the photolysis. It decayed steadily and disappeared after ca. 4 hours of irradiation. This impurity seems to be the most important precursor of SbH. The latter species underwent secondary photolysis, as evidenced by a

maximum formed on its concentration curve after approximately 1 hour of irradiation. Probable product here could be elemental antimony (found in the form of a dark residue covering the substrate window after the experiments).

While photolysis studies on $HCCPH_2$ showed that it may isomerize to CH_3CP and $H_2C{=}C{=}PH$ (Lawzer et al., 2021), analogous isomers could not be detected upon photolysis of either $HCCAsH_2$ or $HCCSbH_2$.

5.2.2.2. Comparison of ethynylpnictinidenes

The electronic structure of HCCN is that of a cyanocarbene (H-Ċ·-C≡N) with a significant allenic (H-Ċ=C=N̲) admixture. When moving from P to Sb, the carbenic and allenic properties become negligible, and the pnictinidene character (H-C≡C-X̲·) predominates. Indeed, the C≡C stretching frequency of HCCN, 1735 cm^{-1}, shifts to 1955.9 cm^{-1} in HCCSb (Dendramis & Leroi, 1977; Lawzer et al., 2021, 2023) pointing to the emergence of a genuine acetylenic unit (cf. **Table 5-3**). This is also reflected in the C-H stretching (increase from 3229.4 to 3297.0 cm^{-1}) and bending frequencies (increase from 458 to 635.1 cm^{-1}). The impact of electronic structure on these vibrational modes is sufficiently strong to overcome the influence of the pnictogen mass (increasing mass, alone, should produce the opposite effect). Additionally, the C-X stretching frequencies (X being either N, P, As, or Sb) decrease, when moving from nitrogen- (1178.5 cm^{-1}) to antimony-bearing compounds (473.3 cm^{-1}). In moving from HCCN to HCCSb, the C-X stretching decreases in energy because unpaired electron density becomes more and more localized on the pnictogen, the π-orbital overlap between carbon and pnictogen becomes smaller, and the mass of the pnictogen atom increases.

Photochemically generated HCCN from 1-azidoalkynes ($HCCN_3$) was reported (Zeng et al., 2014) to appear in solid argon along with HCNC and cyclo-CHCN. No analogous isomers could be detected for HCCAs (Lawzer et al., 2023) or HCCSb.

Table 5-3. IR spectroscopy of ethynylpnictinidenes: Theory and experiment.

Vibrational Modes		**HCCN**	**HCCP**				**HCCAs**				**HCCSb**			
		Ar Matrix (Dendramis & Leroi, 1977)	**Theory (B3LYP/aug-cc-pvtz)**		**Ar matrix** (Lawzer et al., 2021)		**Theory (B3LYP/aug-cc-pvtz)**		**Ar matrix** (Lawzer et al., 2023)		**Theory (B3LYP/ Def2TZVP)**		**Ar matrix This work,** (Lawzer et al., 2023)	
		Frequency (cm^{-1})	**Frequency (cm^{-1})**	**Intensity (km mol^{-1})**	**Frequency (cm^{-1})**	**Relative Intensity (%)**	**Frequency (cm^{-1})**	**Intensity (km mol^{-1})**	**Frequency (cm^{-1})**	**Relative Intensity (%)**	**Frequency (cm^{-1})**	**Intensity (km mol^{-1})**	**Frequency (cm^{-1})**	**Relative Intensity (%)**
ν_1	C-H stretching	3229.0	3307.9	76	3287.8	100	3309.1	67.8	3294.7 3284.6	100	3309.42	60.745	3297.0 3283.9	60
ν_2	C-C stretching	1735.0 [a]	1786.7	4.6	1814.2 1807.9	7.3 7.0	1864.3	10.8	1893.1	13	1935.5	13.313	1955.9	18
ν_3	C-X stretching	1178.5 [b]	678.3	15	696.1	13	518.5	23.5	552.9	10	431.2	36.2	473.3	21
$2\nu_4$	C-C-H bending overtone	-	-	-	-	-	-	-	1201.0	17	-		1256.7	26
ν_4	C-C-H bending	458.0	564.6	36	564.7	73	608.8	36.0	605.9	59	634.9	38.536	635.1	100
$2\nu_5$	C-C-X bending overtone	-	-		-	-	-	-	498.7	6	-	-	-	-
ν_5	C-C-X bending	369.5 [c]	299.6	10	Out of detection range		261.9	11.8	out of detection range	-	221.4	13.96	out of detection range	Out of detection range

a - antisymmetric CCN stretch; *b* - symmetric CCN stretch; *c* - uncertain

5.2.3. Electronic spectroscopy

5.2.3.1. Absorption

The HCCSb molecule features two unpaired electrons distributed across two degenerate, singly occupied molecular orbitals (SOMOs) (**Figure 5-7**). The lowest of the two observed electronic transitions, presumably the fully allowed $1^3\Sigma^-$-$X^3\Sigma^-$, was detected between 33 000 cm^{-1} and 28 000 cm^{-1} (**Figure 5-8**, bottom). It seems to originate mostly in the excitation of an electron from the highest occupied molecular orbital (HOMO) to the SOMO, i.e. $\sigma^2\pi^4\pi^{*2}$ to $\sigma^2\pi^3\pi^{*3}$. Theoretical predictions on the electronic spectroscopy of HCCX species (**Table 5-4**, **Figure 5-12**) were obtained by Dr. Marcin Gronowski, who made use of generalized active space configuration interaction (GASCI) and Fock-space CCSD (FS-CCSD) methods (Lawzer et al. 2023). The second experimentally observed absorption, at 35 600 cm^{-1}, is associated with the fully allowed transition $1^3\Pi$–$X^3\Sigma^-$ dominated by the excitation from HOMO-1 to SOMO ($\sigma^2\pi^4\pi^{*2}$ to $\sigma^1\pi^4\pi^{*3}$).

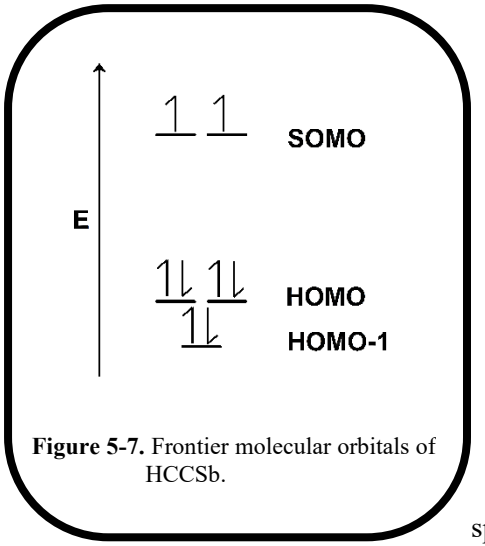

Figure 5-7. Frontier molecular orbitals of HCCSb.

Figure 5-8 shows the UV absorption spectrum of ethynylphosphinidene in solid Ar (Lawzer et al. 2021) and the spectrum of ethynylarsinidene obtained by extensive (1 week) irradiation of Ar matrix-isolated vinylarsine. Both molecules exhibit absorption patterns similar to those of HCCSb, though at slightly higher energies. A general trend observed across the electronic absorption spectra from HCCN to HCCSb is the blue shift of the $1^3\Sigma^-$-$X^3\Sigma^-$ transition (which in HCCN appears between 33 300 cm^{-1} and 29 400 cm^{-1} with a vibronic spacing of 550 cm^{-1}; Dendramis & Leroi 1977). The weakness and complexity of the $1^3\Sigma^-$-$X^3\Sigma^-$ systems observed for HCCP, HCCAs, and HCCSb currently preclude reliable assignment of vibronic transitions.

In HCCN, the $1^3\Pi$–$X^3\Sigma^-$ transition appears as a vibronic progression between approx. 41 700 cm^{-1} and 33 900 cm^{-1}, with a vibronic spacing of 1100 cm^{-1} (M. Nakajima et al., 2013). For HCCP and HCCAs, however, it is observed as a single sharp feature at 38 460 cm^{-1} and 38 170 cm^{-1} respectively (Lawzer et al., 2021, 2023). Theoretically predicted energy differences between the HOMO-1 and SOMO are similar for HCCP and HCCAs. The transition is more red-shifted for HCCSb, appearing strongly at 36 500 cm^{-1}. These single absorption peaks can be assigned to the $1^3\Pi$–$X^3\Sigma^-$ vibrationless (0-0) transitions.

Table 5-4. Results of generalized active space configuration Interaction (GASCI) and Fock-space CCSD (FS-CCSD, inside the parentheses) (Lawzer et al., 2023).

State		HCCSb			HCCAs		
		Relative energy [cm^{-1}]	**Relative energy [eV]**	**Transition dipole moment [Debye]**	**Relative energy [cm^{-1}]**	**Relative energy [eV]**	**Transition dipole moment [Debye]**
$X^3\Sigma^-$	Ω=0	0 (0)	0 (0)	-	0 (0)	0 (0)	-
	Ω=1	640 (660)	0.08 (0.08)	0.02	110 (124)	0.01 (0.02)	0.003
$1^3\Delta$	Ω=3	30 300 (32 300)	3.76 (4.00)	-	30 200 (30 700)	3.74 (3.81)	-
	Ω=2	31 300 (33 300)	3.88 (4.13)	-	30 700 (31 200)	3.81 (3.87)	-
	Ω=1	31 600 (33 400)	3.91 (4.14)	0.04	31 200 (31 800)	3.87 (3.94)	0.01
$1^3\Sigma^+$	Ω=1	32 700 (34 600)	4.06 (4.29)	0.02	31 700 (32 200)	3.93 (4)	0.008
	Ω=0	32 900 (34 500)	4.07 (4.27)	-	31 900 (32 400)	3.96 (4.02)	-
$1^3\Sigma^-$	Ω=0	32 900 (34 800)	4.08 (4.32)	2	33 000 (34 200)	4.09 (4.23)	2.0
	Ω=1	33 900 (35 700)	4.21 (4.42)	0.03	33 200 (34 300)	4.11 (4.25)	0.01
$1^3\Pi$	Ω=2	38 800	4.81	-	41 700	5.17	-
	Ω=1	39 900	4.94	1.1	42 200	5.23	0.9
	Ω=0	41 400	5.14	-	42 800	5.31	-
$1^1\Delta$		7 300 (7 500)	0.91 (0.93)	-	6 900 (6 400)	0.86 (0.8)	-
$1^1\Sigma^+$		13 500 (14 000)	1.67 (1.73)	0.03	12 400 (12 400)	1.54 (1.54)	0.01
$1^1\Sigma^-$		29 400 (30 600)	3.64 (3.79)	-	28 700 (28 900)	3.56 (3.59)	-

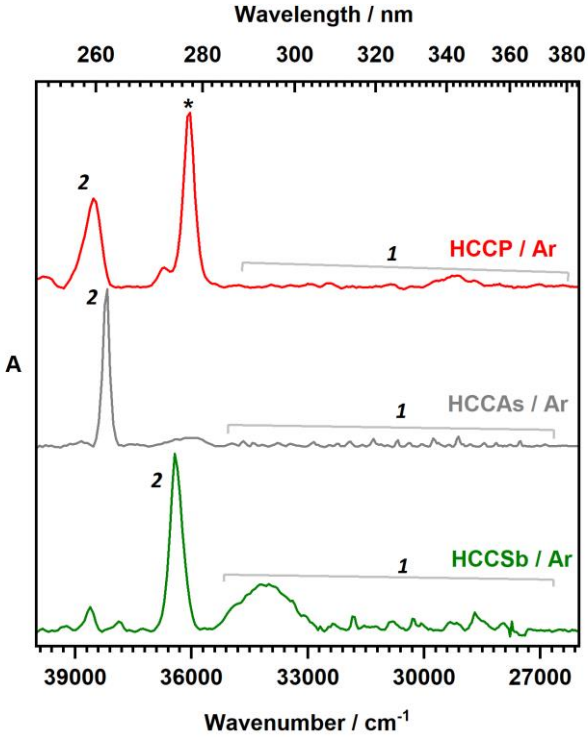

Figure 5-8. UV absorption spectra of ethynylphosphinidene (top; Lawzer et al. 2021), ethynylarsinidene (middle; courtesy of Dr. A. Lawzer), and ethynylstibindene (bottom; this work) isolated in an argon matrix. Spectra measured after the UV photolyses of phosphapropyne, vinylarsine, and ethynylstibine, respectively. Asterisked peak corresponds to an unidentified photoproduct. Bands of the $1^3\Sigma^-$-$X^3\Sigma^-$ and $1^3\Pi$-$X^3\Sigma^-$ systems are marked by **1** and **2**, respectively.

5.2.3.2. Luminescence of HCCSb

A spectrofluorimeter did not provide photoexcitation efficiency necessary to allow detection of ethynylstibinidene luminescence, therefore a tunable optical parametric oscillator (OPO) system was employed as the excitation source. The experimental setup was equipped with a monochromator coupled to a gated CCD camera to record dispersed luminescence (technical details are given in **Section 2.4**). The OPO provided excitation wavelengths between 250 - 350 nm, where UV absorption was previously detected. Excitation at 260.0 nm (38 460 cm^{-1}) revealed two emissions (**Figure 5-9**). The stronger one (30 000 cm^{-1} – 18 000 cm^{-1}), a progression of bands with a vibronic spacing of approximately 1500 cm^{-1}, was due to the $A^3\Sigma_u^+$ - $X^3\Sigma_g^-$ system of O_2 (Fournier et al. 1979), which is a common sample impurity. The other, weaker emission was more interesting. It appeared as a progression in the 18 000 - 12 000 cm^{-1} region with a spacing of about 800 cm^{-1}.

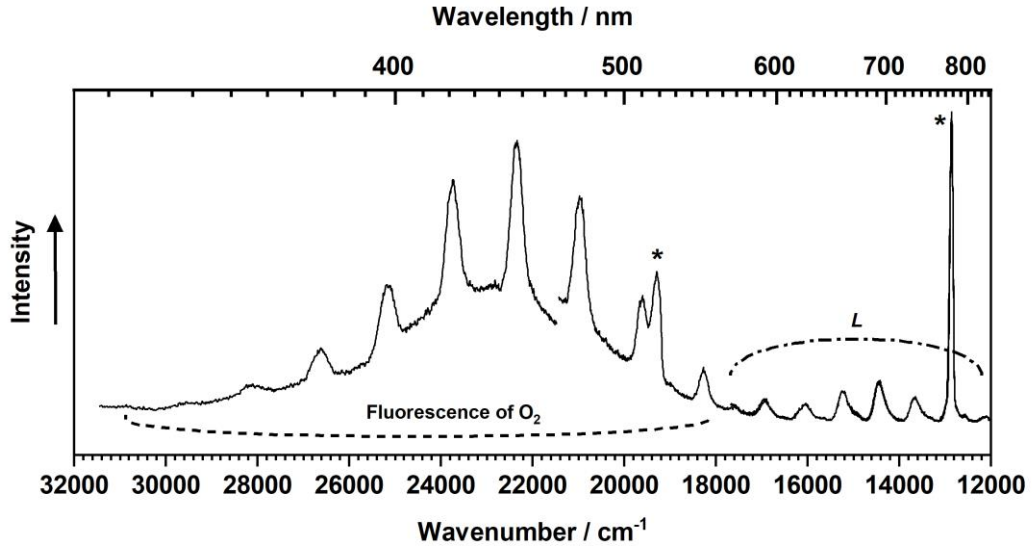

Figure 5-9. Two emission systems observed by exciting (λ_{exc} = 260 nm) a sample of Ar matrix-isolated $HCCSbH_2$ previously photolyzed with a mercury lamp. A discontinuity visible at 21 480 cm^{-1} is the result of a change of the OPO spectral range. Asterisks mark the excitation laser lines appearing in the 2nd and 3rd grating order.

Unfortunately, it was not possible with the available experimental setup to obtain a full, well resolved excitation spectrum for the progression denoted as *L* in **Figure 5-9**. Dispersed emission spectra corresponding to a few distinct excitation wavelength settings were nevertheless recorded. The result, depicted by **Figure 5-10**, suggests that *L* and the two absorption systems of **Figure 5-8** might be due to HCCSb.

It is not easy to strengthen this tentative assignment of *L* to HCCSb by pinpointing a concrete luminescence system responsible for the discovered emission. The spacing of the progression (about 800 cm^{-1}; **Table 5-5**), does not fit any of the vibrational frequencies of ground-state HCCSb which have already been measured using IR spectroscopy (**Table 5-3**). This excludes $X^3\Sigma^-$ as the final state of these transitions, as does the location of the progression origin which is at about 17 600 cm^{-1} or 2.18 eV; see **Table 5-4** or **Figure 5-12** for the predicted energies. A transition between two excited singlet states can be considered. This would involve the population of $1^1\Sigma^-$ by intersystem crossing from a cluster of excited triplet states ($1^3\Sigma^-$, $1^3\Sigma^+$, $1^3\Delta$), facilitated by their close proximity to $1^1\Sigma^-$. The observed progression would then correspond to the $1^1\Sigma^-$ - $1^1\Sigma^+$ system, the origin of which is predicted to be at 1.97 eV (GASCI) or 2.06 eV (FS-CCSD), not far from the measured value, given the accuracy of calculations. We did not detect any $1^1\Sigma^-$ - $1^1\Delta$ emission, although it may be masked by strong fluorescence of O_2.

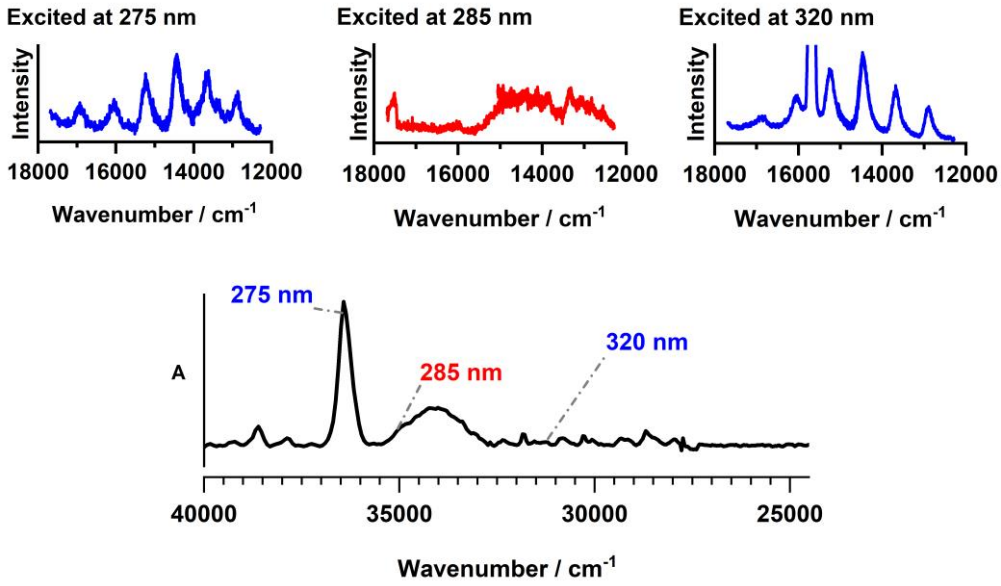

Figure 5-10. Top: Dispersed luminescence spectra measured for a sample of Ar matrix-isolated $HCCSbH_2$ which had been irradiated with a mercury lamp. **Bottom**: Same sample, the electronic absorption spectrum tentatively assigned to HCCSb; wavelengths at which luminescence was excited are indicated.

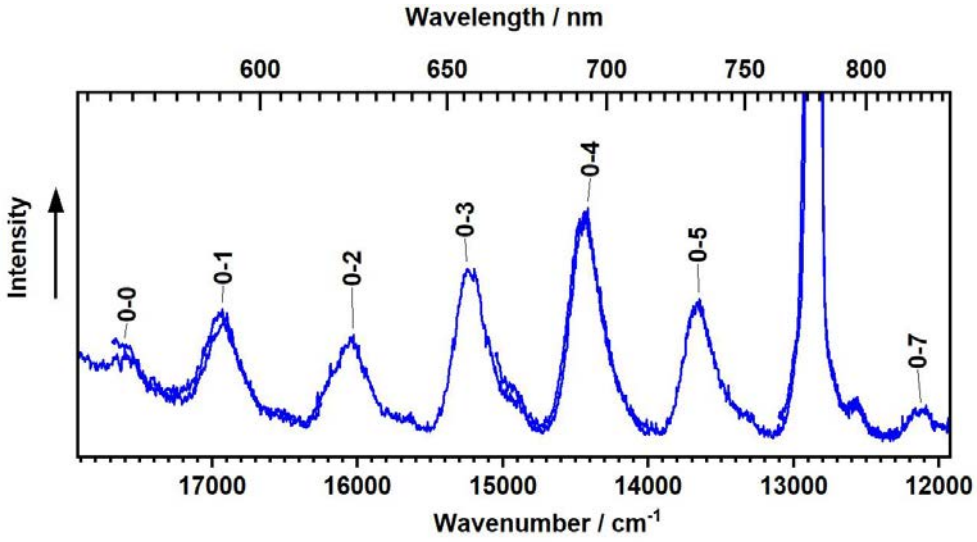

Figure 5-11. Emission L of **Figure 5-9**, tentatively assigned to HCCSb.

Time-resolved measurements, carried out by varying the delay between the excitation pulse and the detection of *L*, indicated a polyexponential decay function (**Figure 5-13**) with at least two components: 18 ± 3 μs and 220 ± 100 μs. If the proposed assignment is correct, intersystem crossing to the $1^1\Sigma^-$ singlet state from the triplets grouped around 4 eV may follow more than one pathway, reflected in luminescence decay kinetics. In other words, although a singlet-singlet luminescence

should be a fast process, the long decay time of this emission may reflect the dynamics of the intersystem crossing.

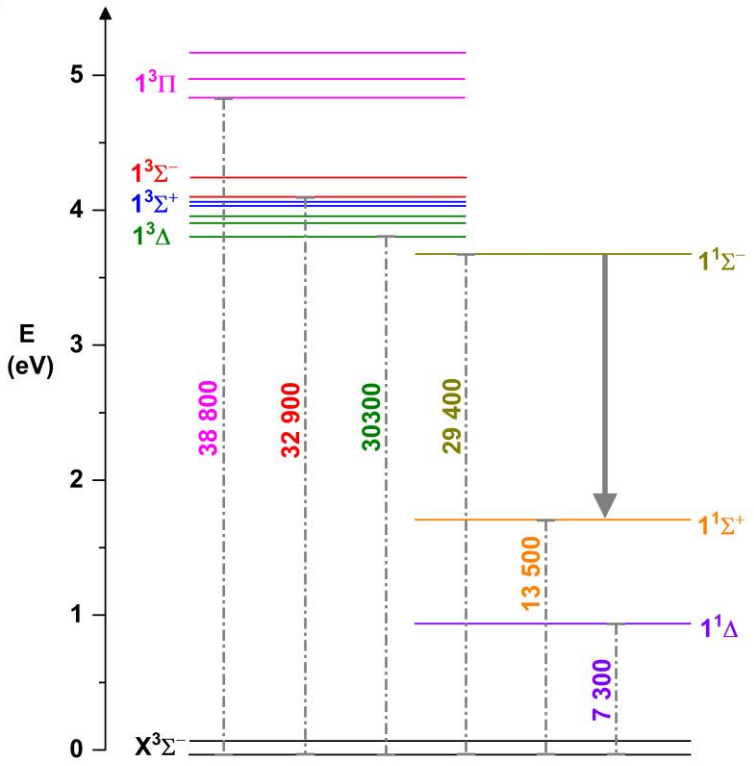

Figure 5-12. Electronic levels of HCCSb (see **Table 5-4**). Energy difference values are provided in cm^{-1}.

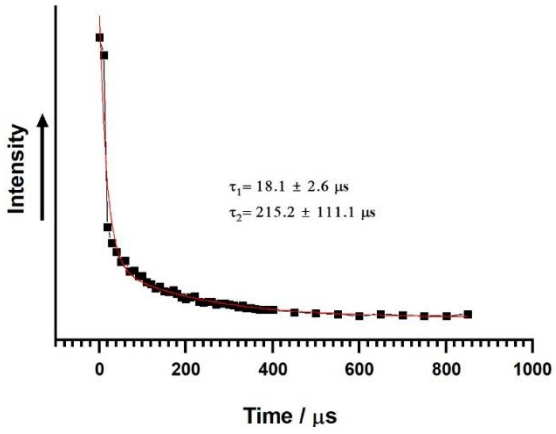

Figure 5-13. Intensity of *L* (see **Figure 5-11**) as a function of time delay between the excitation pulse and detection. Red curve represents the fitting of a biexponential decay function with the indicated τ_1 and τ_2 parameters.

Table 5-5. Vibronic progression (L; see **Figure 5-11**), tentatively assigned to the $1^1\Sigma^-$-$1^1\Sigma^+$ system of HCCSb.

Band	Wavenumber (cm^{-1})
0-0	17 660
0-1	16 900
0-2	16 030
0-3	15 260
0-4	14 440
0-5	13 670
0-6	12 940
0-7	12 170

5.3. Ethynylarsinidene (HCCAs)

HCCAs was generated in solid argon by photolyzing vinylarsine (H_2C=CH-AsH_2) at 254 nm. Its presence in the irradiated sample (see the IR spectrum of **Figure 5-14**) was confirmed based on published results (Lawzer et al., 2023). **Figure 5-15** shows electronic absorption spectra observed upon photolysis of either ethynylarsine (Lawzer et al.) or vinyl arsine and provides evidence that the same photoproduct is obtained starting from either of these precursors. Based on **Table 5-4**, the lowest excited electronic states of HCCAs are expected at energies similar to those predicted for HCCSb. The following section aims to shed light on luminescence of HCCAs which was not reported by Lawzer et al. (2023).

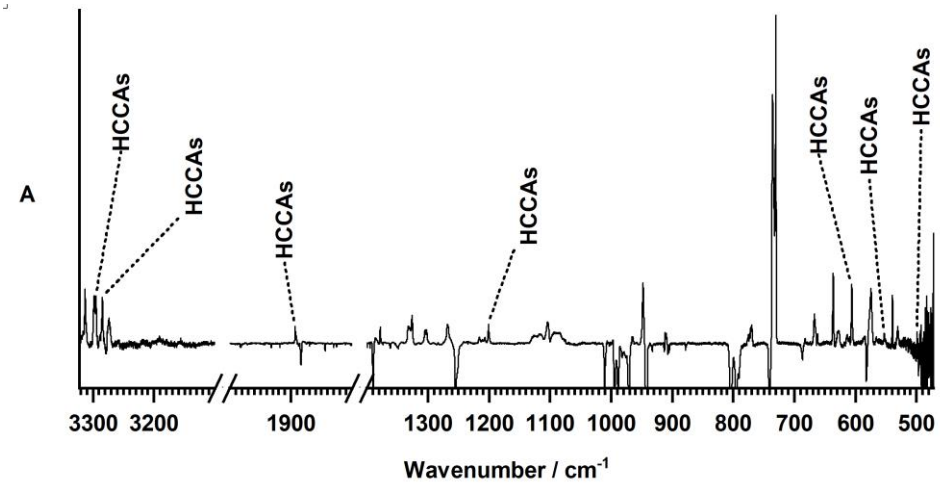

Figure 5-14. A difference spectrum (after-before-photolysis) showing the HCCAs bands generated by 1-day UV photolysis (254 nm) of vinylarsine in solid argon (courtesy of Dr. Arun-Libertsen Lawzer).

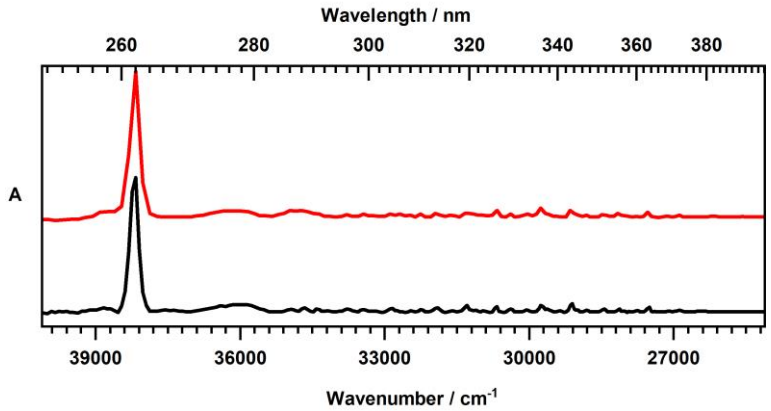

Figure 5-15. UV spectra of Ar matrix-isolated HCCAs obtained by photolyzing (254 nm) ethynylarsine (top) and vinylarsine (bottom).

5.3.1. Luminescence of HCCAs

The emission spectroscopy of HCCAs was studied using the same set-up as for HCCSb (i.e. OPO/spectrograph/CCD camera). Just as in the case of photolyzed ethynylstibinidene, fluorescence of molecular oxygen could be observed when the sample of matrix-isolated and UV-irradiated vinylarsine was excited at λ_{exc} < 280 nm (35 700 cm^{-1}). Another progression of bands (labelled *L'*) was detected. For λ_{exc} > 280 nm (see **Figure 5-16**), oxygen fluorescence disappeared leaving only *L'*. **Figure 5-17** suggests a correlation between *L'* and the UV absorption spectrum assigned to HCCAs (just as *L* was related to the absorption of HCCSb).

The regular vibronic spacing observed in *L'* (~ 900 cm^{-1}) could not be linked to any ground-state vibrational frequency of HCCAs and the presumed origin (0-0 band) of that system (23 080 cm^{-1}) does not correspond to the predicted energy gap between the ground state of HCCAs and any of the excited states (**Table 5-4** and **Figure 5-18**). Energies of the observed *L'* bands are listed in **Table 5-6**.

Time-resolved measurements revealed a biexponential decay curve with a fast component of 1.6 ± 0.3 μs and a slower one of 13.3 ± 0.3 μs (**Figure 5-19**). By analogy to what was proposed for HCCSb in **Section 5.2.3.2**, this emission may represent an electronic system linking two excited singlet states. Considering the predicted energetics, a suitable system could be $1^1\Sigma^-$-$1^1\Delta$ (**Table 5-4** and **Figure 5-18**). The DFT-computed C-C-H bending frequency of the $1^1\Delta$ state is 796 cm^{-1} (see **Table 9-8**), which lends some credence to such an assignment.

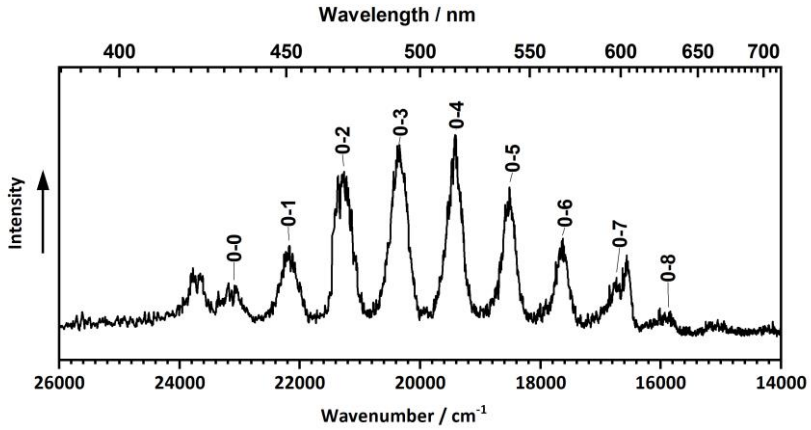

Figure 5-16. Emission *L'* tentatively assigned to HCCAs, observed by exciting (λ_{exc} = 303 nm) the sample of UV-photolyzed vinylarsine isolated in solid argon.

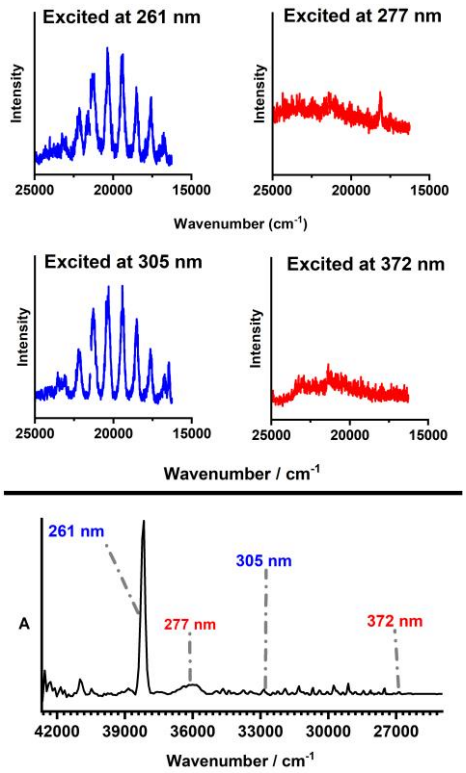

Figure 5-17. **Top**: Dispersed luminescence spectra measured for a sample of Ar matrix-isolated vinylarsine which had been irradiated with a mercury lamp. **Bottom**: Same sample, electronic absorption spectrum assigned to HCCAs; wavelengths at which luminescence was excited are indicated.

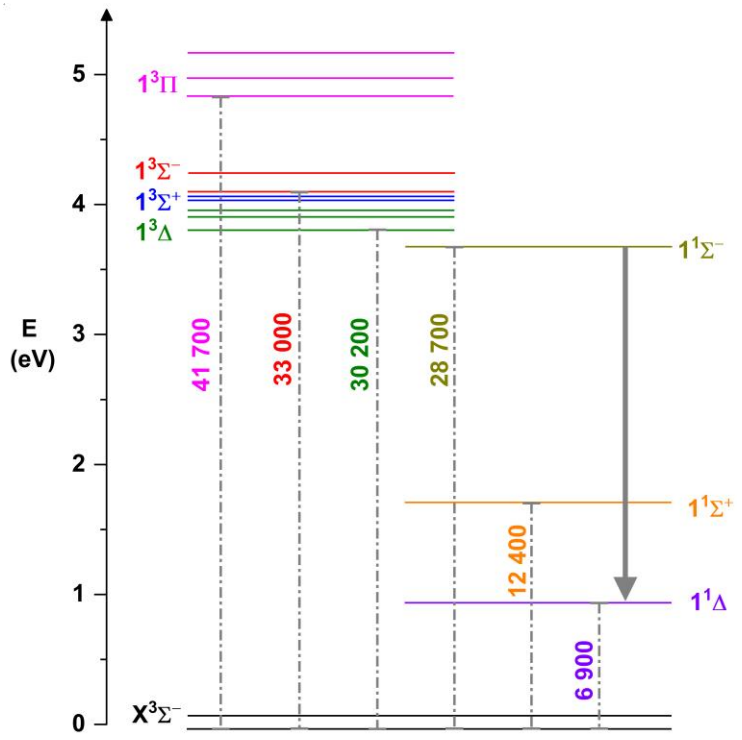

Figure 5-18. Electronic levels of HCCAs, (see **Table 5-4**). Energy difference values are provided in cm^{-1}.

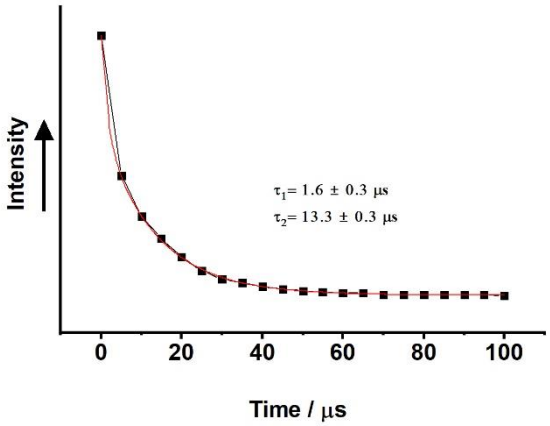

Figure 5-19. Intensity of luminescence *L'* (see **Figure 5-16**) as a function of time delay between the excitation pulse and detection. Red curve represents the fitting of a bioexponential decay function with the indicated τ_1 and τ_2 parameters.

Table 5-6. Luminescence bands of the progression tentatively assigned to the $1^1\Sigma^- - 1^1\Delta$ system of HCCAs.

Band	Wavenumber cm^{-1}
0-0	23 080
1-0	22 170
2-0	21 270
3-0	20 360
4-0	19 420
5-0	18 520
6-0	17 640
7-0	16 740
8-0	15 870

5.4. Conclusions

Photolysis of argon matrix-isolated ethynylstibine ($HCCSbH_2$) with mercury lamp (254 nm) radiation successfully generated the photodehydrogenated photoproduct, triplet ethynylstibinidene (HCCSb). This study is the first to reveal the existence of HCCSb. The compound has been characterized via IR absorption and UV/Vis (both absorption and emission) spectroscopy. Non-detection of radical intermediates (e.g. HCCSbH) suggests that two H atoms are lost in a concerted manner during the photolysis, leading directly to the formation of HCCSb. Together with earlier studies on HCCN, HCCP, and HCCAs, these findings indicate that as the pnictogen atom mass increases in the series, the acetylenic-pnictinidenic electronic structure becomes dominant. In addition to HCCSb, three photoproducts: HCCH, SbH, and CCSb were observed.

UV spectrophotometry revealed the first two excited triplet electronic states of HCCSb with an energetic pattern similar to that observed for HCCAs. The use of a tuneable laser source opened up the way to the excitation of associated electronic emissions. Vibronic progressions observed in the luminescence of products obtained by photolysis of ethynylstibine and vinylarsine can be provisionally assigned to HCCSb and HCCAs, provided that transitions between the excited singlet states of these species are assumed.* Further studies are indispensable to confirm the conjectures outlined above. These should include: (*i*) precise measurements of luminescence excitation spectra, (*ii*) advanced-level theoretical predictions of vibrational frequencies for the lowest singlet states of both compounds, and (*iii*) a search for near-IR luminescence ($1^1\Delta$ - $X^3\Sigma^-$).

* Author's search for luminescence of HCCP has not, does far, been successful.

Chapter-6

Photochemistry of propadienylphosphine (CH_2=C=CH-PH_2) in solid argon

6. Photochemistry of propadienylphosphine (CH_2=C=CH-PH_2) in solid argon

6.1. Literature overview

For more than three decades, phosphaalkynes and phosphaallenes, i.e. molecules featuring multiple carbon-phosphorous bonds, have been used as synthetic building blocks (Nakajima et al., 2015; Nixon, 1995; Regitz, 1990, 1994). Their molecular structures can be stabilized by appropriate bulky or electron-rich substituents (Appel et al., 1986; Märkl & Herold, 1988; Märkl & Reitinger, 1988). Tert-butyl-substituted phosphaethyne (3,3'-dimethylphosphabutyne; Becker et al., 1981) can serve as an example. However, in their free forms, they are typically kinetically unstable and prone to oligomerization (Albrand et al., 1975; Bergstraesser, 2005; Cohen et al., 1987; Ionkin et al., 2009). Synthesis of free phosphaalkynes and phosphaallenes is therefore challenging and studying their properties difficult. Such unstable species can sometimes be generated from less reactive precursors and studied using special techniques. The simplest of phosphaallenes, phosphapropadiene (CH_2=C=PH), was initially theorized as a likely intermediate in base-catalyzed thermal rearrangements of alkynylphosphine to phosphaalkynes (Pellerin et al., 1987). It was later reported as a product of phosphapropyne photorearrangement in solid argon (Lawzer et al., 2021). Using a combination of flow pyrolysis and microwave spectroscopy, highly reactive members of these families were generated and, from a mixture of products, information concerning individual species could be obtained, e.g. HCP, NCCP, HC_3P, and CH_2CHCP (Bizzocchi et al., 2001; Gier, 1961; Kroto et al., 1981a; Laurent et al., 1982; Ohno et al., 1981).

As pointed out in **Section 1.1**, the phosphorus-containing molecules CP, HCP, PN, PO, CCP, and (tentatively) NCCP, have been detected in the interstellar medium (Agúndez et al., 2007, 2014; Saito et al., 1989). Phosphabutadiyne (HC_3P) and vinylphosphaethyne (CH_2CHCP) – the P-bearing analogues of the prominent interstellar molecules cyanoacetylene and vinylcyanide (Sharma, 2019; Walmsley et al., 1980) – have not, thus far, been observed in space. While the microwave (purely rotational) spectra of phosphabutadiyne (HC_3P) and vinylphosphaethyne (CH_2CHCP) have been measured, laboratory investigations of their vibrational and/or electronic transitions are also of value to astrospectroscopy and astrochemistry.

Author's photochemical studies on methylpnictines (**Chapter 4**) and ethynylpnictines (**Chapter 5**) demonstrated the ease of their UV-induced dehydrogenation. In the experiments described below, a phosphaallene, namely propadienylphosphine (CH_2=C=CH-PH_2), is used as a

parent species to generate CH_2CHCP and HC_3P in inert cryogenic matrices. Additionally, the photochemistry of phosphabutyne (CH_3CH_2CP, an isomer of CH_2=C=CH-PH_2), studied in parallel to this research by Dr. Arun-Libertsen Lawzer (Lawzer et al., 2024) is discussed.

6.2. Infrared spectroscopy of propadienylphosphine

Infrared absorption of propadienylphosphine (**1**) has not been studied previously. Present spectra were interpreted with the assistance of DFT computations. Isomers **1a** and **1b** (C_1 symmetry; **Figure 6-1**) exhibit axial chirality which makes them isoenergetic, while **1c** (C_s) is just ~0.3 kcal/mol more stable. The predicted infrared frequencies of these conformers, along with their absolute intensities and possible assignments to the measured IR bands, are listed in **Table 6-1**. Experimental and theoretically predicted spectra are shown in **Figure 6-2**.

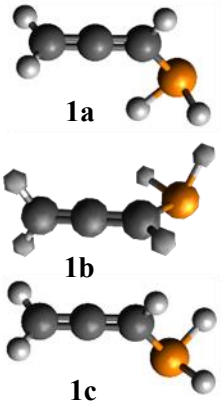

Figure 6-1 The DFT-predicted conformers of species **1**.

The IR bands of matrix-isolated **1** are split into multiplets, which may arise either from microenvironmental effects (various sites) within the matrix or from the presence of conformers. The spectrum revealed also the bands of isomeric species present as inseparable impurities: propargylphosphine ($HCCCH_2PH_2$, **2**) and, to a much lower extent, propynylphosphine (CH_3CCPH_2, **3**). Their identification is shown in **Figure 6-2** and **Figure 6-3**, respectively. The infrared spectrum of pure, Ar martrix-isolated **3**, used here to confirm the presence of this compound, was kindly supplied by Dr. Arun-Libertsen Lawzer. An estimation of the relative concentration of all three isomers showed that isomer **1** is 85 %, **2** is 10 % and **3** is 5 %.

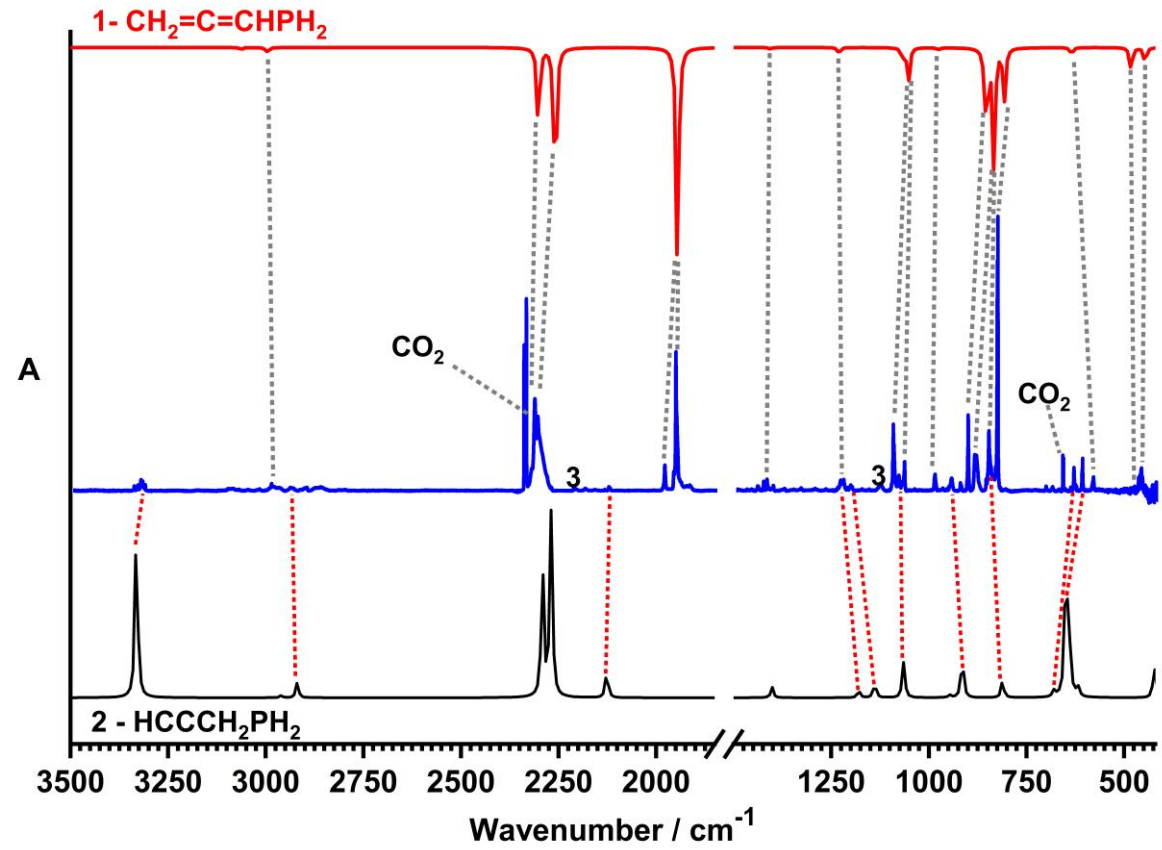

Figure 6-2. Bottom: predicted (B3LYP/aug-cc-pVTZ) infrared spectrum of **2**. **Middle:** spectrum measured for Ar matrix-isolated **1** contaminated with traces of **2** and **3**. **Top:** Predicted (B3LYP/aug-cc-pVTZ) spectrum of **1** (absorbance scale is inversed to facilitate the comparison).

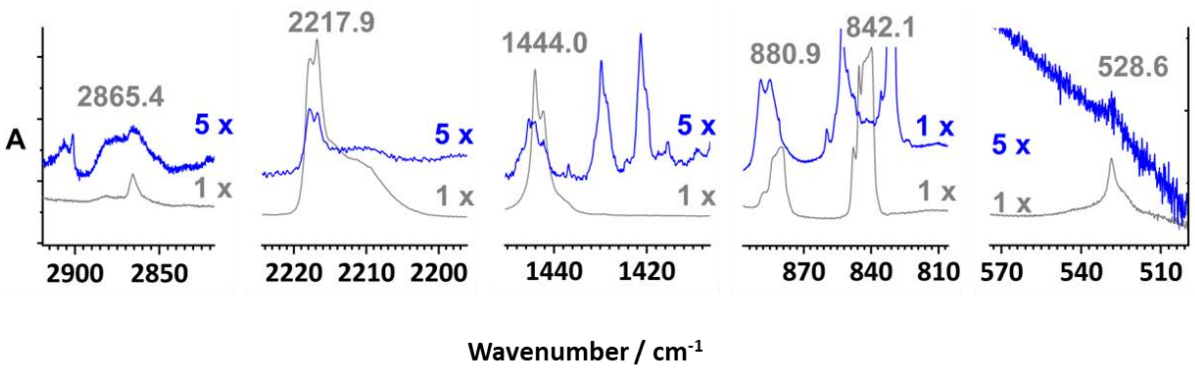

Figure 6-3. Blue: absorption spectrum measured for Ar matrix-isolated **1** contaminated with the isomeric species **2** and **3**. **Grey**: spectrum of pure **3** isolated in Ar (courtesy of Dr. Arun-Libertsen Lawzer).

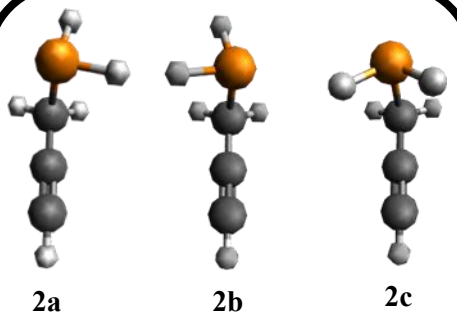

Figure 6-4. DFT predicted conformers of **2**.

The gas phase infrared spectrum of **2** has already been reported (Shay et al., 1988), which helped in identification of this species (**Table 6-2**). Similar to **1**, the observed infrared bands of **2** exhibit splitting, which could either stem from the microenvironmental effects (different sites) within the matrix or from the presence of conformers: the enantiomers **2a**, **2b** (C_1) and a C_s-symmetry species **2c** (see **Figure 6-4**).

Table 6-1. Infrared spectroscopy of propadienylphosphine **1.**

Mode	B3LYP/aug-cc-pVTZ				In solid Ar, 10 K	
	Conformers 1a & 1b		Conformer 1c		Frequency (cm^{-1})	Relative Intensity
	Frequency (cm^{-1})	Absolute intensity (km/mol)	Frequency (cm^{-1})	Absolute intensity (km/mol)		
CH stretching	3062 2999 2994	0.9 0.8 1.7	3070 3003 3000	0.2 1.4 0.2	3022.7 2992.8	1 7
PH_2 antisymmetric, stretching	2303	40.1	2265	66.1	2317.2 2310	100
PH_2 symmetric, stretching	2261	73.1	2264	73.9	2218.0	1
CC stretching	1946	105	1946	121.7	1984.9	6
					1961.7 1956.2	42
CH_2 scissoring	1406	0.7	1402	2.0	1445.1 1436.9 1429.4 1421.2	1 1 1 3
CH_2 scissoring, allene stretching, CH bending, PH_2 twisting	1230	3	1212	15.1	1232.4* 1226.9 1206.7	- 9 2
PH_2 scissoring, allene stretching, CH bending	1068	4.9	1078	12.9	1130.0 1098.1 1083.6	6 14 2
PH_2 scissoring, allene stretching	1053	16.6	1059	14.3	1069.0	8
CH_2 rocking	977	1	974	1	990.6	23
CH_2 twisting, PH_2 wagging, CH bending	857	15.1	-	-	906.0 887.3	7 21
CH_2 wagging, CH bending	851	26.01	867	39	853.4 859.7	18
CH_2 wagging	834	52.7	833	60.9	830.0	46
CH_2 twisting, PH_2 twisting	-	-	825	0.0	-	-

PH_2 wagging	809	23	826	31.9	-	-
CP stretching	634	3.3	667	0.3	706.4	1
Allene twisting	482	10.8	464	0.8	468.9	4
C-C-C bending	447	7.2	456	19.5	462.8	8
CH_2 rocking, C-C-C bending	323	8.5	340	7.3	Out of detection range	
C-C-C-P bending	166	0.2	162	1.0		
PH_2 rocking	127	5.4	110	3.4		

*) Intensity could not be determined due to the overlapping bands of other isomers.

Table 6-2. Infrared spectroscopy of propargylphosphine **2.**

Mode	B3LYP/aug-cc-pVTZ				Gas Phase (Shay et al., 1988) cm^{-1}	In solid Ar, 10 K	
	Conformers of 2a & 2b		Conformer 2c				
	Frequency (cm^{-1})	Absolute intensity (km/mol)	Frequency (cm^{-1})	Absolute intensity (km/mol)		Frequency (cm^{-1})	Relative intensity
CH stretching	3331	73.5	3331	75.3	3335	3343.9 3334.2 3326.3	7 9 5
CH_2 asymmetric Stretching	2960	0.9	2946	0.8	2933	2919.5*	-
CH_2 symmetric stretching	2919	6.4	2915	6.9			
PH_2 asymmetric stretching	2291	55.7	2298	55.3	-	-	-
PH_2 symmetric stretching	2272	78.7	2290	37.0	2301	-	-
CC stretching	2126	11.9	2123	15.7	2129	2137.4 2128.2	2 12
CH_2 scissoring	1402	4.6	1395	4.9	1418	1417.5	5
CH_2 wagging	1180	3.2	1194	0.7	1257 1243 1230	1271.1 1253.4	4
						1234.4 1225.5 1214.1	100
CH_2 twisting	1138	6.8	1160	2.5	-	-	-
PH_2 scissoring	1065	15.4	1070	12.9	1095 1083	1104.5* 1091.5*	- -
CH_2 wagging,	-	-	937	3.4	943	956.3	-

PH_2 wagging							
CH_2 wagging, PH_2 twisting	947	1.0	-	-			
CH_2 rocking, PH_2 wagging	914	19.4	-	-	-	-	-
PH_2 wagging	-	-	822	16.1	863	858.3	19
PH bending, CP stretching	812	7.8	-	-	846 833	847.0* 838.0*	- -
CH_2 rocking, PH_2 wagging	679	2.8	-	-		-	-
CH_2 twisting, PH_2 twisting	-		633	45.4		-	-
CH bending	650	43.6	652	1.1		643.3	5
CH bending	642	40.8	630	43.1		635.5	48
CP stretching, PH_2 wagging, CH bending, C-C-P bending	-	-	609	6.7	628	613.1	47
CP stretching, PH_2 twisting, CH bending, C-C-P bending	618	4.4	-	-			
CH_2 wagging, CP stretching, PH2 wagging, C-C-C bending	-	-	432	14.4	432	-	-
CH_2 wagging, PH bending, C-C-C bending	423	14.1	-	-			
CH_2 rocking, PH_2 rocking, C-C-C bending	333	9.2	333	10.4	-	Out of detection	
PH_2 rocking C-C-P bending	167	2.3	169	1.9	-		
PH_2 rocking, CCP bending	142	1.2	-	-	-		
PH_2 wagging, C-C-P bending	-	-	164.	0.1	-		

-intensities couldn't be determined due to overlapping peaks of isomers **1 or **3**.*

6.3. Photochemistry 254 nm

The electronic absorption spectrum of matrix-isolated **1** (with trace **2** and **3**) revealed a broad, weak mid-UV absorption band extending into the 250 nm region (**Figure 6-5**). This feature was targeted for photolysis by using a low-pressure Hg lamp (254 nm).

Based on previous studies of photolysis of methylpnictines and ethynylpnictines, we expect both isomerization and dehydrogenation processes to be operative for **1** with potential C-C bond cleavage. The increasing concentration of isomer **2** shows that isomerization indeed occurs. Photolysis of CH_3PH_2 and CH_3AsH_2 with 254 nm (**Chapter 4**) resulted primarily in double H_2 elimination (ultimately producing HCP and HCAs). A similar loss of H atoms (one or two H_2 molecules) from **1** (also **2** or **3**) might generate phosphabutadiyne (HC_3P), a cyanoacetylene

analogue of potential astrochemical significance whose IR signature has not yet been measured. While no member of the C_3H_3P family (single dehydrogenation) could be detected upon photolysis of **1** using 254 nm light, the doubly dehydrogenated HC_3P species was observed. Coupled-cluster- (Bizzocchi et al., 2000) and DFT-predicted infrared frequencies of HC_3P assisted in the interpretation of experimental data (**Figure 6-6**). One difficulty in identifying this species was the overlap between the HC_3P bands and those of the (growing) isomer **2** (this was overcome by applying VUV photolysis; see **Section 6.4**). In the case of 254 nm irradiation, the concentration of HC_3P increased almost linearly with time, as shown in **Figure 6-7**.

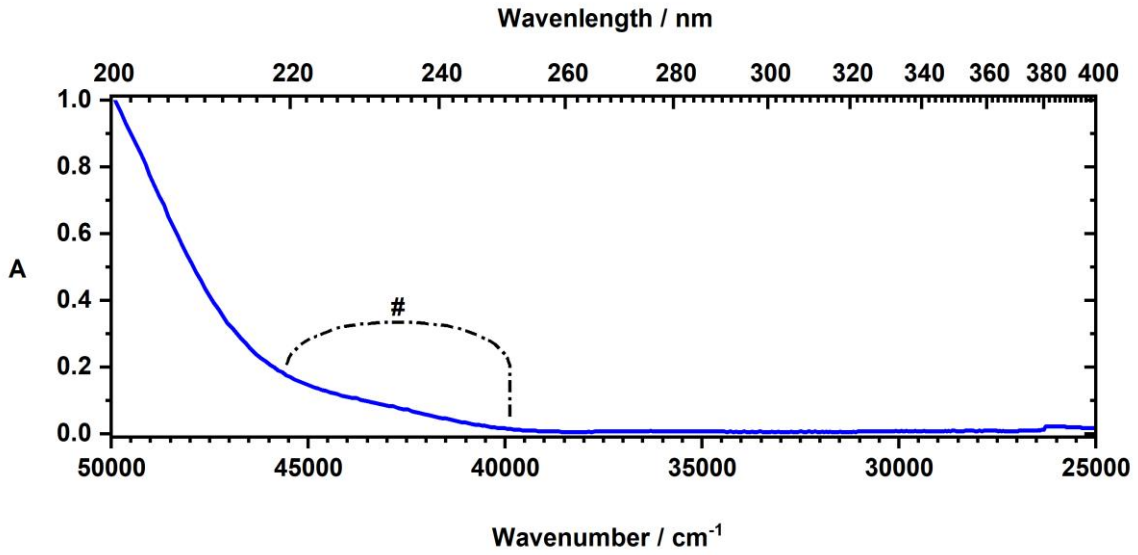

Figure 6-5. UV spectrum of the mixture of isomers **1, 2** and **3** isolated in solid argon tentatively revealing, apart from the scattering, a weak, broad absorption band within the 220-250 nm region (marked as #). No absorption was detected in the visible region.

The C-C bond cleavage products HCP and HCCP were also found. The strong IR absorption bands of HCP, observed at 675.1 cm^{-1}, 681 cm^{-1} and 686 cm^{-1}, were already known from our investigations of the pure substance isolated in solid Ar (**Section 3.2**). Given that HCP is present, it is rational to expect 2-carbon molecules like ethylene or acetylene as complementary photofragments. Bands observed at 731 cm^{-1} and 3270 cm^{-1} can, in fact, be attributed to the C-H bending and stretching vibrational modes of HCCH. However, there was no evidence for the presence of ethylene.

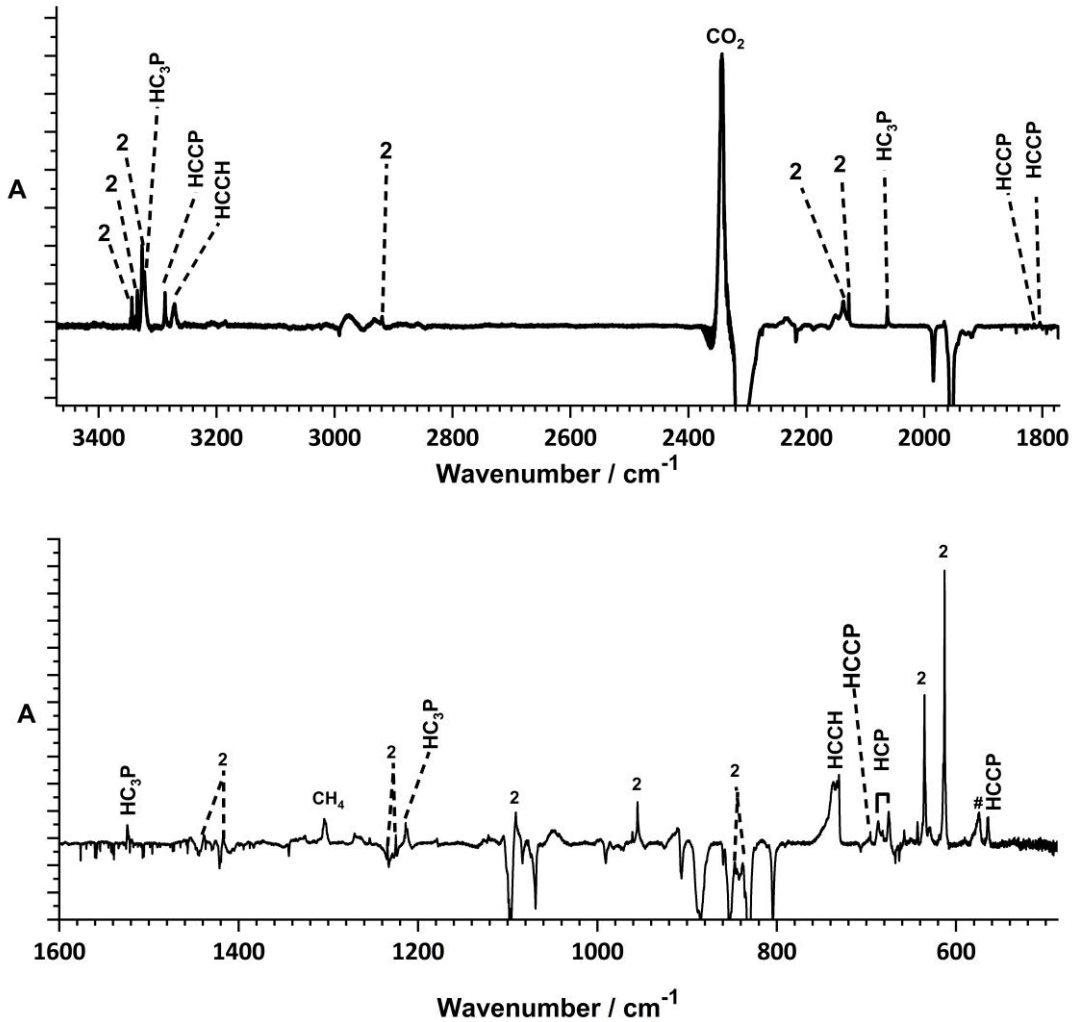

Figure 6-6. Low- and high-wavenumber parts of a baseline-corrected difference spectrum (after-minus-before irradiation) obtained for Ar matrix-isolated propadienylphosphine subjected to 4 days of 254 nm photolysis. An artifact feature originating in the substrate window is marked with #.

The formation of ethynylphosphinidene (HCCP) among the photolysis products could also be firmly confirmed using the reported IR band frequencies of this molecule at 564.7, 696.1, 1807.9, 1814.2, and 3287.8 cm^{-1} (Lawzer et al., 2021). The values reported by Lawzer et al. differ very slightly from those observed following photolysis of **1**, namely: 564.6, 695.8, 1804.3, 1814.3, and 3287.3 cm^{-1}. This is presumably due to differences in the matrix microenvironment of the precursor used in each study which can affect the arrangement of

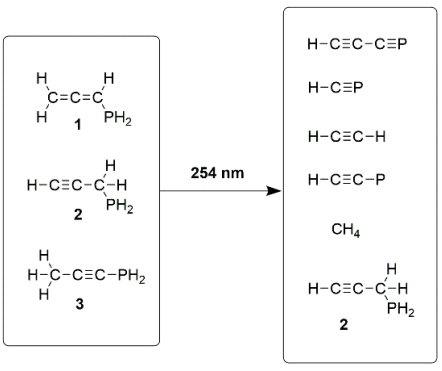

Scheme 6-1. Parent compounds subjected to mercury lamp (254 nm) irradiations and the resultant photoproducts.

photoproducts. Formation of HCCP implies loss of CH_4 from **1**. Methane is therefore expected as a product associated with HCCP. A sharp peak at 1304 cm^{-1} proves its presence. Summing up, the identified photolysis products, apart from species **2**, are HC_3P, HCP, HCCH, HCCP, and CH_4 (see **Scheme 6-1**). The time evolutions of these species, monitored during the photolysis with IR spectroscopy, are shown in **Figure 6-7**.

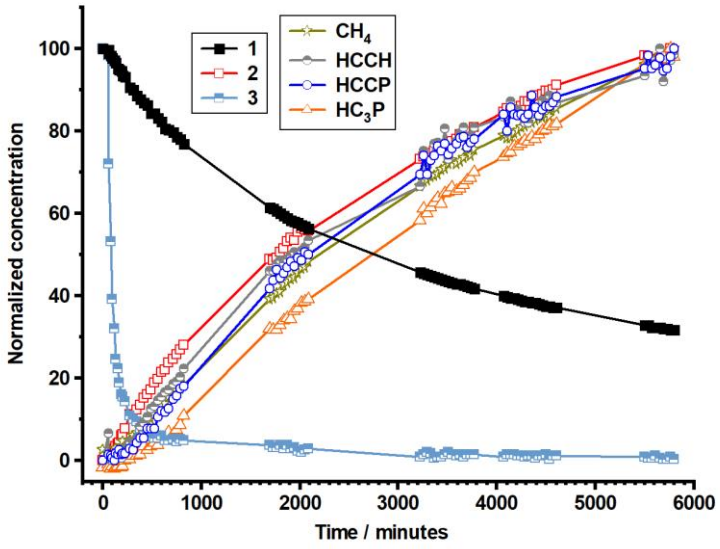

Figure 6-7. Evolution of precursor and product IR absorption band intensities over the course of 254 nm photolysis of propadienylphosphine (**1**, contaminated with traces of **2** and **3**). The monitored bands were: 1956.2 cm^{-1} (**1**), 613.1 cm^{-1} (**2**), 2217.9 cm^{-1} (**3**), 1304 cm^{-1} (CH_4), 3270 cm^{-1} (HCCH), 3287.3 cm^{-1} (HCCP), and 2063 cm^{-1} (HC_3P).

6.4. Photochemistry at 150-190 nm

When an Ar matrix containing **1** (with trace **2** and **3**) was subjected to VUV radiation (150 to 190 nm) of a Xe lamp, all three parent compounds were decomposed and no other C_3H_5P isomers were formed. HC_3P appeared prominently (**Figure 6-8**, **Table 6-3**), along with the single dehydrogenation product, vinylphosphaethyne (H_2C=C(H)-C≡P) which was not detected upon 254 nm irradiation of the sample. The infrared absorption bands of vinylphosphaethyne,

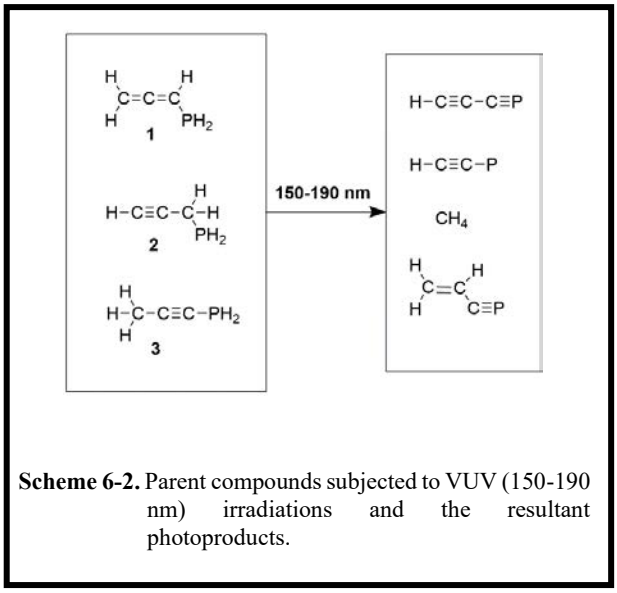

Scheme 6-2. Parent compounds subjected to VUV (150-190 nm) irradiations and the resultant photoproducts.

never reported before, are now assigned based on DFT calculations (**Figure 6-9**, **Table 6-4**). The HC_3P spectrum obtained with VUV photolysis was much cleaner than that observed upon 254-nm irradiation, because the overlapping contributions from the C_3H_5P isomers were eliminated.

While the spectroscopic signatures of neither HCP (675 cm^{-1}) nor acetylene (731 cm^{-1}) were detected, weak bands of HCCP and methane appeared. The observed products of VUV irradiations are summarized in **Scheme 6-2**. Several unassigned, broad spectral features are most likely due to aggregated or polymerized substances.

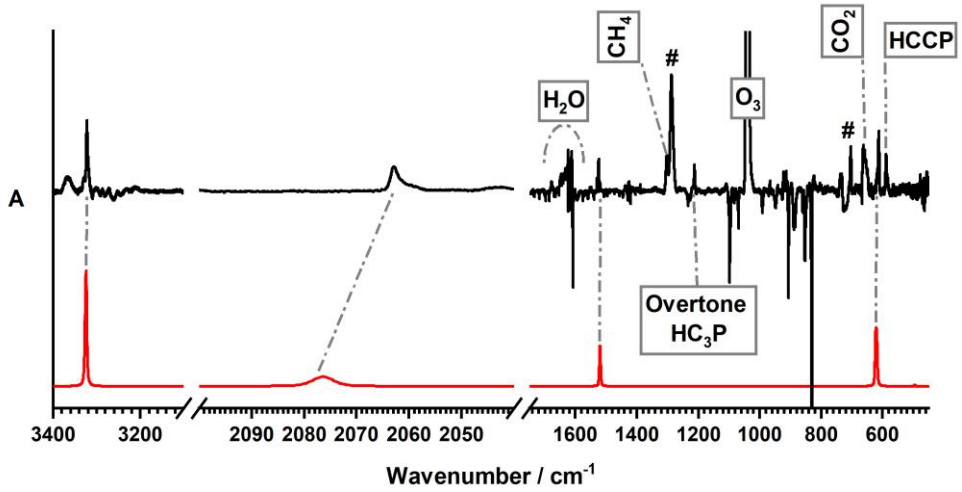

Figure 6-8. **Black**: difference spectrum (after-minus-before irradiation) for Ar matrix-isolated compound **1** (contaminated with traces of **2** and **3**) subjected to VUV xenon lamp (150-190 nm) photolysis. **Red**: B3LYP/aug-cc-pVTZ-predicted IR absorption of HC_3P.

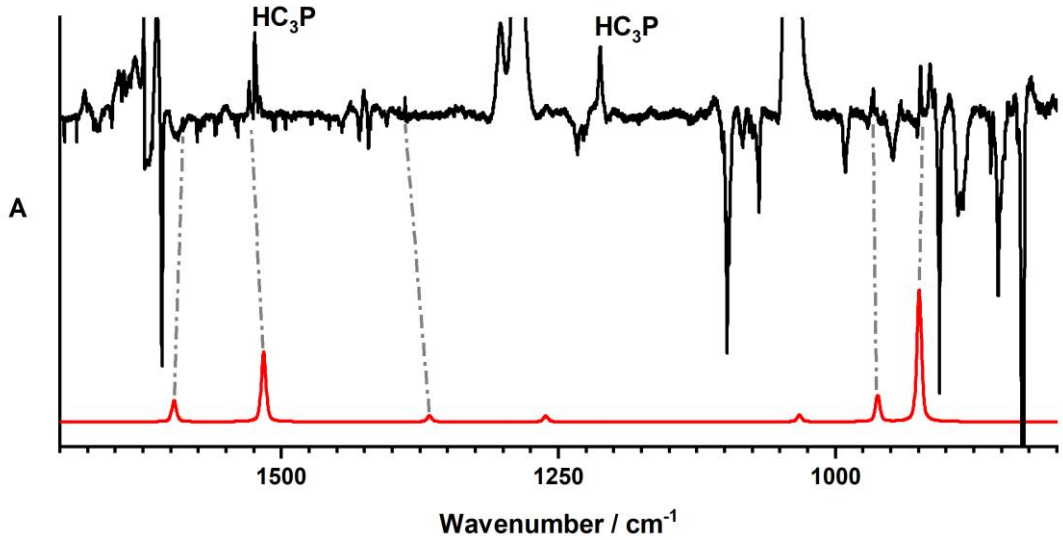

Figure 6-9. Top: difference spectrum (after-minus-before irradiation) obtained for Ar matrix-isolated compound **1** (contaminated with traces of **2** and **3**) subjected to VUV xenon lamp (150-190 nm) photolysis. **Bottom**: B3LYP/aug-cc-pVTZ-predicted IR absorption of vinylphosphaethyne.

Table 6-3. Infrared spectroscopy of HC_3P.

Mode	CCSD(T))/cc-pVQZ [a] (Bizzocchi et al., 2000)	VPT2//B3LYP/aug-cc-pVTZ unharmonic (Lawzer et al., 2024)		B3LYP/aug-cc-pvtz [b] (this work)		In solid Ar [c]	
	Vibrational frequency (cm^{-1})	Vibrational frequency (cm^{-1})	Absolute intensity (km/mol)	Vibrational frequency (cm^{-1})	Absolute intensity (km/mol)	Vibrational frequency (cm^{-1})	Relative Intensity
C-H stretching (ν_1)	3453	3337.7	113.6	3325	102.2	3322.9	100
C-C-stretching (ν_2)	2111	2119.5	12.1	2076	8.7	2063	17
C-P stretching (ν_3)	1544	1563.1	91.2	1520	35.8	1524.0	6
Overtone ($2\nu_5$)	-	1276.6 1255.5	93.8 46.9	-	-	1212.2	16
HCCCP stretching (ν_4)	687	708.7	0.8	680	0.2	-	-
C-H bending (ν_5)	621	635.0	513.8	622 619	40.3 36	614.8 613.8 611.8	76
pseudo-antisymmmetric CCCP chain bending (ν_6)	479	514.0	5.4	496	0.8	Out of detection	
pseudo-symmmetric CCCP chain bending (ν_7)	192	205.4	152.1	196	8		

a) Unscaled harmonic values.
b) Harmonic values, scaling factor 0.96
c) The most reliable measurements (presented here) were carried out for HC_3P generated with VUV radiation.

Table 6-4. Infrared spectroscopy of vinylphosphaethyne

Mode	B3LYP/aug-cc-pVTZ		Ar matrix, 10 K	
	Vibrational frequency (cm^{-1})	Absolute intensity (km/mol)	Vibrational frequency (cm^{-1})	Relative intensity
CH_2 symmetric and antisymmetric stretching	3108	3.5	-	-
	3023	3.3	-	-
CH stretching	2996	3.4	-	-
C-C stretching	1597	7.3	1589.5	29
C-P stretching	1516	23.9	1529.8	82
CH_2 scissoring	1366	2.2	1385.2*	10
CH bending (in-plane)	1262	2.1	-	-
CH_2 rocking	1033	2.4	-	-
CH_2 and CH twisting	962	9	967.4	64
CH_2 wagging	924	44.8	923.8	100
CH bending (in-plane)	720	1.4	-	-
CH bending (out-of-plane)	661	0.8	-	-
C-C-P bending	506	9.6	478.2	40

*-tentative assignment

6.5. Comparison with CH_3CH_2CP photolysis

In parallel with the experiments described here, Dr. Arunlibertsen Lawzer of IPC PAS explored the 254 nm and VUV photolysis of phosphabutyne, CH_3CH_2CP (Lawzer et al., 2024). The UV (254-nm) irradiation of CH_3CH_2CP produced the isomers **1**, **2**, **3**, $HC{\equiv}CPHCH_3$ (**4**), $CH_2{=}C{=}PCH_3$ (**5**), $CH_3CH{=}C{=}PH$ (**6**), as well as $CH_2{=}CHCP$ (**7**), HCCP, HCP, ethylene, and acetylene along with HC_3P*. In a provisional mechanism (**Scheme 6-3**), CH_3CH_2CP serves as the direct precursor of H_2CCH_2/HCP, while HC_3P and HCCH/HCP are likely formed from **3** (CH_3-CC-PH_2) via **7** (vinylphosphaethyne, H_2CCHCP) as an intermediate. According to this scheme, formation of **4**, **5**, and **6** could be due to H-atom and CH_3-group migrations towards the phosphorus center of CH_3CH_2CP. Finally, the HCCP/CH_4 pair forms from **4**.

Currently photolyzed isomers **1**, **2,** and **3** share an important feature that sets them apart from CH_3CH_2CP: a saturated phosphorous centre (the -PH_2 group). This saturation may help explain why the 254 nm-induced isomerization through migration of molecular fragments to the phosphorous atom (to form **4** or **5**) is presently less likely than it was for CH_3CH_2CP. The present lack of ethylene among the products is consistent, within the **Scheme 6-3**, with the absence of CH_3CH_2CP. However, the HC_3P/H_2, HCP/HCCH, and HCCP/CH_4 pairs are formed by the 254 photolysis of **1** (with trace **2** and **3**), even though species **7** and **4** are absent. This suggests that the photoreaction scheme recently proposed for the photolysis of CH_3CH_2CP is not complete. However, a credible completion of this scheme would require advanced quantum chemical calculations of the excited-state potential energy surface and/or further experiments with the specific isomers used as precursors.

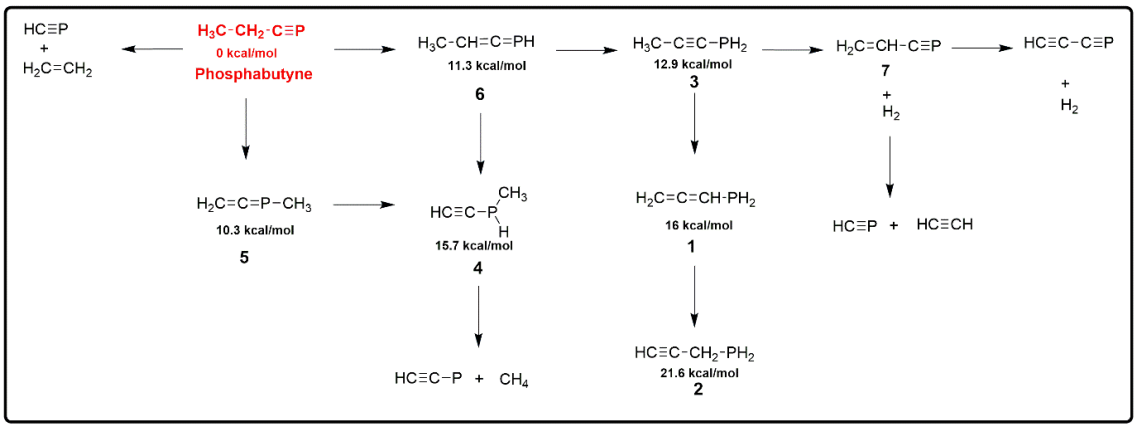

Scheme 6-3. Tentative reaction scheme for the photolysis (254 nm) of phosphabutyne isolated in solid argon. The indicted B3LYP/aug-cc-pVTZ-predicted electronic energy values (Lawzer 2024) are relative, with respect to phosphabutyne.

* The vibrational frequencies of HC_3P measured upon photolysis of CH_3CH_2CP are in exact agreement with those obtained presently with **1** (with trace **2** and **3**) as the parent.

6.6. Conclusions

The 254-nm photolysis of an Ar matrix-isolated mixture of C_3H_5P-stoichiometry isomers propadienylphosphine (**1**, ~85%), propargylphosphine (**2**, ~10%), and propynylphosphine (**3**, ~5%) yields H-C≡C-C≡P, H_2C=C(H)-C≡P, H-C≡P, H-C≡C-H, H-C≡C-P, CH_4, and increases the concentration of **2**. Vacuum-UV photolysis (150-190 nm) decreases the amount of all three initial species, and produces no HCP, HCCH, nor any isomers of the parents. Phosphabutadiyne, HC_3P, is the main photoproduct of the VUV photolysis. Five IR bands of this phosphorus-bearing analogue of cyanoacetylene (HC_3N) have been observed. Spectral signatures of vinylphosphaethyne (H_2C=CHCP) and HCCP + methane (weaker than in the case 254-nm photolysis) were also detected following VUV irradiations. Vinylphosphaethyne, generated via elimination of hydrogen from a C_3H_5P-stoichiometry precursor, is a plausible parent (via further dehydrogenation) to HC_3P. The IR spectra of astrochemically relevant molecules HC_3P and H_2C=CHCP have been measured and analyzed here for the first time.

Chapter 7

Conclusion and future outlook

7. Conclusion and future outlook

7.1. Original research objectives vs. key findings

Goal 1: *Fine-tuning the preparative organic synthesis of pure HCP. If successful, description of the photochemistry of HCP in solid argon.*

Key findings (Chapter 3):

HCP, the heavier analogue of hydrogen cyanide, was successfully synthesized and its vibrational spectroscopy studied in a solid argon. A hydrogen bond interaction between HCP and H_2O was identified via IR absorption for the first time.

UV photolysis of HCP produced CP as the sole detectable photoproduct, enabling the first-ever cryogenic isolation and spectroscopic analysis of CP. Fluorescence from the $B^2\Sigma^+$—$X^2\Sigma^+$ and $B^2\Sigma^+$—$A^2\Pi_i$ systems was observed. Unexpectedly, a very rare case of quartet–doublet phosphorescence was discovered and new electronic systems of CP were described: $a^4\Sigma^+$—$X^2\Sigma^+$ and $a^4\Sigma^+$—$A^2\Pi_i$). The measured quartet state lifetime is 0.1 s.

Goal 2: *Description of differences in photolyzes of the methylpnictines CH_3PH_2, CH_3AsH_2, and CH_3SbH_2. How do these compare to methylamine, CH_3NH_2? Spectroscopic characterization of the respective photoproducts.*

Key findings (Chapter 4):

CH_3PH_2 and CH_3AsH_2, displayed similar photochemical behavior under VUV irradiations, yielding CH_2XH (X represents P or As), HCX, CH_4, and diatomic products (CX, XH). Secondary UV photolysis (254 nm) destroyed CH_2XH with no evidence of monovalent (CH_3-X) or pentavalent (CH_2=XH_3) intermediates.

In contrast, CH_3SbH_2 underwent dehydrogenation to form CH_3-Sb, an exotic compound of monovalent antimony. Cleavage of the C-Sb bond produced SbH and CH_4, a process more efficient than in CH_3PH_2 and CH_3AsH_2.

The photochemistry of methylphosphine and methylarsine in an argon matrix was found to be similar to the methylamine photochemistry, whereas methylstibine followed a different photochemical pathway.

Goal 3: *Finding whether the ethynylstibinidene, HCCSb, can be obtained in a rare gas matrix following the photodehydrogenation route already explored for ethynylarsinidene, HCCAs, and ethynylphosphinidene, HCCP. If successful, spectroscopic (IR and UV/Vis absorption) characterization of HCCSb, as well as the search for electronic luminescence of HCCSb, HCCAs, and HCCP.*

Key findings (Chapter 5):

Photolysis of $HCCSbH_2$ successfully yielded HCCSb, marking its first experimental detection. IR- and UV/Vis-spectroscopic characterization was performed. Luminescence studies revealed electronic emission for both HCCSb and HCCAs, attributed to the radiative relaxation between two singlet excited states. Further experimental and theoretical studies are needed to validate this assignment.

Goal 4: *Attempt to obtain phosphabutadiyne, HC_3P, by photodehydrogenation of a suitable precursor (reported spectroscopy of HC_3P being limited to the radio frequency range). If successful, spectroscopic characterization of this phosphorous-bearing analogue of cyanoacetylene.*

Key findings (Chapter 6):

UV photolysis of propadienylphosphine and its isomers yielded HC_3P together with CH_2=CHCP, HCP, HCCH, HCCP, and CH_4, while VUV irradiations primarily produced HC_3P. Five IR bands of HC_3P were recorded for the first time, along with signatures of vinylphosphaethyne (a possible direct HC_3P precursor) and HCCP. These findings are of relevance to astrochemistry of phosphorus-bearing species.

7.2. Future outlook

Several aspects of the research lines presented in this dissertation remain open to further exploration:

1. **Astrochemical relevance of HCP and HC_3P:** Concentration-dependent studies of intermolecular interactions and radiation-induced reactions of HCP or HC_3P with molecules like acetylene, hydrogen cyanide, carbon monoxide, ammonia, water, etc. should deepen our understanding of the first stages of chemical evolution ultimately leading to biomolecules. Targeted experiments to assess the possibility of HC_3P formation in analogues of icy dust grains may be helpful in detecting this molecule in astrophysical environments.

2. **Theoretical insights into methylpnictine photochemistry:** Advanced theoretical studies are needed to clarify the observed similarities and differences in the photochemical behavior of methylpnictines, particularly the stand-out case of methylstibine.

3. **Luminescence of pnictinidenes:** Reliable theoretical predictions of excited-state potential energy surfaces will assist in (thus far only tentative) interpretation of the detected luminescence spectra of HCCSb and HCCAs.

The Author hopes that his doctoral dissertation provides useful information on the photochemistry and spectroscopy of kinetically unstable pnictogen-containing molecules, also paving the way for further research in this direction.

8. References

A. K. Chaudhury & K. N. Upadhya. (1969). $^2\Sigma^+$-$^2\Pi$ Band System in CP Molecule. *Indian J. Phys*, *43*, 83–91.

Abbiche, K., Marakchi, K., Komiha, N., Francisco, J. S., Linguerri, R., & Hochlaf, M. (2014). Accurate theoretical spectroscopy of the lowest electronic states of CP radical. *Molecular Physics*, *112*(20), 2633–2645. https://doi.org/10.1080/00268976.2014.901567

Agúndez, M., Cernicharo, J., & Guélin, M. (2007). Discovery of Phosphaethyne (HCP) in Space: Phosphorus Chemistry in Circumstellar Envelopes. *The Astrophysical Journal*, *662*(2), L91–L94. https://doi.org/10.1086/519561

Agúndez, M., Cernicharo, J., & Guélin, M. (2014). New molecules in IRC +10216: confirmation of C_5S and tentative identification of MgCCH, NCCP, and SiH_3 CN. *Astronomy & Astrophysics*, *570*, A45. https://doi.org/10.1051/0004-6361/201424542

Ahn, D.-S., Lee, J., Choi, J.-M., Lee, K.-S., Baek, S. J., Lee, K., Baeck, K.-K., & Kim, S. K. (2008). State-selective predissociation dynamics of methylamines: The vibronic and H/D effects on the conical intersection dynamics. *The Journal of Chemical Physics*, *128*(22). https://doi.org/10.1063/1.2937451

Ahn, D.-S., Lee, J., Choon Park, Y., Sup Lee, Y., & Kyu Kim, S. (2012). Nuclear motion captured by the slow electron velocity imaging technique in the tunnelling predissociation of the S1 methylamine. *The Journal of Chemical Physics*, *136*(2). https://doi.org/10.1063/1.3675566

Akimov, A. V., Ganushevich, Y. S., Korchagin, D. V., Miluykov, V. A., & Misochko, E. Y. (2017). The EPR Spectrum of Triplet Mesitylphosphinidene: Reassignment and New Assignment. *Angewandte Chemie International Edition*, *56*(27), 7944–7947. https://doi.org/10.1002/anie.201703629

Albrand, J. P., Anderson, S. P., Goldwhite, H., & Huff, L. (1975). Electric discharge synthesis of phosphorus compounds. *Inorganic Chemistry*, *14*(3), 570–573. https://doi.org/10.1021/ic50145a025

Alpher, R. A., Bethe, H., & Gamow, G. (1948). The Origin of Chemical Elements. *Physical Review*, *73*(7), 803–804. https://doi.org/10.1103/PhysRev.73.803

Appel, R., Winkhaus, V., & Knoch, F. (1986). Niederkoordinierte Phosphor-Verbindungen, 48. Synthese von 1-Phosphaallenen. *Chemische Berichte*, *119*(8), 2466–2472. https://doi.org/10.1002/cber.19861190807

Ashfold, M. N. R., Dixon, R. N., Kono, M., Mordaunty, D. H., & Reed, C. L. (1997). Near ultraviolet photolysis of ammonia and methylamine studied by H Rydberg atom photofragment translational spectroscopy. *Philosophical Transactions of the Royal Society of*

London. Series A: Mathematical, Physical and Engineering Sciences, *355*(1729), 1659–1676. https://doi.org/10.1098/rsta.1997.0082

Bärwald, H., Herzberg, G., & Herzberg, L. (1934). Bandenspektrum und Struktur des CP-Moleküls. *Annalen Der Physik*, *412*(6), 569–593. https://doi.org/10.1002/andp.19344120602

Beck, C., Schinke, R., & Koput, J. (2000). Vibrational spectroscopy of phosphaethyne (HCP). I. Potential energy surface, variational calculations, and comparison with experimental data. *The Journal of Chemical Physics*, *112*(19), 8446–8457. https://doi.org/10.1063/1.481483

Becker, G., Gresser, G., & Uhl, W. (1981). Acyl-und Alkylidenphosphane, XV 2.2-Dimethylpropylidinphosphan, eine stabile Verbindung mit einem Phosphoratom der Koordinationszahl 1/ Acyl- and Alkylidenephosphines, XV 2,2-Dimethylpropvlidynephosphine, a Stable Compound with a Phosphorus Atom of Coordination Number 1. *Zeitschrift Für Naturforschung B*, *36*(1), 16–19. https://doi.org/10.1515/znb-1981-0105

Bergstraesser, U. (2005). Phosphaalkynes (Alkylidynephosphines). *ChemInform*, *36*(41). https://doi.org/10.1002/chin.200541257

Bizzocchi, L., Degli Esposti, C., & Botschwina, P. (2000). Millimeter-wave spectroscopy of HC3P isotopomers and coupled-cluster calculations: the molecular structure of phosphabutadiyne. *Chemical Physics Letters*, *319*(3–4), 411–417. https://doi.org/10.1016/S0009-2614(00)00140-8

Bizzocchi, L., Esposti, C. D., Dore, L., & Puzzarini, C. (2005). Lamb-dip millimeter-wave spectroscopy of HCP: Experimental and theoretical determination of ^{31}P nuclear spin–rotation coupling constant and magnetic shielding. *Chemical Physics Letters*, *408*(1–3), 13–18. https://doi.org/10.1016/j.cplett.2005.03.134

Bizzocchi, L., Thorwirth, S., Müller, H. S. P., Lewen, F., & Winnewisser, G. (2001). Submillimeter-Wave Spectroscopy of Phosphaalkynes: HCCCP, NCCP, HCP, and DCP. *Journal of Molecular Spectroscopy*, *205*(1), 110–116. https://doi.org/10.1006/jmsp.2000.8234

Botschwina, P., Pecul, K., & Preuss, H. (1975). An ab initio Calculation of the Force Constants, Vibrational Frequencies, and Equilibrium Geometry of HCP. *Zeitschrift Für Naturforschung A*, *30*(8), 1015–1017. https://doi.org/10.1515/zna-1975-0815

Bredenbeck, J., Beck, C., Schinke, R., Koput, J., Stamatiadis, S., Farantos, S. C., & Joyeux, M. (2000). The vibrational spectrum of deuterated phosphaethyne: A quantum mechanical, classical, and semiclassical analysis. *The Journal of Chemical Physics*, *112*(20), 8855–8865. https://doi.org/10.1063/1.481500

Bruna, P. J., Krumbach, V., & Peyerimhoff, S. D. (1985). Vertical electronic spectra of the isovalent molecules H_2CNH, H_2SiNH, H_2CPH, and H_2SiPH on the basis of MRD-CI calculations. *Canadian Journal of Chemistry*, *63*(7), 1594–1608. https://doi.org/10.1139/v85-270

Burbidge, E. M., Burbidge, G. R., Fowler, W. A., & Hoyle, F. (1957). Synthesis of the Elements in Stars. *Reviews of Modern Physics*, *29*(4), 547–650. https://doi.org/10.1103/RevModPhys.29.547

Cabana, A., Doucet, Y., Garneau, J.-M., Pépin, C., & Puget, P. (1982). The vibration-rotation spectrum of methinophosphide: The overtone bands $2\nu_1$ and $2\nu_3$, the summation bands $\nu_1 + \nu_2$ and $\nu_2 + \nu_3$, and the difference band ν_1-ν_2. *Journal of Molecular Spectroscopy*, *96*(2), 342–350. https://doi.org/10.1016/0022-2852(82)90198-9

Cabana, A., Savitsky, G. B., & Hornig, D. F. (1963). Vibration—Rotation Spectra of CH_4 and CD_4 Impurities in Xenon, Krypton, and Argon Crystals. *The Journal of Chemical Physics*, *39*(11), 2942–2950. https://doi.org/10.1063/1.1734127

Cachón, J., Recio, P., Zanchet, A., Marggi Poullain, S., & Bañares, L. (2023). Photodissociation dynamics of methylamine in the blue edge of the A-band. II. The $NH_2 + CH_3$ channel. *Journal of Chemical Physics*, *159*(6). https://doi.org/10.1063/5.0159855

Callomon, J. H., & Davey, A. B. (1963). Rotational Analysis of the 3000 Å Absorption System of Cyanogen, C_2 N_2. *Proceedings of the Physical Society*, *82*(2), 335-336–1. https://doi.org/10.1088/0370-1328/82/2/123

Carey, N. A. D., Meinema, H. A., & Noltes, J. G. (1968). Infrared and hydrogen-1 nuclear magnetic resonance spectra of the methylstibines. *Inorganic Chemistry*, *7*(12), 2643–2645. https://doi.org/10.1021/ic50070a036

Chantzos, J., Rivilla, V. M., Vasyunin, A., Redaelli, E., Bizzocchi, L., Fontani, F., & Caselli, P. (2020). The first steps of interstellar phosphorus chemistry. *Astronomy & Astrophysics*, *633*, A54. https://doi.org/10.1051/0004-6361/201936531

Chen, Y., Watt, D. M., Field, R. W., & Lehmann, K. K. (1990). Observation of highly vibrationally excited $\tilde{X}^1\Sigma^+$ HCP by stimulated emission pumping spectroscopy. *The Journal of Chemical Physics*, *93*(3), 2149–2151. https://doi.org/10.1063/1.459041

Cho, H.-G., & Andrews, L. (2012a). Infrared Spectra of CH_3–MH through Methane Activation by Laser-Ablated Sn, Pb, Sb, and Bi Atoms. *The Journal of Physical Chemistry A*, *116*(33), 8500–8506. https://doi.org/10.1021/jp305117d

Cho, H.-G., & Andrews, L. (2012b). Infrared Spectra of CH_3 –MH through Methane Activation by Laser-Ablated Sn, Pb, Sb, and Bi Atoms. *The Journal of Physical Chemistry A*, *116*(33), 8500–8506. https://doi.org/10.1021/jp305117d

Chrostowska, A., Dargelos, A., & Graciaa, A. (2010). UV-photoelectron Spectroscopy of Unhindered Germylenes and Carbon-arsenic Multiple-bonded Species. *Australian Journal of Chemistry*, *63*(12), 1608. https://doi.org/10.1071/CH10325

Chrostowska, A., Dargelos, A., Lemierre, V., Sotiropoulos, J., Guenot, P., & Guillemin, J. (2004). First Synthesis and Characterization by Mass Spectrometry and UV-Photoelectron

Spectroscopy of Methylenearsane. *Angewandte Chemie International Edition*, *43*(7), 873–875. https://doi.org/10.1002/anie.200352445

Cohen, E. A., McRae, G. A., Goldwhite, H., Di Stefano, S., & Beaudet, R. A. (1987). Rotational spectrum, structure, and dipole moment of ethynylphosphine, $H_2PC{\equiv}CH$. *Inorganic Chemistry*, *26*(24), 4000–4003. https://doi.org/10.1021/ic00271a008

Corbett, J. D., & Lynde, R. A. (1971). Bismuth(I) tetrachloroaluminate. Spectrophotometric study of its equilibrium formation in the gas phase. *Inorganic Chemistry*, *10*(8), 1746–1749. https://doi.org/10.1021/ic50102a042

Corby, J. F., McGuire, B. A., Herbst, E., & Remijan, A. J. (2018). The molecular chemistry of diffuse and translucent clouds in the line-of-sight to Sgr B2: Absorption by simple organic and inorganic molecules in the GBT PRIMOS survey. *Astronomy & Astrophysics*, *610*, A10. https://doi.org/10.1051/0004-6361/201730988

Craw, J. S., & de Almeida, W. B. (1991). The infrared spectrum of the methylidyne-phosphine dimer, $(HCP)_2$. *Chemical Physics Letters*, *177*(6), 517–520. https://doi.org/10.1016/0009-2614(91)90077-M

Cubicciotti, D. (1960). The equilibrium 2/3Bi(l) + 1/3BiCl(g) = BiCl(g) and the thermodynamic properties of BiCl gas 1. *The Journal of Physical Chemistry*, *64*(6), 791–794. https://doi.org/10.1021/j100835a022

Curtis, S., Miller, J. M., Fröhlich, C., Sprouse, T., Lloyd-Ronning, N., & Mumpower, M. (2023). Nucleosynthesis in Outflows from Black Hole–Neutron Star Merger Disks with Full GR(ν)RMHD. *The Astrophysical Journal Letters*, *945*(1), L13. https://doi.org/10.3847/2041-8213/acba16

de Lima Batista, A. P., Sampaio de Oliveira-Filho, A. G., & Ornellas, F. R. (2011). Excited Electronic States, Transition Probabilities, and Radiative Lifetimes of CAs: A Theoretical Contribution and Challenge to Experimentalists. *The Journal of Physical Chemistry A*, *115*(30), 8399–8405. https://doi.org/10.1021/jp204497p

del Valle, J. C., & Catalán, J. (2019). Kasha's rule: a reappraisal. *Physical Chemistry Chemical Physics*, *21*(19), 10061–10069. https://doi.org/10.1039/C9CP00739C

Demtröder, W. (2018). *Atoms, Molecules and Photons*. Springer Berlin Heidelberg. https://doi.org/10.1007/978-3-662-55523-1

Dendramis, A., & Leroi, G. E. (1977). Matrix isolation spectroscopic study of the free radical HCCN. *The Journal of Chemical Physics*, *66*(10), 4334–4340. https://doi.org/10.1063/1.433724

Dixon, R. N., Duxbury, G., & Lamberton, H. M. (1966). Arsenic hydride radicals. *Chemical Communications (London)*, *14*, 460b. https://doi.org/10.1039/c1966000460b

Draine, B. T. (2003). Interstellar Dust Grains. *Annual Review of Astronomy and Astrophysics*, *41*(1), 241–289. https://doi.org/10.1146/annurev.astro.41.011802.094840

Dunning, T. H. (1989). Gaussian basis sets for use in correlated molecular calculations. I. The atoms boron through neon and hydrogen. *The Journal of Chemical Physics*, *90*(2), 1007–1023. https://doi.org/10.1063/1.456153

Epshtein, M., Portnov, A., & Bar, I. (2015). Evidence for quantum effects in the predissociation of methylamine isotopologues. *Physical Chemistry Chemical Physics*, *17*(29), 19607–19615. https://doi.org/10.1039/C5CP01193K

Farantos, S. C., Keller, H.-M., Schinke, R., Yamashita, K., & Morokuma, K. (1996). Normal mode and isomerization bending states in HCP: Periodic orbit assignment and spectroscopic signature. *The Journal of Chemical Physics*, *104*(24), 10055–10058. https://doi.org/10.1063/1.471729

Forney, D., Jacox, M. E., & Thompson, W. E. (1993). The Mid- and Near-Infrared Spectra of Water and Water Dimer Isolated in Solid Neon. *Journal of Molecular Spectroscopy*, *157*(2), 479–493. https://doi.org/10.1006/jmsp.1993.1037

Fournier, J., Deson, J., Vermeil, C., & Pimentel, G. C. (1979). Fluorescence and thermoluminescence of N_2O, CO, and CO_2 in an argon matrix at low temperature. *The Journal of Chemical Physics*, *70*(12), 5726–5730. https://doi.org/10.1063/1.437399

Frisch, M. J.; Trucks, G. W.; Schlegel, H. B.; Scuseria, G. E.; Robb, M. A.; Cheeseman, J. R.; Scalmani, G.; Barone, V.; Petersson, G. A.; Nakatsuji, H.; Li, X.; Caricato, M.; Marenich, A. V.; Bloino, J.; Janesko, B. G.; Gomperts, R.; Mennucci, B.; Hratchian, H. P.; Ortiz, J. V.; Izmaylov, A. F.; Sonnenberg, J. L.; Williams-Young, D.; Ding, F.; Lipparini, F.; Egidi, F.; Goings, J.; Peng, B.; Petrone, A.; Henderson, T.; Ranasinghe, D.; Zakrzewski, V. G.; Gao, J.; Rega, N.; Zheng, G.; Liang, W.; Hada, M.; Ehara, M.; Toyota, K.; Fukuda, R.; Hasegawa, J.; Ishida, M.; Nakajima, T.; Honda, Y.; Kitao, O.; Nakai, H.; Vreven, T.; Throssell, K.; Montgomery, J. A., Jr.; Peralta, J. E.; Ogliaro, F.; Bearpark, M. J.; Heyd, J. J.; Brothers, E. N.; Kudin, K. N.; Staroverov, V. N.; Keith, T. A.; Kobayashi, R.; Normand, J.; Raghavachari, K.; Rendell, A. P.; Burant, J. C.; Iyengar, S. S.; Tomasi, J.; Cossi, M.; Millam, J. M.; Klene, M.; Adamo, C.; Cammi, R.; Ochterski, J. W.; Martin, R. L.; Morokuma, K.; Farkas, O.; Foresman, J. B.; Fox, D. J. Gaussian 16, Revision B.01, Gaussian, Inc., Wallingford CT, 2016,

Frosch, R. P., & Robinson, G. W. (1964). Emission Spectrum of NO in Solid Rare Gases: The Lifetime of the $a^4\Pi$ State and the Spectrum of the $a^4\Pi \rightarrow X\,^2\Pi$ and $B^2\Pi \rightarrow X\,^2\Pi$ Transitions. *The Journal of Chemical Physics*, *41*(2), 367–374. https://doi.org/10.1063/1.1725876

Frost, D. C., Lee, S. T., & McDowell, C. A. (1973). The photoelectron spectrum of HCP and comments on the first photoelectron band of HCN. *Chemical Physics Letters*, *23*(4), 472–475. https://doi.org/10.1016/0009-2614(73)89004-9

Ganesan, E., Custer, T., Lawzer, A., Guillemin, J., & Kołos, R. (2022). Unusual Quartet-Doublet Phosphorescence from the Phosphaethynyl Radical, CP. *Angewandte Chemie International Edition*, *61*(43). https://doi.org/10.1002/anie.202210521

Gardner, E. P., & McNesby, J. R. (1982). Vacuum-ultraviolet photolysis of methylamine. *The Journal of Physical Chemistry*, *86*(14), 2646–2651. https://doi.org/10.1021/j100211a019

Garneau, J.-M., & Cabana, A. (1978). The ν_1 and $\nu_1+\nu_2-\nu_2$ infrared absorption bands of $H^{12}CP$. *Journal of Molecular Spectroscopy*, *69*(2), 319–325. https://doi.org/10.1016/0022-2852(78)90067-X

Garneau, J.-M., & Cabana, A. (1980). High-resolution infrared absorption spectrum of $H^{12}CP$. The ν_3 band. *Journal of Molecular Spectroscopy*, *79*(2), 502–506. https://doi.org/10.1016/0022-2852(80)90228-3

Gier, T. E. (1961). HCP a unique phosphorus compound. *Journal of the American Chemical Society*, *83*(7), 1769–1770. https://doi.org/10.1021/ja01468a058

Giles, R. S., Fletcher, L. N., & Irwin, P. G. J. (2017). Latitudinal variability in Jupiter's tropospheric disequilibrium species: GeH_4, AsH_3 and PH_3. *Icarus*, *289*, 254–269. https://doi.org/10.1016/j.icarus.2016.10.023

Goddard, T. D., Huang, C. C., Meng, E. C., Pettersen, E. F., Couch, G. S., Morris, J. H., & Ferrin, T. E. (2018). UCSF ChimeraX: Meeting modern challenges in visualization and analysis. *Protein Science*, *27*(1), 14–25. https://doi.org/10.1002/pro.3235

Goodman, L., & Kasha, M. (1958). The observation and assignment of the lowest multiplicity-forbidden transition in pyrazine. *Journal of Molecular Spectroscopy*, *2*(1–6), 58–65. https://doi.org/10.1016/0022-2852(58)90060-2

Govender, M. G., & Ford, T. A. (2000). The infrared spectrum of matrix-isolated methane—rotation or dimerization? *Journal of Molecular Structure*, *550–551*, 445–454. https://doi.org/10.1016/S0022-2860(00)00399-9

Gu, J., Buenker, R. J., & Hirsch, G. (1994). Ab initio CI study of the electronic spectrum of the interstellar free radical CP. *Chemical Physics*, *185*(1), 39–45. https://doi.org/10.1016/0301-0104(94)00108-1

Guillemin, J., Chrostowska, A., Dargelos, A., Nguyen, T. X. M., Graciaa, A., & Guenot, P. (2008). Methylidynearsine (HC≡As): synthesis and direct characterization by UV-photoelectron spectroscopy and mass spectrometry. *Chemical Communications*, *35*, 4204. https://doi.org/10.1039/b806771f

Habing, H. J., & Olofsson, H. (Eds.). (2004). *Asymptotic Giant Branch Stars*. Springer New York. https://doi.org/10.1007/978-1-4757-3876-6

Hadley, S. G., & Volman, D. H. (1967). Photochemical Formation of Free Radicals from Aliphatic Amines as Studied by Electron Spin Resonance. *Journal of the American Chemical Society*, *89*(5), 1053–1055. https://doi.org/10.1021/ja00981a002

Halmann, M. (1963). 530. Far-ultraviolet absorption spectra of phosphorus compounds in the gas phase. *Journal of the Chemical Society (Resumed)*, 2853. https://doi.org/10.1039/jr9630002853

Hammami, K., Nkem, C., Owono Owono, L. C., Jaidane, N., & Ben Lakhdar, Z. (2008). Rotationally inelastic collisions of methinoposphide (HCP) with para-H_2 at low temperature. *The Journal of Chemical Physics*, *129*(20). https://doi.org/10.1063/1.3009268

Harrison, J. J., & Williamson, B. E. (2005). Magnetic Circular Dichroism and Absorption Spectra of Phosphinidene in Noble-Gas Matrices. *The Journal of Physical Chemistry A*, *109*(7), 1343–1347. https://doi.org/10.1021/jp0453156

Hartford, A., Moehlmann, J. G., & Lombardi, J. R. (1972). Dipole moments of the1A″ and3Δ 1 states of HCP. *The Journal of Chemical Physics*, *56*(11), 5733–5734. https://doi.org/10.1063/1.1677101

Hartford, S. L., Allen, Wm. C., Norris, C. L., Pearson, E. F., & Flygare, W. H. (1973). The molecular Zeeman effect in HCP, HCN, and HCCBr and a comparison with similar molecules. *Chemical Physics Letters*, *18*(2), 153–157. https://doi.org/10.1016/0009-2614(73)80407-5

Harvey, A. B., & Wilson, M. K. (1966). Vibrational Spectrum of Methyl Arsine. *The Journal of Chemical Physics*, *44*(9), 3535–3546. https://doi.org/10.1063/1.1727262

Hensel, K. D., Hughes, R. A., & Brown, J. M. (1995). IR spectrum of the AsH radical in its $X^3\Sigma^-$ state, recorded by laser magnetic resonance. *J. Chem. Soc., Faraday Trans.*, *91*(18), 2999–3004. https://doi.org/10.1039/FT9959102999

Herzberg, G. (1930). A New Band System Probably due to a Molecule CP. *Nature*, *126*(3169), 131–132. https://doi.org/10.1038/126131b0

Hofmann, M., Schleyer, P. V. R., & Regitz, M. (1999). The structures and energies of phosphaalkyne trimers, $(HCP)_3$. *European Journal of Organic Chemistry*, *12*, 3291–3303. https://doi.org/10.1002/(SICI)1099-0690(199912)1999:12<3291::AID-EJOC3291>3.0.CO;2-#

Höltzl, T., Szieberth, D., Nguyen, M. T., & Veszprémi, T. (2006). Formation of Phosphaethyne Dimers: A Mechanistic Study. *Chemistry – A European Journal*, *12*(31), 8044–8055. https://doi.org/10.1002/chem.200600228

Hopkinson, M. J., Kroto, H. W., Nixon, J. F., & Simmons, N. P. C. (1976a). The detection of the reactive molecule 1-phosphapropyne, $CH_3C{\equiv}P$, by microwave spectroscopy. *Chemical Physics Letters*, *42*(3), 460–461. https://doi.org/10.1016/0009-2614(76)80653-7

Hopkinson, M. J., Kroto, H. W., Nixon, J. F., & Simmons, N. P. C. (1976b). The detection of unstable molecules by microwave spectroscopy: phospha-alkenes CF_2=PH, CH_2=PCl, and CH_2=PH. *J. Chem. Soc., Chem. Commun.*, *13*, 513–515. https://doi.org/10.1039/C39760000513

Ionkin, A. S., Marshall, W. J., Fish, B. M., Schiffhauer, M. F., Davidson, F., & McEwen, C. N. (2009). Highly Unsaturated Phosphorus Compounds: Generation and Reactions on Both Multiple Bonds of Vinyl Phosphaalkyne. *Organometallics*, *28*(8), 2410–2416. https://doi.org/10.1021/om801224d

Ishikawa, H., Chen, Y.-T., Ohshima, Y., Wang, J., & Field, R. W. (1996). Stimulated emission pumping spectroscopy of HCP near the isomerization barrier: E VIB≤25 315 cm−1. *The Journal of Chemical Physics*, *105*(17), 7383–7401. https://doi.org/10.1063/1.472601

Ishikawa, H., Field, R. W., Farantos, S. C., Joyeux, M., Koput, J., Beck, C., & Schinke, R. (1999). HCP CPH Isomerization : Caught in the Act. *Annual Review of Physical Chemistry*, *50*(1), 443–484. https://doi.org/10.1146/annurev.physchem.50.1.443

Ishikawa, H., Nagao, C., & Mikami, N. (1999a). Observation of the Highly Excited Vibrational Levels of HCP: Application of IR-UV-SEP Triple Resonance Spectroscopy. *Chemistry Letters*, *28*(9), 941–942. https://doi.org/10.1246/cl.1999.941

Ishikawa, H., Nagao, C., & Mikami, N. (1999b). Observation of the ν_{CH} Excited Vibrational Levels in the $\tilde{A}^1A''$State of HCP by IR-UV Double Resonance Spectroscopy. *Journal of Molecular Spectroscopy*, *194*(1), 52–60. https://doi.org/10.1006/jmsp.1998.7757

Ishikawa, H., Nagao, C., Mikami, N., & Field, R. W. (1997). Observation of the "isomerization states" of HCP by stimulated emission pumping spectroscopy: Comparison between theory and experiment. *The Journal of Chemical Physics*, *106*(7), 2980–2983. https://doi.org/10.1063/1.473417

Jacobson, M. P., & Child, M. S. (2001). Spectroscopic signatures of bond-breaking internal rotation. II. Rotation-vibration level structure and quantum monodromy in HCP. *The Journal of Chemical Physics*, *114*(1), 262–275. https://doi.org/10.1063/1.1330746

Janka, H., Langanke, K., Marek, A., Martinezpinedo, G., & Muller, B. (2007). Theory of core-collapse supernovae. *Physics Reports*, *442*(1–6), 38–74. https://doi.org/10.1016/j.physrep.2007.02.002

Jiang, J., Lu, B., Zhu, B., Li, X., Rauhut, G., & Zeng, X. (2023). Hydrogen-Bonded π Complexes between Phosphaethyne and Hydrogen Chloride. *The Journal of Physical Chemistry Letters*, *14*(18), 4327–4333. https://doi.org/10.1021/acs.jpclett.3c00695

Johns, J. W. C., Shurvell, H. F., & Tyler, J. K. (1969). A spectroscopic study of HCP, the phosphorus analogue of hydrocyanic acid. *Canadian Journal of Physics*, *47*(8), 893–920. https://doi.org/10.1139/p69-114

Jones, C. R., Kearns, D. R., & Wing, R. M. (1973). Investigation of singlet-triplet transitions by phosphorescence excitation spectroscopy. X A simple α, β-unsaturated ketone. *The Journal of Chemical Physics*, *58*(4), 1370–1383. https://doi.org/10.1063/1.1679369

Jones, L. H., Ekberg, S. A., & Swanson, B. I. (1986). Hindered rotation and site structure of methane trapped in rare gas solids. *The Journal of Chemical Physics*, *85*(6), 3203–3210. https://doi.org/10.1063/1.450988

Jovan Jose, K. V., Gadre, S. R., Sundararajan, K., & Viswanathan, K. S. (2007). Effect of matrix on IR frequencies of acetylene and acetylene-methanol complex: Infrared matrix isolation and *ab initio* study. *The Journal of Chemical Physics*, *127*(10). https://doi.org/10.1063/1.2752159

Joyeux, M. (1998). Gustavson's procedure and the dynamics of highly excited vibrational states. *Journal of Chemical Physics*, *109*(6), 2111–2122. https://doi.org/10.1063/1.476724

Joyeux, M., Grebenshchikov, S. Y., & Schinke, R. (1998). Analysis of the highly excited vibrational dynamics of HCP using a high-order Fermi resonance Hamiltonian. *Journal of Chemical Physics*, *109*(19), 8342–8354. https://doi.org/10.1063/1.477497

Jung, M., Winnewisser, B. P., & Winnewisser, M. (1997). High resolution FT-IR spectra of the ν_1, ν_2, and ν_3 bands of H12CP and of the ν_1 and ν_2 bands of $H^{13}CP$. *Journal of Molecular Structure*, *413–414*, 31–48. https://doi.org/10.1016/S0022-2860(96)09751-7

Kalasinsky, V. F., & Pechsiri, S. (1985). Raman spectrum of gaseous phosphaethyne (HCP). *Journal of Raman Spectroscopy*, *16*(3), 190–192. https://doi.org/10.1002/jrs.1250160311

Kanda, Y., Kaseda, H., & Matumura, T. (1964). Singlet—triplet absorption spectra of several carbonyl compounds. *Spectrochimica Acta*, *20*(9), 1387–1396. https://doi.org/10.1016/0371-1951(64)80119-3

Karaev, E., Gerlach, M., Faschingbauer, L., Ramler, J., Krummenacher, I., Lichtenberg, C., Hemberger, P., & Fischer, I. (2023). Bonding in Low-Coordinated Organoarsenic and Organoantimony Compounds: A Threshold Photoelectron Spectroscopic Investigation. *Chemistry – A European Journal*, *29*(35). https://doi.org/10.1002/chem.202300637

Kasha, M. (1950). Characterization of electronic transitions in complex molecules. *Discussions of the Faraday Society*, *9*, 14. https://doi.org/10.1039/df9500900014

Keck, H., Kuchen, W., Tommes, P., Terlouw, J. K., & Wong, T. (1992). The Phosphorus Ylide CH_2PH_3 is Stable in the Gas Phase. *Angewandte Chemie International Edition in English*, *31*(1), 86–87. https://doi.org/10.1002/anie.199200861

Kendall, R. A., Dunning, T. H., & Harrison, R. J. (1992). Electron affinities of the first-row atoms revisited. Systematic basis sets and wave functions. *The Journal of Chemical Physics*, *96*(9), 6796–6806. https://doi.org/10.1063/1.462569

Kim, H.-W., Patel, M. K., & Zeroka, D. (2009). Infrared spectra prediction and potential energy surface studies of methylarsine and methylstibine. *Spectrochimica Acta Part A: Molecular and Biomolecular Spectroscopy*, *73*(4), 730–737. https://doi.org/10.1016/j.saa.2009.03.010

Kim, S. J., Hamilton, T. P., & Schaefer, H. F. (1993). Methylphosphinidene (CH_3P) and its rearrangement to phosphaethylene (CH_2PH): toward the observation of ground-state triplet CH_3P. *The Journal of Physical Chemistry*, *97*(9), 1872–1877. https://doi.org/10.1021/j100111a026

Kim, S. J., Lee, Y. S., & Kim, Y. H. (2001). Spectroscopic studies of the atmospheres of giant planets, Titan, and comets. *Planetary and Space Science*, *49*(2), 117–141. https://doi.org/10.1016/S0032-0633(00)00128-8

Klán, P., & Wirz, J. (2009). *Photochemistry of Organic Compounds*. Wiley. https://doi.org/10.1002/9781444300017

Kollman, P., McKelvey, J., Johansson, A., & Rothenberg, S. (1975). Theoretical studies of hydrogen-bonded dimers. Complexes involving HF, H_2O, NH_3, CH_1, H_2S, PH_3, HCN, HNC, HCP, CH_2NH, H_2CS, H_2CO, CH_4, CF_3H, C_2H_2, C_2H_4, C_6H_6, F- and H_3O^+. *Journal of the American Chemical Society*, *97*(5), 955–965. https://doi.org/10.1021/ja00838a001

Koput, J. (1996). The equilibrium structure and spectroscopic constants of HCP - an ab initio study. *Chemical Physics Letters*, *263*(3–4), 401–406. https://doi.org/10.1016/S0009-2614(96)01252-3

Koput, J., & Carter, S. (1997). The potential energy surface and vibrational - Rotational energy levels of HCP. *Spectrochimica Acta - Part A: Molecular and Biomolecular Spectroscopy*, *53*(8), 1091–1100. https://doi.org/10.1016/S1386-1425(96)01868-9

Krajewska, M., Olbert-Majkut, A., & Mielke, Z. (2002). Matrix infrared spectra and ab initio calculations of the acetylene complexes with nitric and nitrous acids. *Physical Chemistry Chemical Physics*, *4*(18), 4305–4313. https://doi.org/10.1039/b203678a

Kroto, H. W., Nixon, J. F., & Ohno, K. (1981a). The microwave spectrum of phosphabutadiyne, H-C≡C-C≡P. *Journal of Molecular Spectroscopy*, *90*(2), 512–516. https://doi.org/10.1016/0022-2852(81)90143-0

Kroto, H. W., Nixon, J. F., & Ohno, K. (1981b). The microwave spectrum, structure, and dipole moment of the unstable molecule phosphaethene, CH_2=PH. *Journal of Molecular Spectroscopy*, *90*(2), 367–373. https://doi.org/10.1016/0022-2852(81)90134-X

Kroto, H. W., Nixon, J. F., Ohno, K., & Simmons, N. P. C. (1980). The microwave spectrum of phosphaethene, CH_2=PH. *J. Chem. Soc., Chem. Commun.*, *15*, 709a–709a. https://doi.org/10.1039/C3980000709A

Lacombe, S., Gonbeau, D., Cabioch, J. L., Pellerin, B., Denis, J. M., & Pfister-Guillouzo, Genevieve. (1988). Application of photoelectron spectroscopy to molecular properties. Part 34. Phosphaethene. Synthesis by vacuum gas-solid reaction (VGSR) and characterization by photoelectron spectroscopy. *Journal of the American Chemical Society*, *110*(21), 6964–6967. https://doi.org/10.1021/ja00229a005

Lannon, J. A., & Nixon, E. R. (1967). Vibrational spectra and force constants of methylphosphine. *Spectrochimica Acta Part A: Molecular Spectroscopy*, *23*(11), 2713–2732. https://doi.org/10.1016/0584-8539(67)80165-X

Laurent, J. C. T. R. B. St., Cooper, T. A., Kroto, H. W., Nixon, J. F., Ohashi, O., & Ohno, K. (1982). The detection of some new phosphaalkynes, RCP, using microwave spectroscopy. *Journal of Molecular Structure*, *79*, 215–220. https://doi.org/10.1016/0022-2860(82)85054-0

Lawzer, A., Custer, T., Guillemin, J., & Kołos, R. (2021). An Efficient Photochemical Route Towards Triplet Ethynylphosphinidene, HCCP. *Angewandte Chemie*, *133*(12), 6470–6472. https://doi.org/10.1002/ange.202016052

Lawzer, A., Ganesan, E., Gronowski, M., Custer, T., Guillemin, J., & Kołos, R. (2023). Free Ethynylarsinidene and Ethynylstibinidene: Heavier Analogues of Nitrenes and Phosphinidenes. *Chemistry – A European Journal*, *29*(46). https://doi.org/10.1002/chem.202300887

Lawzer, A.-L., Ganesan, E., Custer, T., Guillemin, J.-C., & Kolos, R. (2024). Isomerisation of phosphabutyne and a photochemical route to phosphabutadiyne (HC_3P), a phosphorus analogue of cyanoacetylene. *Physical Chemistry Chemical Physics*. https://doi.org/10.1039/D4CP04182H

Lehmann, K. K., Ross, S. C., & Lohr, L. L. (1985). Experimental and ab initio determination of the bending potential of HCP. *The Journal of Chemical Physics*, *82*(10), 4460–4469. https://doi.org/10.1063/1.448749

Lemierre, V., Chrostowska, A., Dargelos, A., & Chermette, H. (2005). Calculation of Ionization Potentials of Small Molecules: A Comparative Study of Different Methods. *The Journal of Physical Chemistry A*, *109*(37), 8348–8355. https://doi.org/10.1021/jp050254c

Lewis, G. N., & Kasha, M. (1945). Phosphorescence in Fluid Media and the Reverse Process of Singlet-Triplet Absorption. *Journal of the American Chemical Society*, *67*(6), 994–1003. https://doi.org/10.1021/ja01222a032

Li, X., Weissman, S. I., Lin, T., Gaspar, P. P., Cowley, A. H., & Smirnov, A. I. (1994). Observation of a Triplet Phosphinidene by ESR Spectroscopy. *Journal of the American Chemical Society*, *116*(17), 7899–7900. https://doi.org/10.1021/ja00096a058

Liu, L., Ruiz, D. A., Munz, D., & Bertrand, G. (2016). A Singlet Phosphinidene Stable at Room Temperature. *Chem*, *1*(1), 147–153. https://doi.org/10.1016/j.chempr.2016.04.001

Lu, B., & Zeng, X. (2024). Phosphinidenes: Fundamental Properties and Reactivity. *Chemistry – A European Journal*, *30*(15), 1–10. https://doi.org/10.1002/chem.202303283

Lucas, M. F., Michelini, M. C., Russo, N., & Sicilia, E. (2008). On the Nature of the CP Bond in Phosphaalkynes. *Journal of Chemical Theory and Computation*, *4*(3), 397–403. https://doi.org/10.1021/ct700277w

Luna, A., Alcamí, M., Mó, O., & Máñez, M. (2000). Cu+ reactivity trends in sp, sp^2, and sp^3 nitrogen, phosphorus, and arsenic containing bases. *International Journal of Mass Spectrometry*, *201*(1–3), 215–231. https://doi.org/10.1016/S1387-3806(00)00228-1

Maciá-Barber, E. (2019). *The Chemical Evolution of Phosphorus*. Apple Academic Press. https://doi.org/10.1201/9780429265136

Magenheimer, J. J., Varnerin, R. E., & Timmons, R. B. (1969). Photochemistry of methylamine at 1470 A. *The Journal of Physical Chemistry*, *73*(11), 3904–3909. https://doi.org/10.1021/j100845a057

Marchal, R., Bégué, D., Chrostowska, A., & Pouchan, C. (2010). The importance of anharmonicity in predicting the IR spectra of low coordinated organoarsenic compounds. *Chemical Physics Letters*, *493*(1–3), 24–26. https://doi.org/10.1016/j.cplett.2010.04.047

Marchetti, A. P., & Kearns, D. R. (1967). Investigation of Singlet-Triplet Transitions by the Phosphorescence Excitation Method. IV. The Singlet-Triplet Absorption Spectra of Aromatic Hydrocarbons. *Journal of the American Chemical Society*, *89*(4), 768–777. https://doi.org/10.1021/ja00980a007

Mardyukov, A., & Niedek, D. (2018). Photochemical reactions of triplet phenylphosphinidene with carbon monoxide and nitric oxide. *Chemical Communications*, *54*(97), 13694–13697. https://doi.org/10.1039/C8CC08664H

Mardyukov, A., Niedek, D., & Schreiner, P. R. (2017). Preparation and Characterization of Parent Phenylphosphinidene and Its Oxidation to Phenyldioxophosphorane: The Elusive Phosphorus Analogue of Nitrobenzene. *Journal of the American Chemical Society*, *139*(14), 5019–5022. https://doi.org/10.1021/jacs.7b01639

Märkl, G., & Herold, U. (1988). 1-phospha-1,2-butadiene - 1-phospha- 1,2, 5-butatriene. *Tetrahedron Letters*, *29*(24), 2935–2938. https://doi.org/10.1016/0040-4039(88)85051-2

Märkl, G., & Reitinger, S. (1988). 3H-phosphaallen - alkinyl-1H-phosphan - tautomere. *Tetrahedron Letters*, *29*(4), 463–466. https://doi.org/10.1016/S0040-4039(00)80122-7

Mason, M. A., & Lehmann, K. K. (1993). Reinvestigation of the HCP electronic spectrum: Experimental determination of D for the $\tilde{X}$ state and observation of hyperfine quantum beats in the $\tilde{B}$ state. *The Journal of Chemical Physics*, *98*(7), 5184–5190. https://doi.org/10.1063/1.464919

Meng, E. C., Goddard, T. D., Pettersen, E. F., Couch, G. S., Pearson, Z. J., Morris, J. H., & Ferrin, T. E. (2023). <scp>UCSF ChimeraX</scp> : Tools for structure building and analysis. *Protein Science*, *32*(11). https://doi.org/10.1002/pro.4792

Meyer, D. L., Lombeck, F., Huettner, S., Sommer, M., & Biskup, T. (2017). Direct $S_0 \rightarrow T$ Excitation of a Conjugated Polymer Repeat Unit: Unusual Spin-Forbidden Transitions Probed by Time-Resolved Electron Paramagnetic Resonance Spectroscopy. *The Journal of Physical Chemistry Letters*, *8*(7), 1677–1682. https://doi.org/10.1021/acs.jpclett.7b00644

Michael, J. V., & Noyes, W. Albert. (1963). The Photochemistry of Methylamine. *Journal of the American Chemical Society*, *85*(9), 1228–1233. https://doi.org/10.1021/ja00892a004

Milam, S. N., Halfen, D. T., Tenenbaum, E. D., Apponi, A. J., Woolf, N. J., & Ziurys, L. M. (2008). Constraining Phosphorus Chemistry in Carbon- and Oxygen-Rich Circumstellar Envelopes: Observations of PN, HCP, and CP. *The Astrophysical Journal*, *684*(1), 618–625. https://doi.org/10.1086/589135

Miller, S. L. (1953). A Production of Amino Acids Under Possible Primitive Earth Conditions. *Science*, *117*(3046), 528–529. https://doi.org/10.1126/science.117.3046.528

Milovanović, M. Z., & Jerosimić, S. V. (2013). An ab initio study of antimony dicarbide (C_2Sb). *Chemical Physics Letters*, *565*, 28–34. https://doi.org/10.1016/j.cplett.2013.02.047

Milovanović, M. Z., & Mitić, M. L. (2020). Ab initio investigation of dicyanoacetylene cation in the ground electronic state: Vibronic coupling and photoionization selection rules. *Journal of Molecular Spectroscopy*, *372*, 111330. https://doi.org/10.1016/j.jms.2020.111330

Mó, O., Yáñez, M., Guillemin, J.-C., Riague, E. H., Gal, J.-F., Maria, P.-C., & Dubin Poliart, C. (2002). The Gas-Phase Acidity of HCP, CH_3CP, HCAs, and CH_3CAs: An Unexpected Enhanced Acidity of the Methyl Group. *Chemistry - A European Journal*, *8*(21), 4919–4924. https://doi.org/10.1002/1521-3765(20021104)8:21<4919::AID-CHEM4919>3.0.CO;2-J

Moehlmann, J. G., Hartford Jr., A., & Lombardi, J. R. (1972). Zeeman Effect in the 2782 Å Band of HCP. *Canadian Journal of Physics*, *50*(15), 1705–1710. https://doi.org/10.1139/p72-231

Moore, J. H., Davis, C. C., Coplan, M. A., & Greer, S. C. (2009). *Building Scientific Apparatus*. Cambridge University Press. https://doi.org/10.1017/CBO9780511609794

Mukhopadhyay, D. P., Gerlach, M., Hartweg, S., Fischer, I., & Loison, J.-C. (2022). Photoelectron spectroscopy of low valent organophosphorus compounds, $P–CH_3$, $H–P=CH_2$ and $P=CH_2$. *Physical Chemistry Chemical Physics*, *24*(18), 10993–10999. https://doi.org/10.1039/D2CP01082H

Mukhopadhyay, D. P., Schleier, D., Wirsing, S., Ramler, J., Kaiser, D., Reusch, E., Hemberger, P., Preitschopf, T., Krummenacher, I., Engels, B., Fischer, I., & Lichtenberg, C. (2020). Methylbismuth: an organometallic bismuthinidene biradical. *Chemical Science*, *11*(29), 7562–7568. https://doi.org/10.1039/D0SC02410D

Mutunga, F. M., & Anderson, D. T. (2015). Infrared Spectroscopy and 193 nm Photochemistry of Methylamine Isolated in Solid Parahydrogen. *The Journal of Physical Chemistry A*, *119*(11), 2420–2428. https://doi.org/10.1021/jp508476j

Nakajima, K., Takata, S., Sakata, K., & Nishibayashi, Y. (2015). Synthesis of Phosphabenzenes by an Iron-Catalyzed [2+2+2] Cycloaddition Reaction of Diynes with Phosphaalkynes. *Angewandte Chemie International Edition*, *54*(26), 7597–7601. https://doi.org/10.1002/anie.201502531

Nakajima, M., Toyoshima, H., Sato, S., Tanaka, K., Hoshina, K., Kohguchi, H., Sumiyoshi, Y., Ohshima, Y., & Endo, Y. (2013). Electronic spectroscopy of the HCCN radical. *The Journal of Chemical Physics*, *138*(16). https://doi.org/10.1063/1.4802003

Namai, M., Sasaki, T., Ishikawa, H., Morikuni, H., & Mikami, N. (2009). Predissociation Mechanism and Dynamics of HCP. *The Journal of Physical Chemistry A*, *113*(47), 13081–13088. https://doi.org/10.1021/jp900450t

Nanbu, S., Gray, S. K., Kinoshita, T., & Aoyagi, M. (2000). Theoretical study of the potential energy surfaces and bound states of HCP. *The Journal of Chemical Physics*, *112*(13), 5866–5876. https://doi.org/10.1063/1.481159

Nguyen, M. T., Landuyt, L., & Vanquickenborne, L. G. (1993). A theoretical study of the dimerization of phosphaethyne (HC.tplbond.P): head-to-tail versus head-to-head cycloaddition? *The Journal of Organic Chemistry*, *58*(10), 2817–2821. https://doi.org/10.1021/jo00062a027

Nina Hall. (2004). The quest for the chemical roots of life. *Chemical Communications*, *11*, 1247. https://doi.org/10.1039/b401124b

Nishi, N., Shinohara, H., & Hanazaki, I. (1980). Photochemical conversion from methylamine to hydrogencyanide with an arf laser at 193 nm. *Chemical Physics Letters*, *73*(3), 473–477. https://doi.org/10.1016/0009-2614(80)80698-1

Nixon, J. F. (1995). Phospha-alkynes, RCP: new building blocks in inorganic and organometallic chemistry. *Chem. Soc. Rev.*, *24*(5), 319–328. https://doi.org/10.1039/CS9952400319

Ohno, K., Kroto, H. W., & Nixon, J. F. (1981). The microwave spectrum of 1-phosphabut-3-ene-1-yne, CH_2=CHC≡P. *Journal of Molecular Spectroscopy*, *90*(2), 507–511. https://doi.org/10.1016/0022-2852(81)90142-9

Pang, W.-X., Wu, H.-Y., Zhao, J.-J., Lu, Y., & Sun, Y.-B. (2017). DFT anharmonic force field, and spectroscopic constants for phosphaethene, CH_2PH. *Main Group Chemistry*, *16*(3), 207–216. https://doi.org/10.3233/MGC-170237

Pellerin, B., Guenot, P., & Denis, J.-M. (1987). Methylidenephosphine. *Tetrahedron Letters*, *28*(47), 5811–5814. https://doi.org/10.1016/S0040-4039(01)81060-1

Peter Atkins, & Julio de Paula. (2010). *Physical Chemistry, Ninth Edition* (Ninth Edition). Oxford University Press.

Peterson, K. A., & Woods, R. C. (1989). Ground state spectroscopic and thermodynamic properties of AlO^-, SiN^-, CP^-, BS^-, BO^-, and CN^- from Moller–Plesset perturbation theory. *The Journal of Chemical Physics*, *90*(12), 7239–7250. https://doi.org/10.1063/1.456201

Pettersen, E. F., Goddard, T. D., Huang, C. C., Meng, E. C., Couch, G. S., Croll, T. I., Morris, J. H., & Ferrin, T. E. (2021). UCSF ChimeraX: Structure visualization for researchers, educators, and developers. *Protein Science*, *30*(1), 70–82. https://doi.org/10.1002/pro.3943

Potapov, A., Jäger, C., & Henning, T. (2020). Ice Coverage of Dust Grains in Cold Astrophysical Environments. *Physical Review Letters*, *124*(22), 221103. https://doi.org/10.1103/PhysRevLett.124.221103

Qian, W., Schreiner, P. R., & Mardyukov, A. (2024). Preparation and Photochemistry of Parent Triplet Vinylarsinidene. *Journal of the American Chemical Society*, *146*(1), 930–935. https://doi.org/10.1021/jacs.3c11432

Qin, Z., Zhao, J., & Liu, L. (2019). Theoretical study on low-lying electronic states of CP radical: Energy levels, Einstein coefficients, Franck-Condon factors and radiative lifetimes. *Journal of Quantitative Spectroscopy and Radiative Transfer*, *230*, 36–47. https://doi.org/10.1016/j.jqsrt.2019.03.023

Ram, R. S., & Bernath, P. F. (1987). Fourier transform spectroscopy of the $A^2\Pi_i$-$X^2\Sigma^+$ system of CP. *Journal of Molecular Spectroscopy*, *122*(2), 282–292. https://doi.org/10.1016/0022-2852(87)90005-1

Ram, R. S., Brooke, J. S. A., Western, C. M., & Bernath, P. F. (2014). Einstein A-values and oscillator strengths of the $A^2\Pi$–$X^2\Sigma^+$ system of CP. *Journal of Quantitative Spectroscopy and Radiative Transfer*, *138*, 107–115. https://doi.org/10.1016/j.jqsrt.2014.01.030

Ram, R. S., Tam, S., & Bernath, P. F. (1992). The $A^2\Pi_i$-$X^2\Sigma^+$ system of CP: Observation of new bands. *Journal of Molecular Spectroscopy*, *152*(1), 89–100. https://doi.org/10.1016/0022-2852(92)90119-9

Recio, P., Cachón, J., Zanchet, A., Marggi Poullain, S., & Bañares, L. (2023). Photodissociation dynamics of methylamine in the blue edge of the A -band. I. the H-atom elimination channel. *Journal of Chemical Physics*, *158*(23). https://doi.org/10.1063/5.0152993

Reed, C. L., Kono, M., & Ashfold, M. N. R. (1996). Near-UV photolysis of methylamine studied by H-atom photofragment translational spectroscopy. *Journal of the Chemical Society, Faraday Transactions*, *92*(24), 4897. https://doi.org/10.1039/ft9969204897

Regitz, M. (1990). Phosphaalkynes: new building blocks in synthetic chemistry. *Chemical Reviews*, *90*(1), 191–213. https://doi.org/10.1021/cr00099a007

Regitz, M. (1994). Organophosphorus compounds. **75**. Phosphaalkynes — new building blocks in heterocyclic chemistry. *Journal of Heterocyclic Chemistry*, *31*(3), 663–677. https://doi.org/10.1002/jhet.5570310307

Rey-Villaverde, R., Cybulski, H., Flores, J. R., & Fernández, B. (2013). A high-accuracy theoretical study of the CH_nP Systems n = 1-3. *Journal of Computational Chemistry*, *34*(23), 2020–2031. https://doi.org/10.1002/jcc.23357

Rozhenko, A. B., Schoeller, W. W., & Povolotskii, M. I. (1999). Ab initio calculation of NMR shielding in phosphaalkenes X—P=CY_2. *Magnetic Resonance in Chemistry*, *37*(8), 551–563. https://doi.org/10.1002/(SICI)1097-458X(199908)37:8<551::AID-MRC503>3.0.CO;2-3

Saito, S., Yamamoto, S., Kawaguchi, K., Ohishi, M., Suzuki, H., Ishikawa, S.-I., & Kaifu, N. (1989). The microwave spectrum of the CP radical and related astronomical search. *The Astrophysical Journal*, *341*, 1114. https://doi.org/10.1086/167570

Schoeller, W. W., Begemann, C., Tubbesing, U., & Strutwolf, J. (1997). On the π-bond strengths in higher element homologues of methylenephosphane and diphosphene. *Journal of the Chemical Society, Faraday Transactions*, *93*(17), 2957–2962. https://doi.org/10.1039/a701636k

Sharma, M. K. (2019). Vinyl cyanide (CH_2CHCN) in interstellar space: potential spectral lines for its detection. *Heliyon*, *5*(8), e02384. https://doi.org/10.1016/j.heliyon.2019.e02384

Shay, R. H., Diel, B. N., Schubert, D. M., & Norman, A. D. (1988). Synthesis and borane coordination of primary alkenyl- and alkynylphosphines. *Inorganic Chemistry*, *27*(13), 2378–2382. https://doi.org/10.1021/ic00286a031

Shestakov, O., Breidohr, R., Demes, H., Setzer, K. D., & Fink, E. H. (1998). Electronic States and Spectra of BiO. *Journal of Molecular Spectroscopy*, *190*(1), 28–77. https://doi.org/10.1006/jmsp.1998.7538

Shi, D. H., Xing, W., Sun, J. F., Zhu, Z. L., & Liu, Y. F. (2012). Extensive ab initio study of the electronic states of CP radical including spin–orbit coupling. *Journal of Molecular Spectroscopy*, *276–277*(1), 1–9. https://doi.org/10.1016/j.jms.2012.06.011

Slanina, Z. (1992). A computational evaluation of the thermodynamics of $HCP_{(g)}$ dimerization. *Thermochimica Acta*, *198*(1), 45–52. https://doi.org/10.1016/0040-6031(92)85056-2

Slanina, Z., De Almeida, W. B., & Craw, J. S. (1992). $(HCP)_2$ isomeric system: coexistence of T-shaped and linear structures. *Journal of Molecular Structure: THEOCHEM*, *253*(C), 357–361. https://doi.org/10.1016/0166-1280(92)87120-O

Smith, H. H., Hyde, A. S., Simkus, D. N., Libby, E., Maurer, S. E., Graham, H. V., Kempes, C. P., Sherwood Lollar, B., Chou, L., Ellington, A. D., Fricke, G. M., Girguis, P. R., Grefenstette, N. M., Pozarycki, C. I., House, C. H., & Johnson, S. S. (2021). The Grayness of the Origin of Life. *Life*, *11*(6), 498. https://doi.org/10.3390/life11060498

Soleilhavoup, M., & Bertrand, G. (2020). Stable Carbenes, Nitrenes, Phosphinidenes, and Borylenes: Past and Future. *Chem*, *6*(6), 1275–1282. https://doi.org/10.1016/j.chempr.2020.04.015

Tripathi, R., Rai, S. B., & Upadhya, K. N. (1981). The B-A system of CP molecule. *Pramana*, *17*(3), 249–255. https://doi.org/10.1007/BF02846471

Tyler, J. K. (1964). Microwave Spectrum of Methinophosphide, HCP. *The Journal of Chemical Physics*, *40*(4), 1170–1171. https://doi.org/10.1063/1.1725278

Viana, R. B. (2017). Reactivity, vibrational spectroscopy, internal rotation and thermochemical aspects of methylarsine. *Spectrochimica Acta Part A: Molecular and Biomolecular Spectroscopy*, *171*, 383–394. https://doi.org/10.1016/j.saa.2016.08.016

Viana, R. B., & da Silva, A. B. F. (2014). The CH_3PH_2 and CH_3PH isomers: isomerization, hydrogen release, thermodynamic, and spectroscopy properties. *Journal of Molecular Modeling*, *20*(8), 2372. https://doi.org/10.1007/s00894-014-2372-8

Walmsley, C. M., Winnewisser, G., & Toelle, F. (1980). Cyanoacetylene and cyanodiacetylene in interstellar clouds. *Astronomy and Astrophysics*, *81*, 245–250. https://doi.org/1980A&A....81..245W

Wang, X., Souter, P. F., & Andrews, L. (2003). Infrared Spectra of Antimony and Bismuth Hydrides in Solid Matrixes. *The Journal of Physical Chemistry A*, *107*(21), 4244–4249. https://doi.org/10.1021/jp034379y

Waschewsky, G. C. G., Kitchen, D. C., Browning, P. W., & Butler, L. J. (1995). Competing Bond Fission and Molecular Elimination Channels in the Photodissociation of CH_3NH_2 at 222 nm. *The Journal of Physical Chemistry*, *99*(9), 2635–2645. https://doi.org/10.1021/j100009a022

Watts, J. D., Rittby, M., & Bartlett, R. J. (1989). Calculation of molecular ionization potentials using single- and multireference coupled-cluster methods. Application of methyleneamine, CH_2NH, and methylenephosphine, CH_2PH. *Journal of the American Chemical Society*, *111*(12), 4155–4160. https://doi.org/10.1021/ja00194a002

Weigend, F. (2006). Accurate Coulomb-fitting basis sets for H to Rn. *Physical Chemistry Chemical Physics*, *8*(9), 1057. https://doi.org/10.1039/b515623h

Weigend, F., & Ahlrichs, R. (2005). Balanced basis sets of split valence, triple zeta valence and quadruple zeta valence quality for H to Rn: Design and assessment of accuracy. *Physical Chemistry Chemical Physics*, *7*(18), 3297. https://doi.org/10.1039/b508541a

Wentrup, C. (2018). Carbenes and Nitrenes: Recent Developments in Fundamental Chemistry. *Angewandte Chemie - International Edition*, *57*(36), 11508–11521. https://doi.org/10.1002/anie.201804863

Woon, D. E., & Herbst, E. (2009). Quantum chemical predictions of the properties of known and postulated neutral interstellar molecules. *The Astrophysical Journal Supplement Series*, *185*(2), 273–288. https://doi.org/10.1088/0067-0049/185/2/273

Wu, M., Chen, W., Wang, D., Chen, Y., Ye, S., & Tan, G. (2023a). Triplet bismuthinidenes featuring unprecedented giant and positive zero field splittings. *National Science Review*, *10*(10). https://doi.org/10.1093/nsr/nwad169

Wu, M., Li, H., Chen, W., Wang, D., He, Y., Xu, L., Ye, S., & Tan, G. (2023b). A triplet stibinidene. *Chem*, *9*(9), 2573–2584. https://doi.org/10.1016/j.chempr.2023.05.005

Yang, J., & Clouthier, D. J. (2011). Electronic spectroscopy of the previously unknown arsenic carbide (AsC) free radical. *The Journal of Chemical Physics*, *135*(5). https://doi.org/10.1063/1.3618955

Yu, N., Wang, J.-J., & Xu, J.-L. (2019). Chemical evolution of HC_3N in dense molecular clouds. *Monthly Notices of the Royal Astronomical Society*, *489*(4), 4497–4512. https://doi.org/10.1093/mnras/stz2431

Yuan, J., Chen, R., Tang, X., Tao, Y., Xu, S., Jin, L., Chen, C., Zhou, X., Zheng, C., & Huang, W. (2019). Direct population of triplet excited states through singlet–triplet transition for visible-light excitable organic afterglow. *Chemical Science*, *10*(19), 5031–5038. https://doi.org/10.1039/C8SC05198D

Zeng, X., Beckers, H., Seifert, J., & Banert, K. (2014). The Photochemical and Thermal Decomposition of Azidoacetylene in the Gas Phase, Solid Matrix, and Solutions. *European Journal of Organic Chemistry*, *2014*(19), 4077–4082. https://doi.org/10.1002/ejoc.201402153

Zhang, J., & Zhu, Z. (2021). Radiative lifetimes of $A^2\Pi$, $B^2\Sigma^+$, $a^4\Sigma^+$, and $b^4\Delta$ states of CP radical. *Journal of Quantitative Spectroscopy and Radiative Transfer*, *270*, 107664. https://doi.org/10.1016/j.jqsrt.2021.107664

9. Appendices

9.1. Closed-cycle two-stage helium refrigerator

Cryogenic temperatures are achieved by passing He gas through the cryostat with the help of the compressor and an *expander* (**Figure 9-1**, **Figure 9-2**). Two lines are used to cycle He: the first of these supplies high-pressure gas from the compressor to the expander, and the other one returns the low-pressure gas to the compressor. After two adiabatic expansion stages, the temperature below 10 K is attained at the sample holder made of copper. A substrate window (CsI, CaF_2, or KBr) is attached to the holder, the proper thermal contact being secured with indium washers. The vacuum shroud of the cryostat is equipped with external windows made of CsI, KBr, CaF_2, fused silica or MgF_2 (see **Table 9-1**, for the transparency ranges of these materials).

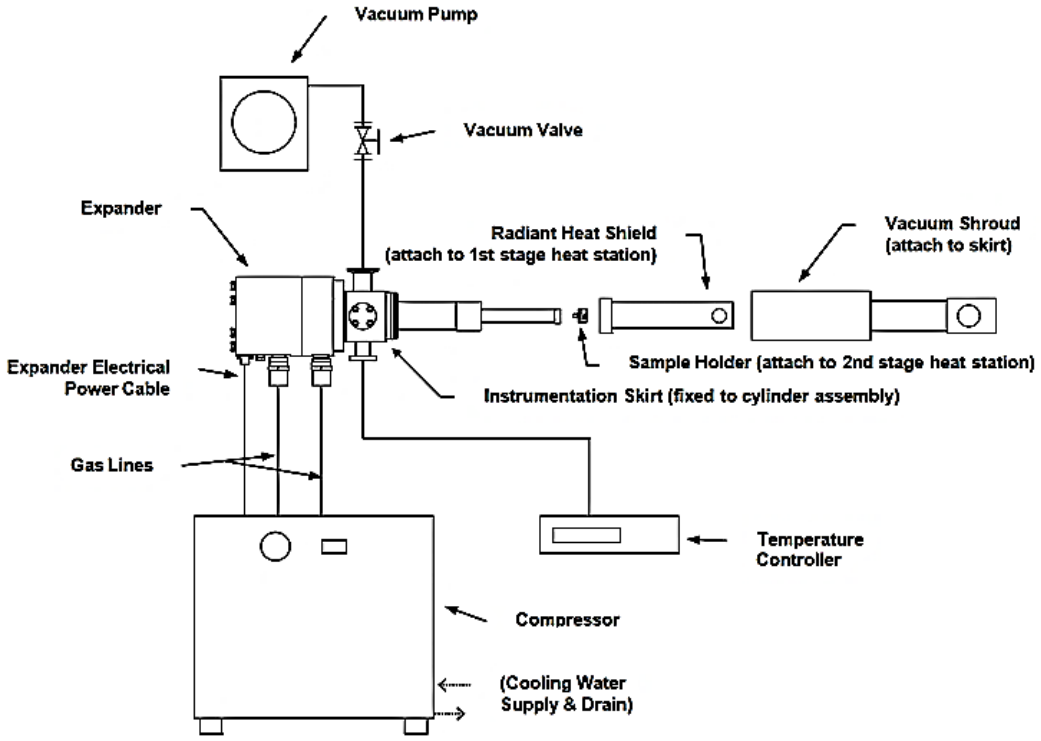

Figure 9-1. Cryostat components, Source: ARS official website.

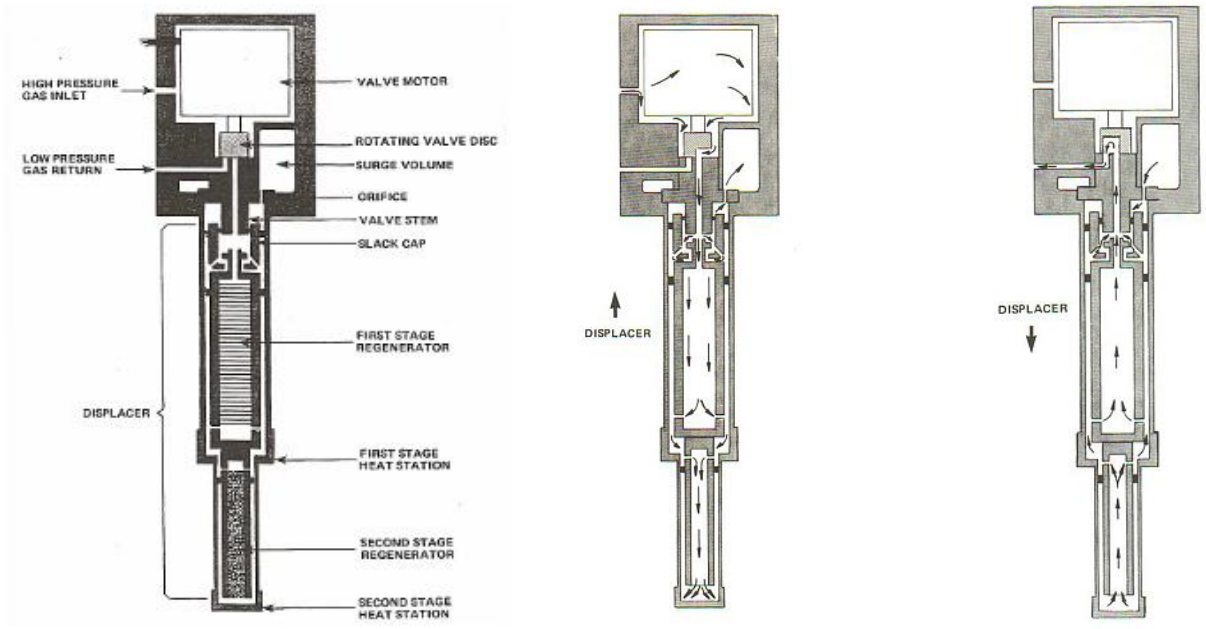

Figure 9-2. Cryostat, principle of operation; Source: ARS official website.

9.2. Spectral transparency of optical materials

Table 9-1. Transparency ranges of select materials used in IR and UV/Vis (Moore et al., 2009).

	CsI	**Sapphire**	**Fused silica** [a]	**KBr**	**MgF_2**
Range (cm^{-1})	150 – 33 000	2000 – 66 000	3000 – 55 600	400 – 33 000	1000 – 100 000

a) high-purity quartz

9.3. Results of quantum chemical calculations

Table 9-2. B3LYP/aug-cc-pVTZ)-derived vibrational frequencies, absolute infrared intensities, and electronic energies for several *a priori* possible products of methylphosphine photolysis.

Molecule	Infrared frequency (cm^{-1})	Relative Intensity (%)	Absolute Intensity (km/mol)	Energy + ZPE (Hartree)
CH_2PH_3	283.561 459.446 645.641 678.105 912.702 929.496 949.557 1115.16 1132.97 1332.12 2058.72 2348.66 2366.65 3014.56 3101.02	1.38374 31.5632 2.21126 7.96961 10.9213 6.63309 3.26196 43.3618 1.89747 2.48572 100 14.1505 7.51789 0.275399 0.272134	5.04 115.03 8.06 29.05 39.80 24.17 11.89 158.03 6.92 9.06 364.45 51.57 27.40 1.00 0.99	-382.435938
CH_3PH	214.594 650.589 699.02 752.386 990.482 1257.72 1401.91 1404.12 2242.67 2902.26 2960.79 2989.59	1.53975 16.1432 0.503948 0.767086 33.4249 1.34516 5.63687 7.37155 100 10.1127 7.21983 7.98892	1.38 14.46 0.45 0.69 29.94 1.21 5.05 6.60 89.57 9.06 6.47 7.16	-381.87749
CP	1225.24	100	0.905	-379.338873

Table 9-3. B3LYP/aug-cc-pVTZ)-derived molecular geometries for several *a priori* possible products of methylphosphine photolysis.

Molecule	Molecular geometry	Cartesian coordinates
CH_2PH_3		C -1.1983920000 0.0009360000 -0.061754000 P 0.4781400000 0.0000820000 0.0050460000 H -1.6971980000 0.9207670000 0.2107210000 H -1.6940930000 -0.9216810000 0.2071910000 H 1.0390540000 1.1073170000 -0.6585330000 H 1.3399360000 0.0134300000 1.1663550000 H 1.0305550000 -1.1266780000 -0.630900000
CH_3PH		C 0.0565630000 1.1505290000 0.0000000000 H -0.4534180000 1.5406920000 0.8823050000 H 1.0824530000 1.5143640000 0.0000000000 P 0.0565630000 -0.7096810000 0.0000000000 H -0.4534180000 1.5406920000 -0.8823050000 H -1.3634410000 -0.8537140000 0.0000000000
CP		C 0.0000000000 0.0000000000 -1.1127910000 P 0.0000000000 0.0000000000 0.4451160000

Table 9-4. B3LYP/aug-cc-pVTZ)-derived vibrational frequencies, absolute infrared intensities, and electronic energies for several *a priori* possible products of methylarsine photolysis.

S.no	Molecule	Infrared frequency (cm^{-1})	Relative Intensity (%)	Absolute Intensity (km/mol)	Energy + ZPE (Hartree)
1.	CH_2AsH_3	288.797 510.937 544.367 555.669 751.906 879.921 906.617 955.428 1001.8 1334.09 1863.54 2182.94 2198.58 2957.34 3040.6	2.03294 3.73199 4.29961 25.7444 7.88452 1.34355 3.13848 28.5886 0.124869 0.0599704 100 10.1279 7.58049 1.30394 1.30165	9.78 17.95 20.68 123.81 37.92 6.46 15.09 137.48 0.60 0.29 480.90 48.71 36.46 6.27 6.26	-2 276.976656
2.	CH_3AsH	184.01 540.055 638.106 728.644 910.667 1225.05 1402.91 1403.32 2043.2 2915.91 2986.34 3004.88	0.0125689 10.4236 0.974733 0.923029 18.4533 0.489687 3.25028 4.01569 100 7.20163 4.13296 4.92151	0.02 14.60 1.37 1.29 25.84 0.69 4.55 5.62 140.03 10.08 5.79 6.89	-2 276.460974
3.	CH_2AsH_2	173.076 453.49 574.291 595.478 710.873 873.801 929.485 1329.31 2054.29 2075.34 3009.72 3114.64	1.0332 32.8158 13.4432 1.06039 11.5319 9.26802 21.7407 2.86104 87.214 100 5.28148 1.2108	1.17 37.05 15.18 1.20 13.02 10.46 24.54 3.23 98.46 112.89 5.96 1.37	-2 276.414746
4.	CH_3As(singlet)	482.405 639.949 751.959 1199.26 1246.87 1401.29 2818.77 2942.16 2992.82	22.5206 56.8748 79.6667 42.5545 25.1213 79.9749 13.8993 100 0.432437	5.91 14.93 20.91 11.17 6.59 20.99 3.65 26.25 0.11	-2 275.799267
5.	CH_3As(triplet)	537.243 733.322 733.783 1214.17 1390.99 1391.33 2903.22 2978.71 2979.27	100 10.0538 10.0196 0.135971 42.2118 42.4409 47.0465 25.989 26.2059	17.28 1.74 1.73 0.02 7.30 7.34 8.13 4.49 4.53	-2 275.84248
6.	$CHAsH_2$ (singlet)	206.946	22.1918	24.02	-2 275.735457

		536.821 740.967 789.573 906.629 958.228 2046.87 2206.6 2896.4	38.8886 2.16851 17.7289 6.37334 57.1899 100 20.7692 15.6623	42.10 2.35 19.19 6.90 61.91 108.25 22.48 16.95	
7.	$CHAsH_2$ (triplet)	275.19 555.896 651.173 695.69 796.714 936.519 2041.22 2047.08 3049.78	20.7996 1.82639 18.8598 6.96693 26.347 23.2376 92.8972 100 4.09348	18.99 1.67 17.22 6.36 24.05 21.21 84.80 91.28 3.74	-2 275.736474
8.	CH_2As	684.666 797.577 802.021 1343.06 2972.66 3054.49	1.29418 100 4.82063 1.61452 3.88317 0.252806	1.04 80.26 3.87 1.30 3.12 0.20	-2,275.223225
9.	CHAsH	547.248 684.732 750.735 854.243 1985.56 3081.82	24.0397 53.3483 21.2349 1.62252 100 0.314796	24.41 54.18 21.57 1.65 101.56 0.32	-2,275.164198
10.	CAs	1010.39	100	1.251	-2,273.912938

Table 9-5. B3LYP/aug-cc-pVTZ)-derived molecular geometries for several *a priori* possible products of methylarsine photolysis.

S.No.	Molecule	Molecular geometry	Cartesian coordinates		
1	CH_2AsH_3	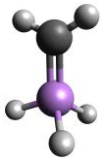	C -0.0030980000 1.4845470000 0.0000000000 As -0.0030980000 -0.2995740000 0.0000000000 H -0.9284220000 2.0312680000 0.0000000000 H 0.9572410000 1.9673630000 0.0000000000 H 1.3974700000 -0.8300540000 0.0000000000 H -0.6527400000 -1.0949530000 -1.1409500000 H -0.6527400000 -1.0949530000 1.1409500000		
2	CH_3AsH	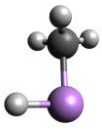	C 0.0353540000 1.5479150000 0.0000000000 H -0.4747440000 1.9254160000 0.8851850000 H 1.0643160000 1.8996970000 0.0000000000 As 0.0353540000 -0.4388800000 0.0000000000 H -0.4747440000 1.9254160000 -0.8851850000 H -1.4936160000 -0.5549900000 0.0000000000		
3	CH_2AsH_2	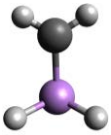	C -0.0398480000 1.5415880000 0.0000000000 H 0.9795350000 -0.5712520000 1.1182520000 H -0.2025020000 2.0789630000 -0.9236740000 As -0.0398480000 -0.3716650000 0.0000000000 H -0.2025020000 2.0789630000 0.9236740000 H 0.9795350000 -0.5712520000 -1.1182520000		
4	CH_3As(singlet)	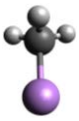	C 1.5075550000 0.0000140000 -0.0216750000 As -0.4445350000 0.0000000000 -0.0028650000 H 1.9644420000 0.9028940000 -0.4208780000 H 1.9645380000 -0.9024680000 -0.4216860000 H 1.6953570000 -0.0005140000 1.0671700000		
5	CH_3As(triplet)	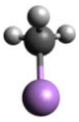	C 1.5298800000 0.0000000000 -0.0000030000 As -0.4511540000 -0.0000010000 0.0000130000 H 1.9025820000 0.8896640000 -0.5076680000 H 1.9026480000 -0.8844980000 -0.5165850000 H 1.9035640000 -0.0051410000 1.0238560000		
6	$CHAsH_2$ (singlet)	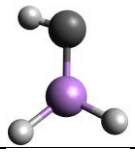	C -1.5128870000 0.1662950000 0.0629790000 H -1.9487260000 -0.8439480000 0.0334080000 As 0.2709810000 -0.0065540000 -0.0417310000 H 0.9821320000 1.2170140000 0.4517790000 H 1.1015320000 -1.1545400000 0.5140500000		
7	$CHAsH_2$ (triplet)	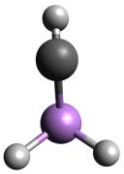	C 1.5580710000 -0.0000660000 0.1808950000 H 2.3875010000 0.0002940000 -0.5166290000 As -0.3156010000 0.0000440000 -0.0732060000 H -0.6607830000 1.1066450000 0.9242300000 H -0.6603100000 -1.1079910000 0.9228110000		
8	CH_2As	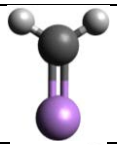	C 1.4003170000 0.0000020000 0.0001560000 As -0.3746440000 0.0000010000 -0.0000420000 H 1.9806420000 -0.9167580000 0.0002300000 H 1.9806970000 0.9167260000 0.0002310000		
9	CHAsH		C 0.0197910000 1.4378420000 0.0000000000 H -1.5084620000 -0.4958970000 0.0000000000 As 0.0197910000 -0.3145100000 0.0000000000 H 0.7366170000 2.2476760000 0.0000000000		
10	CAs		C 0.0000000000 0.0000000000 -1.4164370000 As 0.0000000000 0.0000000000 0.2575340000		

Table 9-6. B3LYP/aug-cc-pVTZ)-derived vibrational frequencies, absolute infrared intensities, and electronic energies for several *a priori* possible products of methylstibine photolysis.

S.no	Molecule	Infrared frequency (cm^{-1})	Relative Intensity (%)	Absolute Intensity (km/mol)	Energy + ZPE (Hartree)
1.	CH_2SbH_3	256.594 388.9 402.497 508.715 701.175 786.648 791.038 795.871 895.174 1327.23 1695.33 1949.8 1959.96 2914.78 2996.65	2.46645 9.66986 7.43299 7.53701 14.2339 1.6656 4.62126 39.8416 1.34261 0.0688668 100 16.8391 17.8299 2.10428 2.29811	11.74 46.03 35.38 35.88 67.75 7.93 22.00 189.64 6.39 0.33 475.99 80.15 84.87 10.02 10.94	-281.332925
2.	CH_3Sb(singlet)	465.657 602.103 638.781 1171.04 1267.03 1397.89 2874.58 2969.28 3010.59	65.3691 53.681 100 32.7176 18.8047 84.583 22.9004 88.2127 3.6642	13.24 10.88 20.26 6.63 3.81 17.14 4.64 17.87 0.74	-280.192640
3.	CH_3Sb(triplet)	474.811 687.405 688.078 1175.81 1393.74 1394.17 2917.65 2999.8 3000.38	100 17.5184 17.5844 12.1777 33.0009 33.0992 59.5033 28.8298 29.1074	19.52 3.42 3.43 2.38 6.44 6.46 11.62 5.63 5.68	-280.231892
4.	$CHSbH_2$ (singlet)	282.246 482.082 576.837 585.555 796.878 846.069 1810.01 1899.4 2845.66	10.5703 22.6351 2.95452 43.4047 43.6044 8.47816 100 67.9516 24.4717	13.60 29.12 3.80 55.84 56.09 10.91 128.64 87.41 31.48	-280.089622
5.	$CHSbH_2$ (triplet)	239.608 486.115 562.077 575.947 689.386 783.811 1808.69 1813.48 3033.82	11.0611 0.943009 10.6319 3.27425 24.5418 18.9427 89.5099 100 4.27092	18.12 1.55 17.42 5.36 40.20 31.03 146.62 163.81 7.00	-280.103414
6.	CH_2SbH	556.591 680.322 692.395 758.063 783.304 1344.25 1821.5	2.14641 10.3099 1.93942 34.5994 12.6331 0.0693491 100	4.46 21.42 4.03 71.89 26.25 0.14 207.79	-280.208129

		3010.43 3109.33	2.05809 0.0743542	4.28 0.15	
7.	CH_2Sb	634.579 674.883 738.423 1330.2 2984.34 3074.94	3.27879 4.61561 100 0.00145173 5.60458 0.529324	2.94 4.13 89.55 0.0 5.02 0.47	-279.597593
8.	CHSbH	461.587 601.754 631.065 705.501 1783.46 3067.73	8.18574 31.339 16.1512 1.34222 100 0.397912	13.89 53.19 27.41 2.28 169.71 0.68	-279.528092
9.	HCSb	575.787 575.787 892.761 3146.64	100 100 2.8743 5.54216	102.99 102.99 2.96 5.71	-278.968231
10.	CSb	806.82	100	0.017	-278.279262

Table 9-7. B3LYP/aug-cc-pVTZ)-derived molecular geometries for several *a priori* possible products of methylsibine photolysis.

Molecule	Molecular geometry	Cartesian coordinates		
CH_2SbH_3	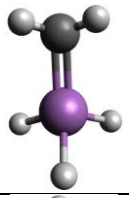	C 1.8065150000	-0.0000560000	-0.1154080000
		Sb -0.2364140000	-0.0000020000	0.0068320000
		H 2.1739520000	-0.8955500000	0.3930930000
		H 2.1737220000	0.8956190000	0.3929620000
		H -0.8470330000	-1.3165800000	-0.8581270000
		H -1.4359660000	-0.0007440000	1.2727230000
		H -0.8466380000	1.3176970000	-0.8566410000
CH_3Sb(singlet)	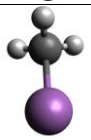	C 1.8267320000	-0.0001340000	-0.0151610000
		Sb -0.3438750000	-0.0000080000	-0.0011060000
		H 2.2511710000	-0.9018720000	-0.4504980000
		H 2.0755540000	0.0044010000	1.0551640000
		H 2.2505070000	0.8986700000	-0.4572850000
CH_3Sb(triplet)	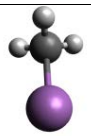	C 1.8404580000	0.0000010000	0.0000020000
		Sb -0.3464290000	0.0000000000	0.0000010000
		H 2.2084070000	0.7801980000	0.6658220000
		H 2.2082820000	0.1865550000	-1.0085960000
		H 2.2084380000	-0.9667360000	0.3427140000
$CHSbH_2$ (singlet)	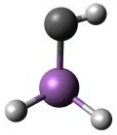	C 1.8336020000	0.1649200000	-0.0709010000
		Sb -0.2296300000	-0.0040550000	0.0463690000
		H 2.2282730000	-0.8695840000	-0.0517850000
		H -0.7040430000	1.3244560000	-0.8982620000
		H -0.8147030000	-1.2375900000	-0.9893620000
$CHSbH_2$ (triplet)	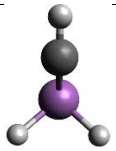	C 1.8342440000	-0.1685210000	0.0258860000
		Sb -0.2473010000	0.0530520000	-0.0083180000
		H 2.6858030000	0.4989450000	-0.0766670000
		H -0.5405080000	-1.2882400000	-1.0436230000
		H -0.5384250000	-0.9052080000	1.3891880000
CH_2SbH	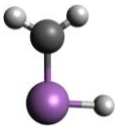	C 1.6998030000	0.0187590000	-0.0001560000
		Sb -0.2801310000	-0.0357310000	0.0000270000
		H 2.2738550000	-0.9001800000	-0.0001530000
		H 2.2795020000	0.9326030000	-0.0002570000
		H -0.4655020000	1.6772890000	-0.0000500000
CH_2Sb	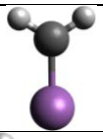	C -0.0000270000	-1.6911040000	0.0000000000
		Sb -0.0000270000	0.2881910000	0.0000000000
		H 0.0007750000	-2.2755510000	0.9144150000
		H 0.0007750000	-2.2755510000	-0.9144150000
CHSbH	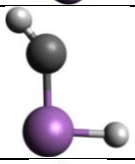	C 0.0179100000	1.7140600000	0.0000000000
		Sb 0.0179100000	-0.2444560000	0.0000000000
		H 0.6822580000	2.5706680000	0.0000000000
		H -1.7031440000	-0.3877580000	0.0000000000
HCSb		C 0.0000000000	0.0000000000	-1.6054370000
		Sb 0.0000000000	0.0000000000	0.2414790000
		H 0.0000000000	0.0000000000	-2.6828070000
CSb		C 0.0000000000	0.0000000000	-1.6835640000
		Sb 0.0000000000	0.0000000000	0.1980660000

Table 9-8.B3LYP/aug-cc-pVTZ)-derived vibrational frequencies, absolute infrared intensities, and electronic energies for singlet ($1^1\Delta$) HCCAs

S.no	Molecule	Infrared frequency (cm^{-1})	Relative Intensity (%)	Absolute Intensity (km/mol)	Energy (Hartree)
1.	HCCAs singlet ($1^1\Delta$)	204.698 303.69 338.962 548.631 796.345 1853.57 3310.03	9.61576 26.0791 77.4707 13.4507 14.1177 1.035 100	8.339 22.617 67.186 11.665 12.243 0.898 86.724	-2,312.656559

Table 9-9. B3LYP/aug-cc-pVTZ)-derived molecular geometry for singlet ($1^1\Delta$) HCCAs.

S.No.	Molecule	Molecular geometry	Cartesian coordinates			
1.	HCCAs singlet ($1^1\Delta$)		C	0.0000000000	0.0000000000	-2.3153390000
			H	0.0000000000	0.0000000000	-3.3779870000
			C	0.0000000000	0.0000000000	-1.0889180000
			As	0.0000000000	0.0000000000	0.7213190000

List of figures

List of tables